AD755480

CALCULATION OF POTENTIAL FLOW ABOUT ARBITRARY THREE-DIMENSIONAL LIFTING BODIES

Final Technical Report

October 1972

Report No. MDC J5679-01

by

John L. Hess

Prepared Under Contract N00019-71-C-0524

for

Naval Air Systems Command

Department of the Navy

by

Douglas Aircraft Company
McDonnell Douglas Corporation
Long Beach, California

165

UNCLASSIFIED

Security Classification

DOCUMENT CONTROL DATA - R&D

(Security classification of title, body of abstract and indexing annotation must be entered when the overall report is classified)

1. ORIGINATING ACTIVITY (Corporate author) Douglas Aircraft Company McDonnell Douglas Corporation 3855 Lakewood Blvd., Long Beach, California 90846	2a. REPORT SECURITY CLASSIFICATION UNCLASSIFIED 2b. GROUP Aerodynamics Research

3. REPORT TITLE
Calculation of Potential Flow About Arbitrary Three-Dimensional Lifting Bodies

4. DESCRIPTIVE NOTES (Type of report and inclusive dates)
Final Technical Report

5. AUTHOR(S) (Last name, first name, initial)
Hess, John L.

6. REPORT DATE	7a. TOTAL NO. OF PAGES	7b. NO. OF REFS
October 1972	165	20

8a. CONTRACT OR GRANT NO. N00019-C-71-0524	9a. ORIGINATOR'S REPORT NUMBER(S) MDC J5679/01
b. PROJECT NO.	
c.	9b. OTHER REPORT NO(S) (Any other numbers that may be assigned this report)
d.	

10. AVAILABILITY/LIMITATION NOTICES

This document has been approved for public release and sale; its distribution is unlimited.

11. SUPPLEMENTARY NOTES	12. SPONSORING MILITARY ACTIVITY
	Naval Air Systems Command Department of the Navy Washington, D. C. 20360 (AIR-53014)

13. ABSTRACT

This report presents a complete discussion of a method for calculating potential flow about arbitrary lifting three-dimensional bodies without the approximations inherent in lifting-surface theories. The basic formulation of three-dimensional lifting flow is pursued at some length and some difficulties are pointed out. All aspects of the flow calculation method are discussed, and alternate procedures for various aspects of the calculation are compared and evaluated. Particular emphasis is placed on the handling of the bound vorticity and the application of the Kutta condition, and it is concluded that the approach used in the method of this report has certain advantages over alternate schemes used by other existing methods. A considerable number of calculated results for various configurations are presented to illustrate the power and scope of the method. Included are: wing-fuselages, a wing with endplates, and a wing-fuselage with external stores. For some configurations, wind tunnel data are available for comparison with the calculated results. Any discrepancy between calculation and experiment appears to be due to viscosity, which is rather important in lifting cases.

UNCLASSIFIED
Security Classification

14 KEY WORDS	LINK A		LINK B		LINK C	
	ROLE	WT	ROLE	WT	ROLE	WT
Aerodynamics						
Computer Program						
Finite-Element Methods						
Flow Field						
Fluid Dynamics						
Integral Equations						
Interference Problems						
Kutta Condition						
Lifting Bodies						
Multipole Expansion						
Numerical Analysis						
Pressure Distribution						
Surface Singularity						
Three-Dimensional Flow						
Vorticity						
Wind-Tunnel Interference						
Wing-Body						

DD FORM 1 NOV 65 1473 (BACK)
S/N 0102-014-6800

UNCLASSIFIED
Security Classification

A-31409

CALCULATION OF POTENTIAL FLOW ABOUT ARBITRARY THREE-DIMENSIONAL LIFTING BODIES

Final Technical Report

October 1972

Report No. MDC J5679-01

by

John L. Hess

Prepared Under Contract N00019-71-C-0524

for

Naval Air Systems Command

Department of the Navy

by

Douglas Aircraft Company

McDonnell Douglas Corporation

Long Beach, California

CALCULATION OF POTENTIAL FLOW ABOUT
ARBITRARY THREE-DIMENSIONAL
LIFTING BODIES

Final Technical Report

Report No. MDC J5679-01 Issued October 1972

by

John L. Hess

Prepared Under Contract N00019-71-C-0524

for

Naval Air Systems Command
Department of the Navy

by

Douglas Aircraft Company
McDonnell Douglas Corporation
Long Beach, California

Approved by:

John L. Hess

J. L. Hess, Chief
Basic Research Group
Aerodynamics Subdivision

A. M. O. Smith

A.M.O. Smith
Chief Aerodynamics Engineer
Research

O. R. Dunn
Director of Aerodynamics

1.0 ABSTRACT

This report describes an investigation into the problem of the "exact" calculation of three-dimensional lifting potential flows. The designation "exact" is used to denote a method that makes no approximations in its basic formulation, such as small-perturbation or lifting-surface theories do. Obviously, numerical realities require some approximate techniques in the computer, but "exact" methods can be numerically refined in principle to give any degree of accuracy.

The first part of the study is a look at the problem of three-dimensional lifting potential flow from a fundamental standpoint, something almost totally lacking in the literature. Unlike nonlifting flow whose "physics" and mathematical description seem basically related, the mathematical description of the lifting problem is merely a model to describe by means of an inviscid flow a phenomenon that is ultimately due to viscosity. This is true even in two dimensions, but in three dimensions it leads to certain logical difficulties.

The method of this report and all current "exact" methods of calculating lifting flows are based on the author's previous work on three-dimensional nonlifting flows. This report describes the present method in general and in detail, including all formulas and logic. Alternatives are discussed, some of which are discarded, while others are incorporated into the program. The present method differs from other current methods mainly in its use of finite-strength surface vorticity distributions instead of concentrated line vorticity interior to the body and in its application of the Kutta condition. Comparisons indicate advantages for the formulation of the present method.

A variety of cases calculated by the present method are presented to illustrate its versatility and usefulness. Comparisons of the calculations with experimental data are presented. The importance of viscosity in the experimental results is illustrated.

2.0 TABLE OF CONTENTS

1.0 Abstract 1
2.0 Table of Contents 2
3.0 Index of Figures 4
4.0 Principal Notation 7
5.0 Introduction 11
- 5.1 Statement of the Problem of Potential Flow 11
- 5.2 Potential-Flow Model for Lift 13
- 5.3 Some Logical Difficulties in the Potential-Flow Model 18

6.0 General Features of the Method of Solution 21
- 6.1 The Method for Nonlifting Three-Dimensional Flow 21
- 6.2 Surface Elements for the Lifting Case 23
- 6.3 Bound and Trailing Vorticity 26
- 6.4 Use of a Dipole Distribution to Represent Vorticity 34
- 6.5 The Kutta Condition 35
- 6.6 Symmetry Planes 45
- 6.7 Multiple Angles of Attack 47
- 6.8 Some Special Situations 48
- 6.9 Summary of the Logic of the Calculation 50

7.0 Details of the Method of Solution. 54
- 7.1 Order of the Input Points 54
- 7.2 Formation of the Elements from Input Points 54
- 7.3 Form of the Surface Dipole Distribution 61
  - 7.3.1 General Form. Order of the Input Points 61
  - 7.3.2 Variation Across the Span of a Lifting Strip 65
  - 7.3.3 Variation Over a Trapezoidal Element 65
  - 7.3.4 Variation Between Elements of a Lifting Strip 67
- 7.4 Overall Logic of the Calculation of the Velocity Induced by a Lifting Element at a Point in Space 69
- 7.5 Far-Field Formulas for the Velocity Induced by a Lifting Element 72
- 7.6 Intermediate-Field or Multipole Formulas for the Velocity Induced by a Lifting Element 74
- 7.7 Near-Field Formulas for the Velocity Induced by a Lifting Element 77
- 7.8 Some Alternate Near-Field Formulas for Use in the Plane of the Element 83

7.9 The Velocity Induced by a Wake Element. 84
7.10 Option for a Semi-Infinite Last Wake Element 87
7.11 Formation of the Vorticity Onset Flows 89
7.12 The Linear Equations for the Values of Surface Source Density . 94
7.13 Application of the Kutta Condition 95
7.13.1 Flow Tangency in the Wake 96
7.13.2 Pressure Equality on Upper and Lower Surface at the Trailing Edge 97
7.14 Final Flow Computation 99
7.15 Computation Time, Effort, and Cost 100
8.0 Numerical Experiments to Illustrate Various Aspects of the Method. . 102
8.1 Element Number on an Isolated Lifting Wing 102
8.2 Two Forms of the Kutta Condition 103
8.3 Step Function and Piecewise Linear Bound Vorticity 104
8.4 Order of the Input Points 105
8.5 Location of the Trailing Vortex Wake 107
8.6 A Wing in a Wall. Fuselage Effects 108
8.7 A Sudden Change in Element Shape 109
8.8 An Extreme Geometry 110
9.0 Comparison of Calculated Results with Experimental Data 111
9.1 General Remarks 111
9.2 An Isolated Wing 112
9.3 Wing-Fuselages 112
9.4 A Wing-Fuselage in a Wind Tunnel 115
10.0 Interference Studies 117
10.1 Wing-Fuselage with External Stores 117
10.2 Wing with Endplates 119
10.3 Wing in a Wind Tunnel 120
10.4 Wing with Endplates in a Wind Tunnel 120
11.0 Acknowledgement 122
12.0 References 123
Appendix A. Relation Between Dipole and Vortex Sheets of Variable Strength 125
Appendix B. Literature Review of Shapes of Trailing Vortex Wakes 132

3.0 INDEX OF FIGURES

1. Potential flow about a three-dimensional body. 11
2. Nomenclature for a three-dimensional wing. 15
3. Circulation on a three-dimensional wing. 16
4. Wing planforms showing various tip geometries. 19
5. Examples of terminating trailing edges 20
6. Representation of a nonlifting body by quadrilateral surface elements 22
7. Typical lifting configuration. 24
8. Representation of the bound vorticity by concentrated vortex filaments lying in the mean camber surface 27
9. Representation of the bound vorticity by a finite-strength vorticity distribution lying on the wing surface 29
10. Two forms of the spanwise variation of bound surface vorticity . . . 29
11. Surface pressure distributions on a Karman-Trefftz airfoil of large camber at 1.205 degrees angle of attack 32
12. Surface pressure distributions on a conventional airfoil section at 6.9 degrees angle of attack 33
13. Theoretical behavior of the vortex wake at the trailing edge of a wing 41
14. Behavior of the vortex wake near the trailing edge for small values of the trailing edge velocity component 42
15. Calculated lift coefficients for a two-dimensional airfoil as functions of the distance from the trailing edge of the point of application of the Kutta condition. Airfoil is 10-percent thick symmetric section at 10 degrees angle of attack 44
16. Reflection of an element and its associated N-lines in symmetry planes 46
17. Handling of a wing-pylon intersection 48
18. Handling of a wing-fuselage intersection 49
19. Adjustment of the input points to form a plane trapezoidal element . 55
20. A plane trapezoidal element 58
21. Variation of dipole strength along an N-line 62
22. Three variations of dipole strength along a section curve (N-line) 63
23. An example of division of a single physical lifting portion of a body into two lifting sections 93
24. Special procedures at the ends of a lifting section for the parabolic fit used with the piecewise linear vorticity option . . . 94

25. Planform of a swept tapered wing showing lifting strips used in the calculations 134

26. Spanwise distributions of section lift coefficient calculated for a swept tapered wing at 8 degrees angle of attack using various numbers of lifting strips 135

27. Spanwise distributions of bound vorticity on a swept tapered wing at 8 degrees angle of attack computed by the two bound vorticity options 136

28. Spanwise distributions of section lift coefficient on a swept tapered wing at 8 degrees angle of attack computed by the two bound vorticity options 136

29. Spanwise distributions of bound vorticity on a swept tapered wing at 8 degrees angle of attack computed with two orders for the input points 137

30. Spanwise distributions of section lift coefficient on a swept tapered wing at 8 degrees angle of attack computed with two orders for the input points 137

31. A wing protruding from a plane wall showing three element distributions used for the wall 138

32. Calculated effects of a finite and an infinite plane wall on the spanwise distribution of section lift coefficient for a wing of rectangular planform at 10 degrees angle of attack 139

33. Two element distributions on a wing of rectangular planform mounted on a round fuselage 140

34. Comparison of results calculated for a rectangular wing mounted on a round fuselage using two different element distributions at 6 degrees angle of attack 141

35. Geometry of an extreme test case with a large flap deflection . . . 142

36. Comparison of calculated and experimental results on a swept tapered wing at 8 degrees angle of attack 143

37. A rectangular wing mounted as a midwing on a round fuselage. 144

38. Comparison of calculated and experimental results on a rectangular wing mounted as a midwing on a round fuselage at 6 degrees angle of attack 145

39. A supercritical wing mounted as a high wing on a fuselage 146

40. Comparison of calculated and experimental results on a supercritical wing mounted as a high wing on a fuselage at 7 degrees angle of attack 147

41. A conventional wing mounted as a low wing on a fuselage. 148

42. Comparison of calculated and experimental results on a conventional wing mounted as a low wing on a fuselage at 6.9 degrees angle of attack and a freestream Mach number of 0.5 149

43. A W-wing on a fuselage mounted on a strut in a rectangular wind tunnel 150

44. Comparison of calculated and experimental results on a W-wing mounted on a fuselage. Calculations performed with and without support strut and wind tunnel walls 151

45. Two external-store configurations 152

46. Comparison of calculated results on a clean wing, a wing with tip tank, and a wing with pylon-mounted external store, all in the presence of a round fuselage at 6 degrees angle of attack. 154

47. A rectangular wing of aspect ratio 1.4 with endplates 155

48. Comparison of calculated results on a rectangular wing at 10 degree angle of attack with and without endplates 156

49. A rectangular wing of aspect ratio 1.4 in a rectangular wind tunnel 157

50. Comparison of calculated results on a rectangular wing at 10 degrees angle of attack with and without the wind tunnel sidewalls 158

51. A rectangular wing of aspect ratio 1.4 with endplates in a rectangular wind tunnel 159

52. Comparison of calculated results for a rectangular wing at 10 degrees angle of attack in free air with those for the same wing with endplates in a wind tunnel 160

4.0 PRINCIPAL NOTATION

A_{ij} — velocity induced at the i-th control point by a unit value of source density on the j-th element. If there are N on-body control points where a normal-velocity boundary condition is applied, this is an N x N matrix. It is the coefficient matrix for the linear equations for the values of source density. The same coefficient matrix applies to all onset flows.

B — Constant of proportionality for the dipole strength along an N-line. Local dipole strength along an N-line equals B times the arc length along the N-line from the trailing edge. By theorem of Appendix A, this means B equals the value of bound vorticity at the spanwise location of the N-line. Used with superscript k to indicate value of B at the midspan of the k-th lifting strip.

b_{32}, b_{41} — intercepts of slanted sides of a trapezoidal element with the x-axis of its own coordinate system (figure 20).

C_L — lift coefficient for a complete body.

C_p — pressure coefficient. Equals difference of local static pressure from freestream static pressure divided by freestream dynamic pressure.

c — denotes an integration path. Also a constant multiplying a second order dipole term used to produce continuity.

c_ℓ — section lift coefficient. Lift force on a strip of elements on a wing divided by the projected area of the strip in a plane containing the chord line and by freestream dynamic pressure.

d — used with double subscript to denote length of a side of a quadrilateral element.

F, S — subscripts and superscripts used to denote quantities associated with the two N-lines bounding a strip of elements. F denotes "first" N-line and S the "second" N-line. F is also used to denote number of uniform onset flows.

I_{nm} — normalized moment of the area of a trapezoidal element with respect to the axis of the element coordinate system, equations (7.2.24) and (7.2.27).

i — a subscript used to denote quantities associated with the i-th control point, particularly velocities at that point. Used as superscript to denote input point.

ij — double subscript used to denote effect of j-th element at i-th control point, particularly induced velocity.

$\vec{i}_E$, $\vec{j}_E$, $\vec{k}_E$	unit vectors along the axes of a coordinate system based on an element.
k	subscript used in various ways. $k = 1, 2, 3, 4$ denotes quantities associated with the four corner points of an element. Also used as subscript and superscript to denote k-th lifting strip or vorticity onset flow associated with that strip.
L	arc length along an N-line. Also denotes total number of lifting strips of surface elements.
M	used in figure 42 to denote freestream Mach number
m_{32}, m_{41}	slopes of the slanted sides of a trapezoidal element with respect to the y-axis of its own coordinate system (figure 20).
N	total number of surface elements at which normal-velocity boundary conditions are applied. Includes both lifting and nonlifting elements.
N-line	curve in wing surface, usually a fixed spanwise location, along which input points are given. N-line continues aft to define the trailing vortex wake. A strip of elements lies between two consecutive N-lines.
$\vec{n}$	unit normal vector.
O	number of off-body points at which flow is to be computed
P	a general point in space.
r	distance between two points. Used with subscript o to denote distance from centroid of an element to point where velocity is being computed. Used with subscript k to denote distance between such a point and the corner point of an element.
S	denotes a body surface on which a normal-velocity boundary condition is applied.
s	arc length, especially arc length along an N-line.
[illegible]	maximum diagonal of an element (figure 20).
$\vec{V}$	total flow velocity.
$\vec{V}_i$	total flow velocity at i-th control point.
[illegible]	velocity of an onset flow, especially a uniform onset flow.
[illegible]	combined onset flow including freestream and vorticity onset flows, equation (7.11.2)
[illegible]	k-th vorticity onset flow. With superscript [illegible] denotes uniform onset flow.

$\vec{v}$	perturbation velocity due to body.
$\vec{v}_i^{(k)}$	total flow velocity at i-th control point due to flow induced about the body by the k-th vorticity onset flow. With superscript (∞) the nonlifting flow about the body in a uniform freestream,equation (7.13.4).
V_x, V_y, V_z	velocity components induced by an element at a point space with respect to the coordinate system of the element.
$\vec{V}_{ij}$	velocity induced at the i-th control point by a unit value of source density on the j-th element.
$\vec{V}_{ij}^{(F)}$, $\vec{V}_{ij}^{(S)}$	velocities induced at the i-th control point by a dipole distribution on the j-th trapezoidal element that varies linearally from zero on one parallel side to unity on the other. Superscript denotes the N-line containing the side with nonzero dipole strength.
w	width of a trapezoidal element in direction normal to the parallel sides (figure 20). Also used with subscript k to denote width of lifting strip for parabolic fit (section 7.11).
x, y, z	coordinates of a point in element coordinate system.
x', y', z'	coordinates of a point in the reference coordinate system used to input the body.
x_0, y_0, z_0	coordinates of the centroid of an element in the reference coordinate system.
α, β, γ	direction cosines of a point in space with respect to the coordinate system of an element based on the centroid as origin. Also used with subscript k to denote the same direction cosines with origin shifted to a corner point.
Γ	total circulation around a closed path.
γ	circulation about a closed path due to perturbation velocity field of the body.
μ	dipole strength per unit area.
ξ, η	x, y coordinates of a point of an element in its own coordinate system. Used with subscripts k to denote coordinates of the corner points.
ρ_1, ρ_2	distance criteria used to decide when multipole and far-field formulas are to be used.
σ	source density per unit area. Used with subscript j to denote value on j-th element and with superscript k to denote values calculated for k-th vorticity onset flow.

ϕ	velocity potential especially that due to a body or that due to a surface element.
ϕ_{pq}	velocity potential due to a dipole distribution on an element that varies as the p-th power of ξ and the q-th power of η_1 equation (7.4.4).

5.0 INTRODUCTION

5.1 Statement of the Problem of Potential Flow

The problem considered is that of the flow of an incompressible inviscid fluid in the region R' exterior to (or interior to) a given boundary surface S. For definiteness S is shown as a single three-dimensional surface in figure 1, but S may consist of several disjoint surfaces, and the problem may be either two- or three-dimensional. It is convenient to express the fluid velocity field $\vec{V}$ at any point P as the sum of two velocities:

$$\vec{V} = \vec{V}_\infty + \vec{v} \tag{5.1.1}$$

The velocity $\vec{V}_\infty$ is denoted the onset flow and is defined as the velocity field that would exist if all boundaries were simply transparent to fluid motion. It is assumed that $\vec{V}_\infty$ is known. Most commonly $\vec{V}_\infty$ represents a uniform parallel stream and is thus a constant vector. The vector $\vec{v}$ is the disturbance velocity field due to the boundary surface S. Since the flow is incompressible, both $\vec{V}_\infty$ and $\vec{v}$ have zero divergence. It is further assumed

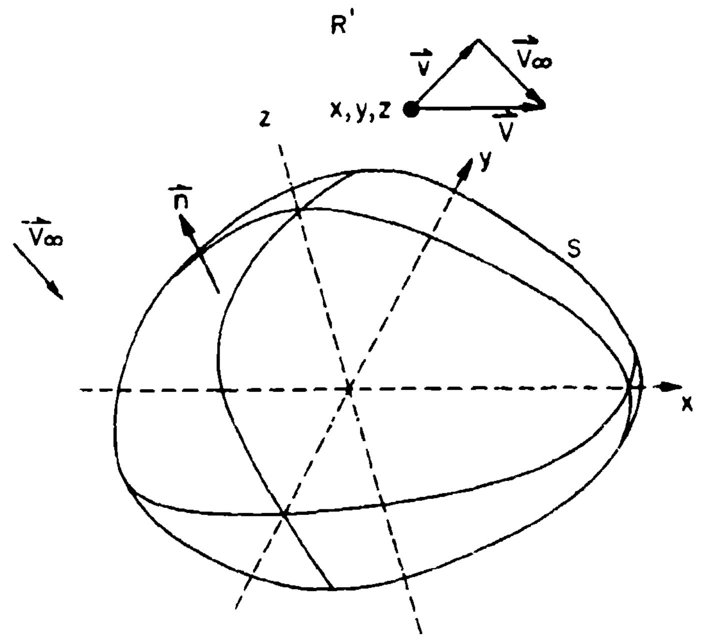

Figure 1. Potential flow about a three-dimensional body.

that $\vec{v}$ is irrotational, i.e., has zero curl. Thus, $\vec{v}$ may be expressed as the negative gradient of a potential function ϕ,

$$\vec{v} = -\text{grad}\ \phi \tag{5.1.2}$$

The con..ion of zero divergence then yields Laplace's equation for ϕ,

$$\nabla^2\phi = 0 \quad \text{in} \quad R' \tag{5.1.3}$$

The boundary condition on S is derived from the requirement that on a stationary impervious surface S the normal component of fluid velocity must vanish. Thus,

$$\frac{\partial\phi}{\partial n} = \text{grad}\ \phi \cdot \vec{n} = \vec{V}_\infty \cdot \vec{n} \quad \text{on} \quad S \tag{5.1.4}$$

where $\vec{n}$ is the unit outward normal vector to S. Since the right side is known, equation (5.1.4) expresses a Neumann boundary condition for ϕ. If the boundary S is moving or if a nonzero normal velocity is prescribed, the right side of (5.1.4) is modified in an obvious way.

A regularity condition at infinity is also required. In the usual exterior problem the condition is

$$|\text{grad}\ \phi| \to 0 \text{ at infinity} \tag{5.1.5}$$

In addition to the above equations, some applications require certain auxiliary conditions to be satisfied. However, in the absence of such conditions and for a simply connected region R', the equations (5.1.3), (5.1.4), and (5.1.5) comprise a well-posed problem for the potential ϕ.

In two-dimensional exterior problems, the region R' is not simply connected, and equations (5.1.2), (5.1.3), (5.1.4), and (5.1.5) do not define a unique velocity field. Define the total circulation Γ around any closed path c in the fluid as the line integral

$$\Gamma = \int_c \vec{V} \cdot \vec{ds} = \int_c \vec{V}_\infty \cdot \vec{ds} + \int_c \vec{v} \cdot \vec{ds} = \Gamma_\infty + \gamma \tag{5.1.6}$$

where

$$\gamma = \int_{c} \vec{v} \cdot \vec{ds} \qquad (5.1.7)$$

is the circulation associated with the disturbance velocity due to the body. In the above

$$\vec{ds} = \vec{t}\, ds \qquad (5.1.8)$$

where S is arc length along c, and $\vec{t}$ is the unit tangent vector. If c does not enclose all or part of S, then $\gamma = 0$. If S is a single surface, it can be shown (reference 1) that the velocity field $\vec{v}$ is rendered unique by specifying γ for any c that encloses S. If S consists of several disjoint surfaces, γ must be specified for a set of paths, each of which encloses exactly one of the disjoint surfaces that comprise S. The potential ϕ is unique if and only if $\gamma = 0$ for all closed paths.

5.2 Potential-Flow Model for Lift

The reasoning leading up to the formulation of the potential flow problem in terms of equations (5.1.3), (5.1.4), and (5.1.5) seems very plausible. However, when the problem defined by these equations is solved, the resulting flow gives zero net force on a closed three-dimensional body. This is due to the fact that all components of force on a body — both the lift, which is perpendicular to the freestream, and the drag, which is parallel to the freestream — are ultimately due to viscosity. Nevertheless, the goal of calculating at least the lift component of the force by a purely inviscid technique has been continuously pursued. It is important to realize that any such formulation is simply a potential-flow model of real lifting flow, and that the two flows are not necessarily related in any fundamental way. Formulation of the commonly accepted potential-flow model of three-dimensional lifting flow has relied heavily on results for the two-dimensional case.

In two-dimensional flow advantage can be taken of the indeterminacy of the solution as described in section 5.1. For a single closed body in a uniform stream, the drag force is zero, and the lift is proportional to the circulation γ, which is arbitrary. (For a uniform onset flow the total circulation Γ equals γ, the circulation due to the disturbance velocity.) Thus, in two-dimensions the problem is not that no lift is obtained but that the lift can have any magnitude. Some auxiliary condition is needed to fix the value of lift. For bodies with continuous slope no satisfactory auxiliary condition has ever been formulated. However, a conventional airfoil has a sharp corner at its trailing edge, and there is a unique value of γ (and thus a unique lift) that makes the potential-flow surface velocity finite at this corner. Determining the value of circulation in this way also insures that a streamline of the flow leaves the airfoil at the trailing edge with a direction along the bisector of the trailing-edge. This condition of finite velocity at the trailing edge, the so-called Kutta condition, is so well accepted that it is normally not considered a mere modeling device but is assumed to have a more fundamental connection with the real flow. However, the Kutta condition is inapplicable to smooth bodies, and for airfoils with sharp trailing edges it gives values of lift that differ from experimental values by up to 20 percent.

The theorem that guarantees a unique solution for the flow about a two-dimensional body with prescribed circulation γ is quite general. However, in a specific calculation procedure the question arises of how the condition of prescribed circulation is to be applied. All procedures accomplish this with the help of vorticity. A distribution of vorticity, consisting of either concentrated filaments or finite-strength surface or volume distributions are hypothesized to lie on or within the body in question. The total strength of the vorticity distribution establishes the prescribed circulation.

Consideration of the above two-dimensional model suggests certain elements of a model for lifting flow about a three-dimensional wing of the type shown in figure 2. If the trailing edge of the wing is a sharp corner, a plausible three-dimensional Kutta condition requires that the velocity remain finite there all across the span, which means that a stream surface leaves the wing from the trailing edge. Define the circulation about a particular wing section as the line integral of the velocity in the form of equation (5.1.7) about a closed curve lying in the wing surface as shown in figure 2. The precise definition of this so-called section curve is not considered now. A reasonable definition is that the curve lie in a plane parallel to the plane

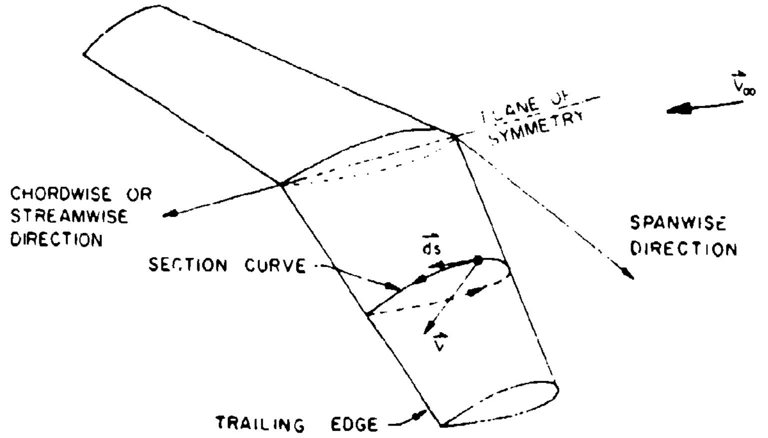

Figure 2. Nomenclature for a three-dimensional wing.

of symmetry of the wing. But for certain purposes the curve could lie in a plane normal to the leading or trailing edge. In any case the value of the circulation is different for curves at different locations, so that there is a "spanwise" variation in "section circulation." By analogy with two-dimensions, it is expected that a proper adjustment of this spanwise variation could render the velocity finite all along the trailing edge. Presumably, the circulation can be generated by some distribution of vorticity lying on or within the wing. It seems evident that the direction of this so-called "bound vorticity" should be generally along the span, roughly parallel to the trailing edge. The net vorticity strength through each "section" is proportional to the circulation around that section.

Define γ_1 and γ_2 as the values of circulation about two sections of the wing, where the positive sense of the integral of (5.1.7) is taken as clockwise to an observer at the wing midplane looking towards the right wing tip. Unlike the two-dimensional case, the region exterior to a closed three-dimensional body is simply connected, so that if the flow is potential, i.e., has zero curl, and is free from singularities, then

$$\int_C \vec{V} \cdot \vec{ds} = 0 \tag{5.2.1}$$

for any closed path c, which implies $\gamma_1 = \gamma_2 = 0$. Thus, to obtain nonzero values of section circulation, there must be some form of singularity in the exterior flow. The nature of the singularity can be exhibited by considering the path c shown in figure 3a. The line integral of velocity around this path is

$$\int_c \vec{v} \cdot \vec{ds} = \gamma_1 - \gamma_2 + \int_I (\vec{v}_+ - \vec{v}_-) \cdot \vec{ds} \tag{5.2.2}$$

where I is the straight path joining the two section curves and $\vec{v}_+$ and $\vec{v}_-$ are the limiting velocities obtained by approaching I from two different directions on the surface. If the line integral of (5.2.2) is to vanish, then either $\gamma_1 = \gamma_2$ or $\vec{v}_+ \neq \vec{v}_-$, and there is a discontinuity of tangential velocity along I. If sharp corners in streamlines are to be avoided, such a discontinuity can occur only across a stream surface of the flow, and thus either I is a locus from which a stream surface leaves or joins the body or else I is a portion of a streamline on the surface. In any event I represents the intersection of a sheet of vorticity with the body surface. To complete the potential flow model, the first possibility, a stream surface

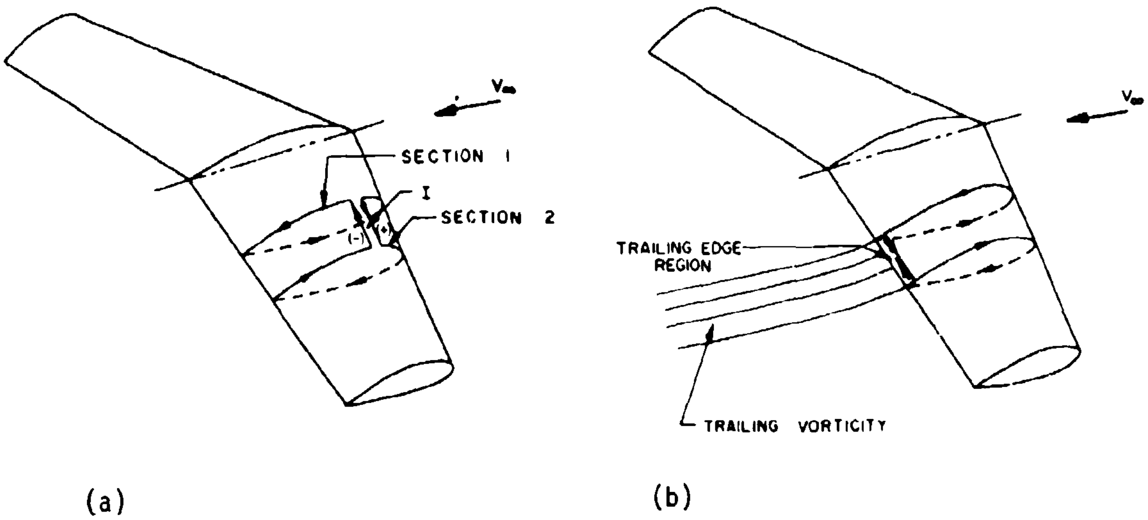

Figure 3. Circulation on a three-dimensional wing. (a) Integration path c. (b) Discontinuity at the trailing edge.

leaving the body, is selected, essentially on physical grounds. It is reasoned that vorticity is introduced only to the fluid that passes by the body and that the path I of (5.2.2) must lie along the trailing edge of the wing (figure 3b). Thus, a vortex sheet issues from the trailing edge and for steady flow it proceeds to infinity. The average strength of the sheet along I is proportional to the difference $\gamma_1 - \gamma_2$. Taking the limit as the two section curves approach each other gives the result that the local strength of the trailing vortex sheet is proportional to the "spanwise" derivative of the "section circulation."

It follows from the above that the local strength of the "trailing vorticity" that issues from the wing trailing edge equals the "spanwise" derivative of the "bound vorticity." Thus, trailing vorticity is of precisely the right form so that the entire bound-plus-trailing vorticity system may be thought of as being composed of constant-strength vortex lines of infinitesimal strength, each of which proceeds "spanwise" along the wing and then turns and proceeds "streamwise" to infinity, the familiar "horseshoe" vortices. This is crucial because, as pointed out in reference 2, the velocity field due to a variable-strength vortex filament or a nonclosed constant-strength vortex filament of finite length is not a potential flow. Only infinite or closed vortex lines of constant strength give rise to irrotational velocity fields.

As mentioned above, the trailing vortex sheet must be a stream surface of the flow. Also, on physical grounds the pressure must be continuous across the sheet. In principle, these two conditions allow the complete shape of the trailing vortex sheet to be calculated. The basic flow problem is nonlinear because the location of the sheet changes for different onset flows. In particular, the sheet changes location if the angle of attack of the freestream changes.

The above contains the general features of the potential-flow model of three-dimensional lift. It is considerably more complicated than the simple formulation of equations (5.1.3), (5.1.4), and (5.1.5), which represent the nonlifting case. However, the nonlifting formulation appears to be fundamental, while the lifting formulation is basically a model adopted to simulate certain properties of real viscous flow by means of a potential flow. The nonfundamental nature of the lifting model leads to some logical difficulties which may or may not be important in a particular case. Some of these are discussed in the next section.

5.3 Some Logical Difficulties in the Potential-Flow Model

The principal device by which lift is introduced into potential flow of either two or three dimensions is the trailing edge. To some extent the definition of a trailing edge is a matter of legislation by the user of the method rather than a fundamental concept. Accordingly, difficulties may arise. In two-dimensions the situation is rather simple. There is no logical difficulty if the trailing edge is a sharp corner (the agreement of the model with real flow may or may not be acceptable). On the other hand, if there is no sharp corner, the difficulty is crucial, because the trailing edge cannot be rationally defined. In three-dimensions some rather subtle borderline cases arise in ordinary design applications. In regions where the wing has a sharp corner as shown in figure 2, the choice of trailing edge is straightforward. Difficulty arises where the locus of the sharp corner ends. The question arises whether the trailing edge ends or continues, and, if the latter, in what matter.

A wing tip is the place where the above-mentioned difficulty most frequently arises. Consider the type of tip shown in figure 4a, whose planform is a semicircle. The trailing edge is well-defined by a sharp corner out to the beginning of the tip. On the tip itself, the downstream side of a "section" curve has a finite radius of curvature which approaches zero at the point A. Should the trailing edge end at A or should it continue over the tip region despite the fact that there is no sharp corner? If the "section" curves on the tip region had sharp corners, presumably the trailing edge would continue into the tip region all the way to the point B. For highly yawed flow, the point B appears to be part of the leading edge. Where should the trailing edge end in that case? The tip in figure 4b is a half-body of revolution formed by rotating the symmetric section curve at AA' about its symmetry line. In this case, ending the trailing edge at the point A would probably be the choice of most users. However, the tips in figures 4a and 4b differ mainly in their values of the ratio of "spanwise"

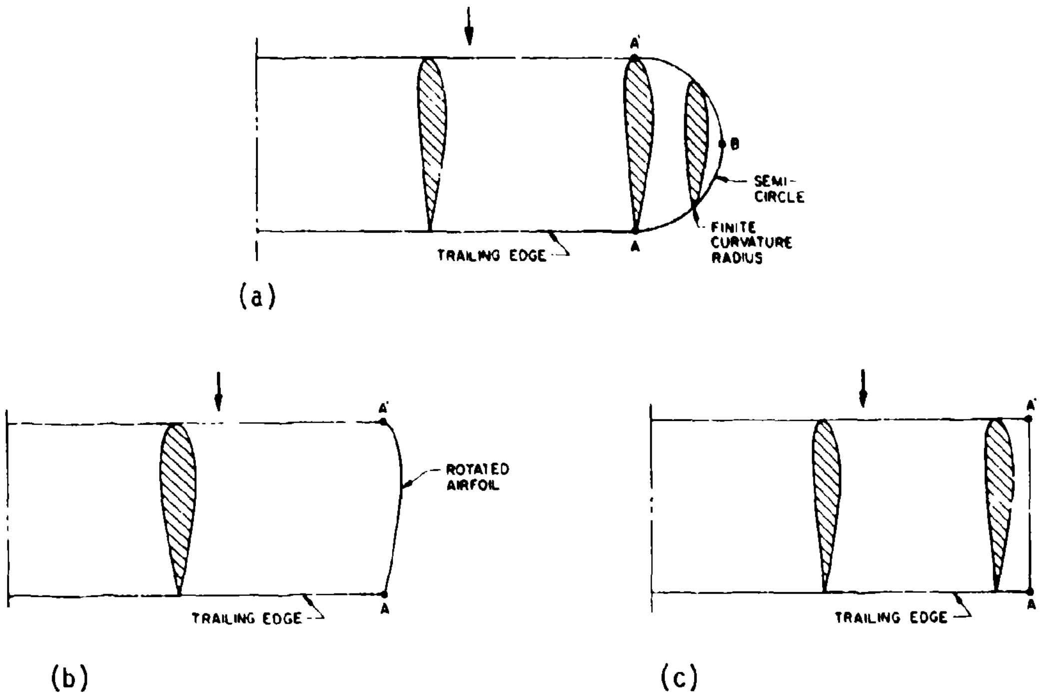

Figure 4. Wing planforms showing various tip geometries.

extent to "streamwise" extent. For the "squared-off" tip shown in figure 4c agreement to terminate the trailing edge at the point A would be virtually unanimous. Nevertheless, the question arises as to what exactly does happen on the tip itself. This type of tip occurs, for example, at the edge of deflected flaps. Objections of the sort mentioned here are basic to the potential-flow model and do not depend on the particular implementation used to produce an actual program.

One "answer" to the above is that certain viscous effects are important at wing tips, and potential flow is not expected to apply in that region. The "tip vortex" leaves the wing well forward of the trailing edge with a finite diameter (see Appendix B) in contradiction to the potential flow model. Thus, the assumed potential flow model treats wing tips in an approximate fashion and is not applicable to very low "aspect ratios".

A wing-fuselage junction (figure 5a) is another important application where the trailing edge must end at point A. It would make little sense to

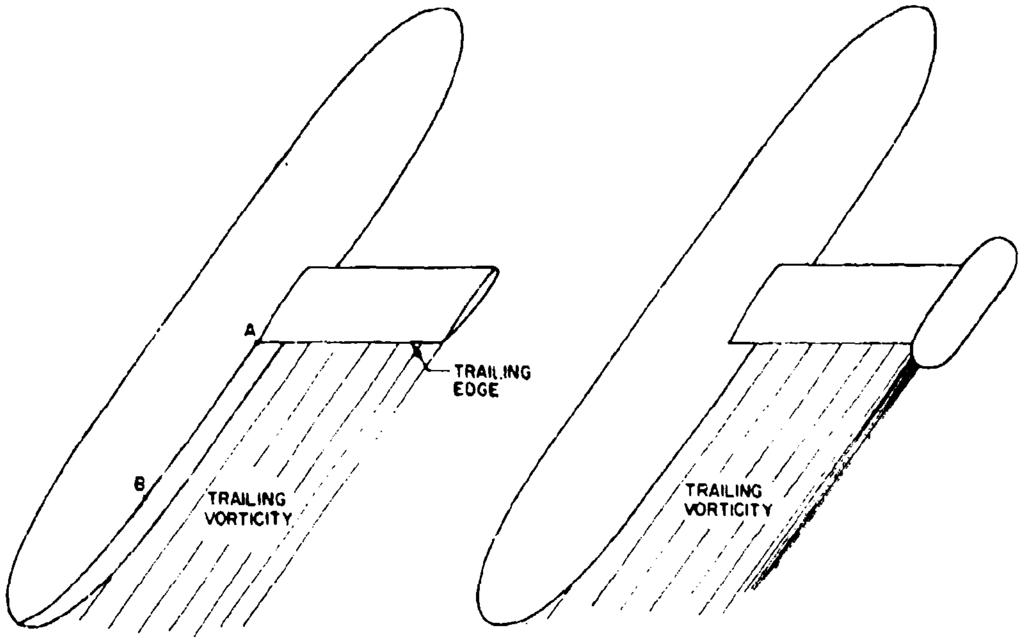

(a) (b)

Figure 5. Examples of terminating trailing edges. (a) Wing-fuselage intersection. (b) A tip tank.

continue the trailing edge downstream along, say, the line AB. However, the trailing vortex wake intersects the fuselage along AB and must do so without numerical problems. The question arises of what happens to the "bound vorticity" at a wing-fuselage junction, but that is as much a problem of implementation as a problem in the basic formulation (see section 6.8).

A situation with elements of both the above is a wing with a tip tank (figure 5b). Depending on its size, the tank may be considered a small fuselage or a big wing tip. Unlike the usual situation for a fuselage, the flow about the tip tank has no right-and-left symmetry, and there is vorticity trailing downstream from the tip tank, which must be accounted for.

There are certainly other situations where the details of the potential-flow model of three-dimensional lift are unclear. The examples of this section simply serve to illustrate that such basic problems exist, regardless of the particular implementation used to reduce the model to practice. The implementations of course lead to problems of their own.

6.0 GENERAL FEATURES OF THE METHOD OF SOLUTION

6.1 The Method for Nonlifting Three-Dimensional Flow

References 1 and 2 review the long-term effort of the author and his colleagues in the field of potential-flow calculation. Among the methods described are those for lifting two-dimensional flows and nonlifting three-dimensional flows. The latter is described in somewhat greater detail in reference 3. This nonlifting method forms the basis on which is built the lifting method to be described here. By way of introduction, the nonlifting program is outlined briefly here, but the references are relied on to supply all details.

All the potential flow methods of references 1 and 2 are based on a distribution of source density over the surface of the body about which flow is to be computed. The normal component of fluid velocity is given on the surface of the body. Usually the normal velocity is zero. Application of the normal-velocity boundary condition yields an integral equation for the distribution function of the source density, where the domain of integration is the body surface. Once this equation is solved for the source distribution, flow velocities both on and off the body surface can be calculated. Implementing this method for the computer requires an approximate representation of the body surface and a numerical integration routine.

In the nonlifting program of reference 3, the body is specified to the computer by a set of points, which presumably lie exactly on the body surface. These points are associated into groups of four "adjacent" points and a least-squares plane passed through them. The four points are then projected into this plane to form the corners of a plane quadrilateral surface element. When this process is completed for all of the points, the body surface is approximated by a set of plane quadrilaterals. A hypothetical example is shown in figure 6. Because of the process of projection, the edges of adjacent elements may be not quite coincident, but errors from this source are small compared to errors from the other numerical approximations inherent in the method.

Certain features of the method of approximating the body surface are of importance to the lifting application. The points defining the body are input in such an order that they define a family of approximately parallel curves lying in the body surface. These curves, which have some of the features of surface coordinates have been designated "N-lines," as shown in figure 6. (In reference 3 the designation "column" is used instead of "N-line." Both have the same meaning.) First all points along a certain N-line are input in order from bottom to top, and then the same is done for the adjacent N-line to the right. Two adjacent N-lines bound a "strip" of elements of approximately constant width. The elements are general quadrilaterals and do not necessarily have two parallel sides or two sides of equal length. As a logical device a number of N-lines can be associated into a "section." Often a section is simply an entire body, but separate sections are often used to represent geometrically different parts of the same body; for example, a wing and a fuselage. Also sections are used to concentrate elements in certain regions of a body. Logically, the concept of a section means only that the last (or first) N-line of the section is not associated with the next (or previous) N-line to form a strip of elements.

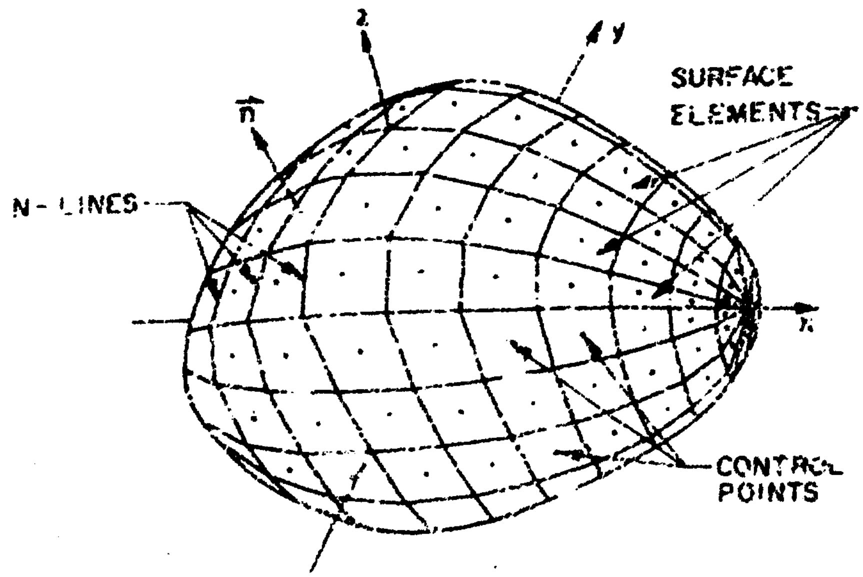

Figure 6. Representation of a non-lifting body by quadrilateral surface elements.

On each element one point is selected where the normal velocity boundary condition is to be applied and where flow velocities are to be computed. This point, which is designated the control point of the element, has been defined various ways in the past but currently is identified with the centroid of the element. Formulas have been derived that give the components of velocity induced at a general point in space by a unit value of source density on a general quadrilateral element. These formulas allow the velocities induced by the elements on each other's control points to be calculated. Equating the normal velocity induced by all elements at each control point to the negative of the normal component of the onset flow (for the case of zero total normal velocity) yields a set of linear algebraic equations for the values of source density on the elements. Once these are solved, flow velocities can be computed at the centroids and at any selected point in the flow field. For the lifting application it is important to point out that the onset flow need not be a uniform stream. Moreover, solutions for several onsets may be obtained simultaneously. The onset flow affects only the right side of the linear equations for the source density not the coefficient matrix. Thus, if a direct matrix solution is employed, several onset flows may be treated in nearly the same computing time as a single onset flow.

6.2 Surface Elements for the Lifting Case

A lifting body and its trailing vortex wake are approximated by quadrilateral surface elements in a manner very similar to that described in reference 3 for a nonlifting body. The approximation procedure is outlined here with emphasis on the differences from the nonlifting case.

As pointed out in section 5.3, certain portions of a general aerodynamic configuration do not have well-defined trailing edges and are not normally thought of as having their own bound vorticity; e.g., a fuselage. These portions are denoted nonlifting portions to signify that they do not possess independent bound vorticity and that a Kutta condition is not applied on them. However, in general, the fluid exerts nonzero pressure forces on nonlifting portions due to interference pressures from other nearby portions of the configuration and due to extentions of the bound vorticity from lifting portions (see section 6.8). Nonlifting portions are approximated by general plane quadrilateral elements in exactly the same way as in the nonlifting method of reference 3. In the main calculation such elements have source density but not vorticity. The organization of the input data by sections (see above) is a natural way of isolating lifting and nonlifting portions.

Portions of a general configuration that possess definite trailing edges (usually sharp corners) and contain bound vorticity are denoted lifting portions. The most frequently occurring application with both lifting and nonlifting portions is a wing-fuselage. Accordingly, this configuration is used as an illustrative example in figure 7. On a lifting portion the N-lines are approximately in the freestream direction. On each N-line points are input beginning at the trailing edge, continuing around a "section curve" of the wing, returning to the trailing edge, and proceeding downstream to define the trailing vortex wake. The wake may be defined as far downstream as desired. Provision has been made to consider the last element of the wake semiinfinite so that wake definition may be terminated at any point aft of which the wake curvature in the stream direction may be neglected. Usually a lifting portion such as a wing is considered a single lifting section, but it may be divided

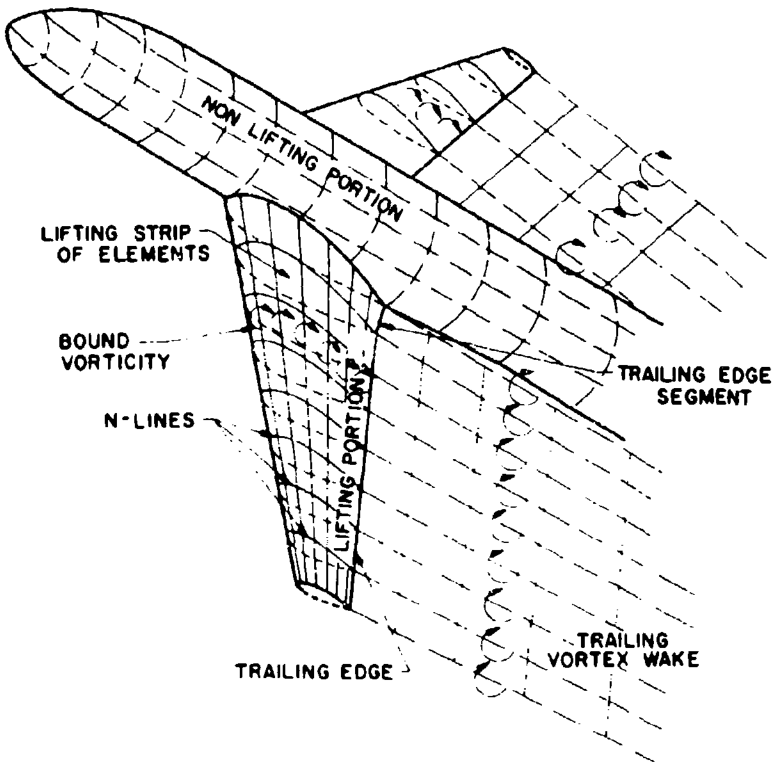

Figure 7. Typical lifting configuration.

into several lifting sections if desired. Within each lifting section all N-lines must contain the same number of input points. Points on adjacent N-lines of a lifting section are associated to form surface elements. The set of elements formed from points on a pair of adjacent N-lines is denoted a "lifting strip" of elements. The strip contains elements both on the body and in the wake. Although two adjacent N-lines are not quite parallel in general, they are nearly parallel in most cases.

Elements of lifting sections are taken as plane trapezoids. Each of the two parallel sides is formed from two input points on the same N-line. Thus the parallel sides are approximately along the N-lines. Of course, in the general case the four input points that are associated to form an element do not even lie in the same plane, much less form a trapezoid. They must be "adjusted" to do this. In the nonlifting program of reference 3 the input points are adjusted to lie in the same plane but not to be trapezoidal. Thus, the "adjustment" required is somewhat more for lifting elements than for non-lifting. Adjacent elements have two input points in common, but the adjustment that these points are subject to is usually different for the two elements. Thus, in general, after adjustment the sides of adjacent elements are not coincident, and there are gaps between the elements. Such gaps exist for both lifting and nonlifting elements. For the nonlifting case the unimportance of the gaps is discussed in references 1 and 3. For lifting elements the gaps are presumably greater than for nonlifting elements, but it seems that in both cases the gaps should have the same order of magnitude. Thus, errors from this source should be unimportant. It is pointed out in references 1 and 3 that for some bodies the gaps between elements vanish. For lifting bodies the important case for which this occurs is an untwisted wing, possibly swept and tapered, having the same airfoil section at all spanwise locations.

The centroids of the elements are used as control points. Thus, for each lifting strip the locus of control points is approximately midway between the two N-lines used to generate the strip. Elements of lifting strips have source densities whose strengths are determined to give zero (or prescribed) normal velocity at the control points.

6.3 Bound and Trailing Vorticity

In addition to the source densities on the elements, lifting portions also possess a distribution of bound vorticity. As pointed out in section 5.2, the form of the bound vorticity uniquely determines the strength distribution of the trailing vorticity, which lies along the input wake. The form assumed for the bound vorticity contains a number of adjustable parameters equal to the number of lifting strips on that lifting portion. The values of these parameters are determined by applying a Kutta condition at the trailing edge segment (figure 7) of each lifting strip. The simplest form of the bound vorticity distribution utilizes a set of individual distributions, each of which is nonzero only on one lifting strip. The complete distribution consists of a linear combination of these individual distributions, each of which is nonzero on a different lifting strip. The combination constants of the linear combination are the required adjustable parameters. This is the type of distribution used in the present method. Other existing methods (references 4, 5, 6, and 7) also use this type of distribution. The value of the parameter multiplying the distribution associated with a particular lifting strip represents the strength of the bound vorticity at the "spanwise" location of that strip. Thus, as expected, the "spanwise" variation of bound vorticity is determined by the Kutta condition. More precisely the "spanwise" variation of vorticity from one lifting strip to another is determined by the Kutta condition. The "spanwise" variation of vorticity within the small but finite span of each individual lifting strip is basically a question of the order of accuracy of a numerical integration (see below for the options of the present method).

Even if the bound vorticity is of the type mentioned above, various forms of this vorticity are possible. In addition, the "chordwise" or "streamwise" variation of vorticity on a "section curve" at a particular "spanwise" location may be chosen at will. In the limit where an infinite number of surface elements are used to approximate the body, it appears that the calculated flow velocities are independent of the assumptions made concerning bound vorticity. However, for practical element numbers, the form assumed for the bound vorticity and its "chordwise" variation have an appreciable effect on the accuracy of the solution. The methods of references 4, 5, 6, and 7 all use the same form for the bound vorticity, which consists of concentrated vortex filaments lying in the camber surface of the wing. Some details are illustrated in figure 8a, which shows a single N-line representing a section curve of the wing. An equal number of elements is placed on the upper and lower surfaces. The input points defining the elements are arranged so that a pair of points, one on the upper surface and one on the lower, lie nearly on the same perpendicular to the mean camber surface. The bound vorticity filaments, which appear as points in figure 8a, lie midway between corresponding points on the upper and lower surface. This arrangement maximizes the distance of the vortex filaments from the wing surface and presumably reduces numerical problems associated with the flow singularities at the filaments. Thus, in general the number of vortex filaments is one less than half the number of surface elements in the lifting strip, although in certain formulations some vortices may be given zero strength. The strengths of the bound vortex filaments are maintained constant over the "span" of each individual lifting strip. Thus,

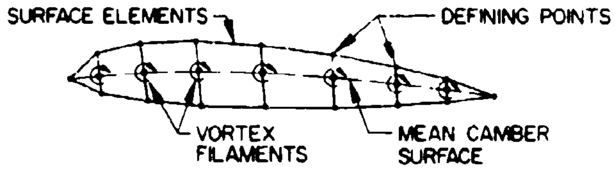

(a)

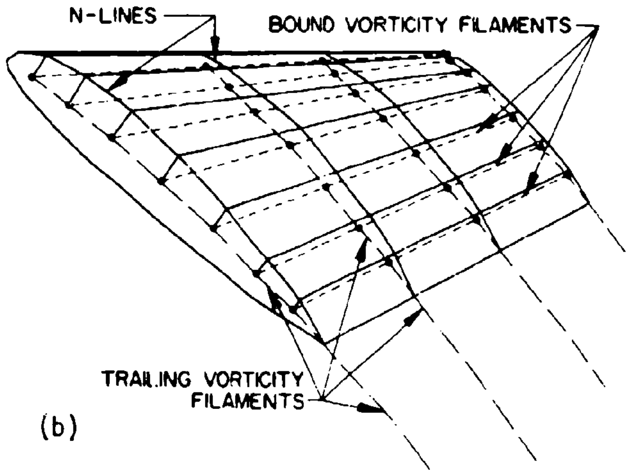

(b)

Figure 8. Representation of the bound vorticity by concentrated vortex filaments lying in the mean camber surface. (a) A section curve of the wing. (b) The complete three-dimensional vortex pattern.

the trailing vorticity is also in concentrated filaments. Forward of the trailing edge these lie in the mean camber surface beneath the edges of the strip, i.e., midway between the portions of the N-lines on the upper and lower surfaces of the wing. Downstream of the trailing edge the trailing vortex filaments lie along the N-lines defining the assumed wake. A view of the entire three-dimensional arrangement is shown in figure 8b. The formulations of the references use different "chordwise" variations of the vortex strengths. Reference 4 presents results for a distribution of zero strength from 0% to 20% chord and from 80% to 100% chord. From 20% to 80% chord the distribution is constant. However, both reference 4 and the subsequent development of the method presented in reference 5 recommend use of a "chordwise" vorticity variation approximately the same as the "chordwise" lift distribution. In a practical case this last might be determined from linear theory or might be estimated from results for similar wings. Quite different are the distributions used in references 6 and 7. Apparently, reference 6 uses a vortex strength proportional to the local thickness of the airfoil section, while reference 7 uses a strength proportional to the square root of the local thickness. Since exact solutions are not available and experimental results are affected by viscosity, compressibility, and testing error, the results of these calculations must be judged largely on their "reasonableness," e.g., lack of extraneous wiggles, etc.

The present method uses a completely different form for the bound vorticity. Instead of concentrated vortex filaments interior to the wing, there is a finite-strength sheet of vorticity on the surface of the wing, i.e., the vorticity lies on the quadrilateral surface elements. The nature of the singularity is thus reduced from a line singularity to a surface singularity. Some features of this formulation are illustrated in figure 9 which may be compared with figure 8. The "chordwise" variation of the surface vorticity strength may be chosen at will. In the present method the strength is taken as constant all around the airfoil section. This choice was influenced by requirements of simplicity and by the fact that constant-strength surface vorticity gives good results in two-dimensional cases (see below). The variation of vorticity over the "span" of a lifting strip of elements has two options: constant and linear. In the former option the "spanwise" variation of vorticity over the wing is a step function (figure 10a) whose values

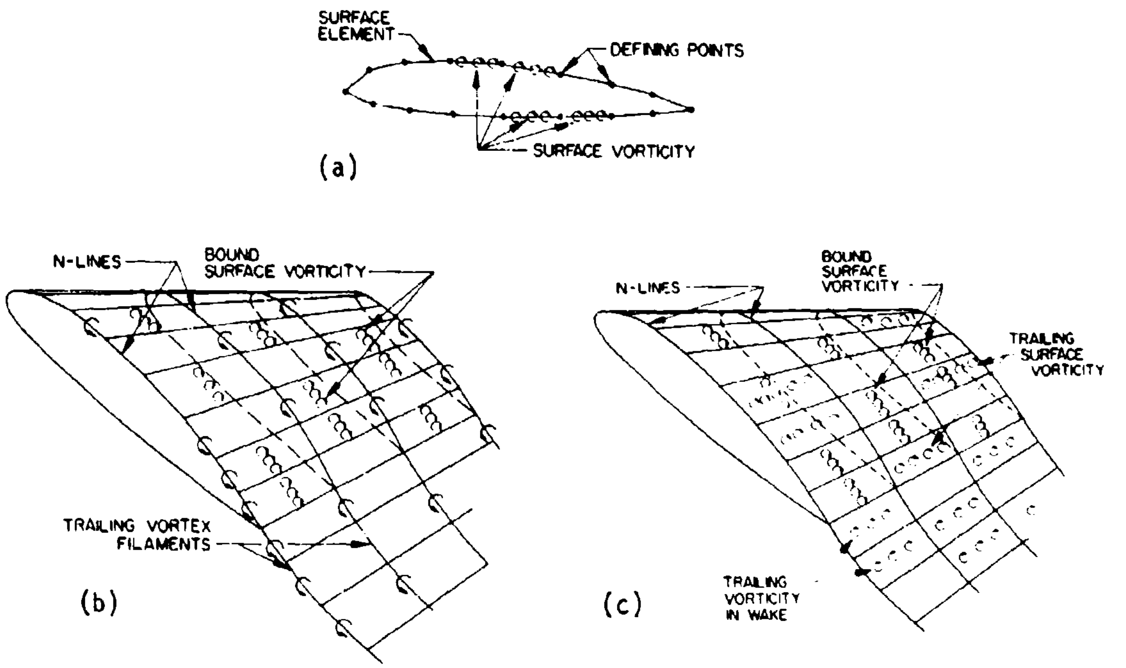

Figure 9. Representation of the bound vorticity by a finite-strength vorticity distribution lying on the wing surface. (a) A section curve of the wing. (b) The complete three-dimensional vorticity pattern using a step function spanwise variation. (c) The complete three-dimensional vorticity pattern using a piecewise linear spanwise variation.

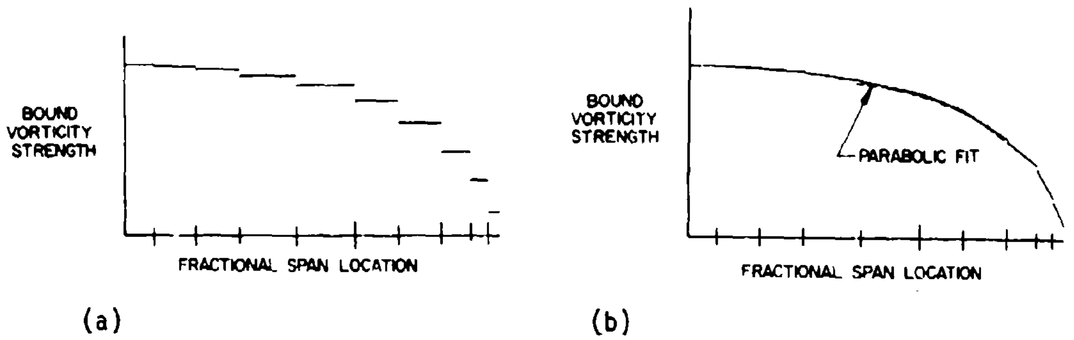

Figure 10. Two forms of the spanwise variation of bound surface vorticity. (a) Step function. (b) Piecewise linear.

are determined by the Kutta condition. This form of the bound vorticity has the advantage of simplicity and does not require special handling at the end of a lifting section, e.g., a wing tip. However, the trailing vorticity takes the form of concentrated vortex filaments along the N-lines (figure 9b). This situation can be avoided by using a linear vorticity variation over the span of the lifting strip. In this case the trailing vorticity takes the form of a vortex sheet over the surface of the strip, i.e., over the surface elements (figure 9c). If the vorticity distribution were exactly continuous at the edges of the strips, i.e., at the N-lines, there would be no vortex filaments on the N-lines. This is not possible in general because, as mentioned in section 6.2, the edges of adjacent elements are not quite coincident. Thus, there are small geometrical discontinuities in the vortex sheet along the N-lines. It is thus not worthwhile to attempt to determine the "spanwise" rate of change of vorticity over a strip from a condition of continuity of strength along the N-lines. Moreover, this type of variation leads to serious numerical difficulties (reference 8). Instead the spanwise rate of change on a strip is determined from a centered parabolic fit over values of bound vorticity at the midspan of three consecutive strips and strict continuity of strength at the N-lines is obtained only if the "spanwise" variation is truly parabolic. However, the discontinuity is of high order, and the vortex sheet may be considered continuous to within the order of the overall approximation. In this option the "spanwise" variation of vorticity is a piecewise linear function as shown in figure 10b. The trailing vorticity continues as a sheet into the wake, so that the velocity has the desired behavior of discontinuity across the wake. The behavior does not occur if the wake is composed of concentrated filaments as it is in the methods of the references and in the above "step function" option of the present method. The chief disadvantage of the "piecewise linear" option is that special handling is required at the first and last lifting strips of a section to determine the "spanwise" rate of change of vorticity (section 7.11). Moreover, in most cases that have been run with the present method using both options for the bound vorticity, the calculated results are not very different.

The accuracy to be obtained using various forms for the bound vorticity may be investigated by considering the two-dimensional case for which exact analytic solutions are available. Indeed this is a very natural procedure because the essential three-dimensional feature is the "spanwise" variation of vorticity which is determined by the Kutta condition. The form of the bound vorticity and its assumed "chordwise" variation have direct two-dimensional analogies, which are very similar numerically to what is being calculated in three dimensions. The two-dimensional cases are obtained by simply considering the "section curves" of figures 8a and 9a as two-dimensional airfoils. The cases were run with the rather small element numbers that are characteristic of the three-dimensional case rather than the much larger element numbers that are available in two dimensions to obtain very high accuracy. Two cases are presented here that illustrate different aspects of the situation.

The first case is a Karman-Trefftz airfoil, for which coordinates of points on the body may be obtained very accurately using analytic expressions. A rather extreme geometry was chosen so that differences in the solutions could be seen more easily. The airfoil is 8.2 percent thick, has a 9° trailing-edge angle and the rather large camber value of 24 percent. A sketch of the shape is given in figure 11. Calculations were performed for an angle of attack of 1.205°. The exact solution from the well-known formulas gives a lift coefficient of 3.37. Using 50 surface elements, calculations were performed with a constant-strength surface vorticity, as is done in the present method, and also with interior vortex filaments whose strength is proportional to the local airfoil thickness, as is done in the method of reference 6. The calculated surface pressure distributions are compared with the exact solution in figure 11. Neither calculated result is very good because of the extreme geometry and the limited element number. However, the error for the surface vorticity approach is about half the error for the interior vortex filament approach. The "wiggles" in the solution generated from the interior vortex filaments are not due to inaccuracies in the points defining the airfoil. These points are exact. The "wiggles" are apparently due to changes in element lengths along the surface. Adjacent elements differ in length by no more than 25 percent, which appears quite reasonable. The solution obtained from the surface vorticity does not respond to this situation and is perfectly smooth.

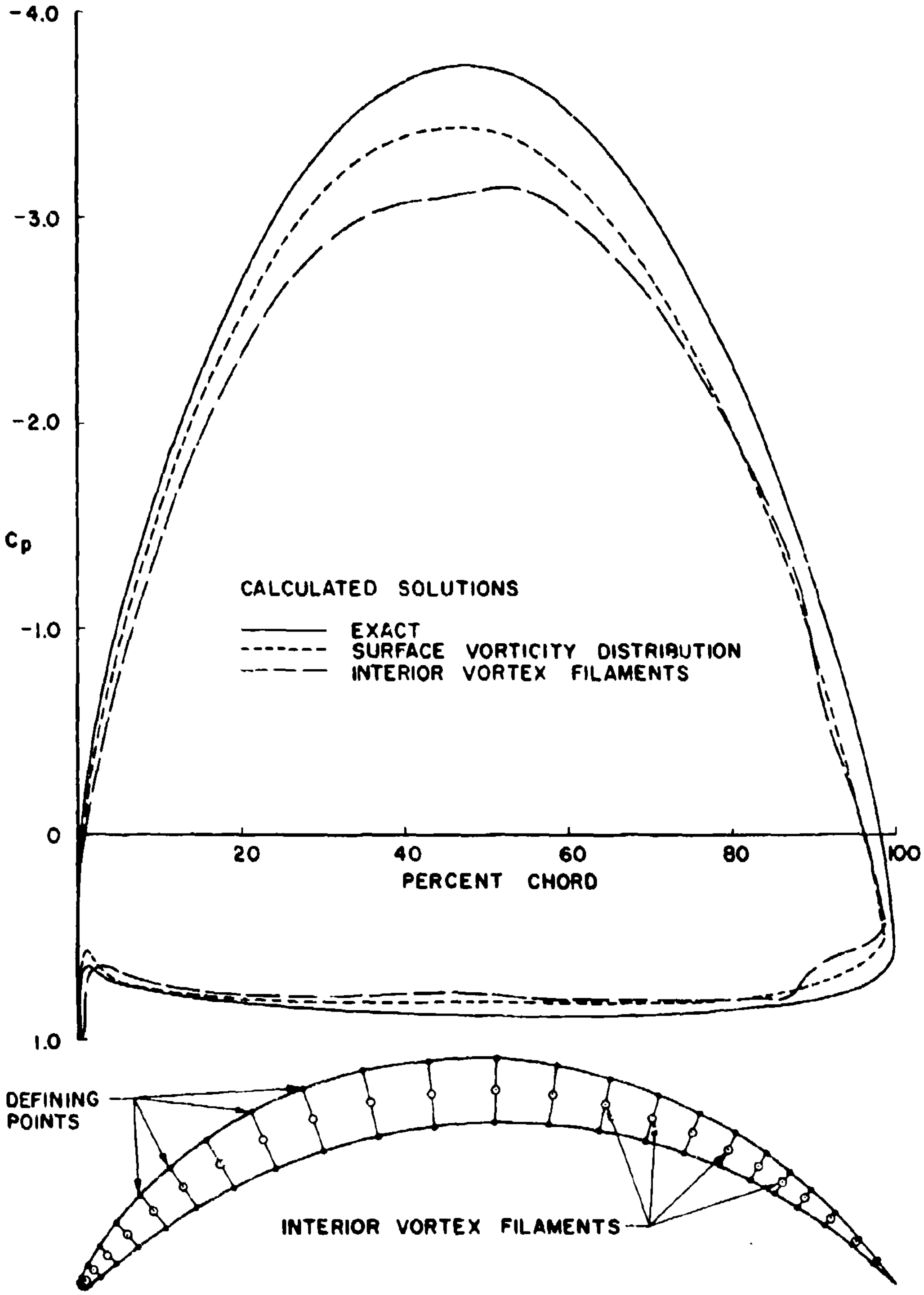

Figure 11. Surface pressure distributions on a Karman-Trefftz airfoil of large camber at 1.205 degrees angle of attack.

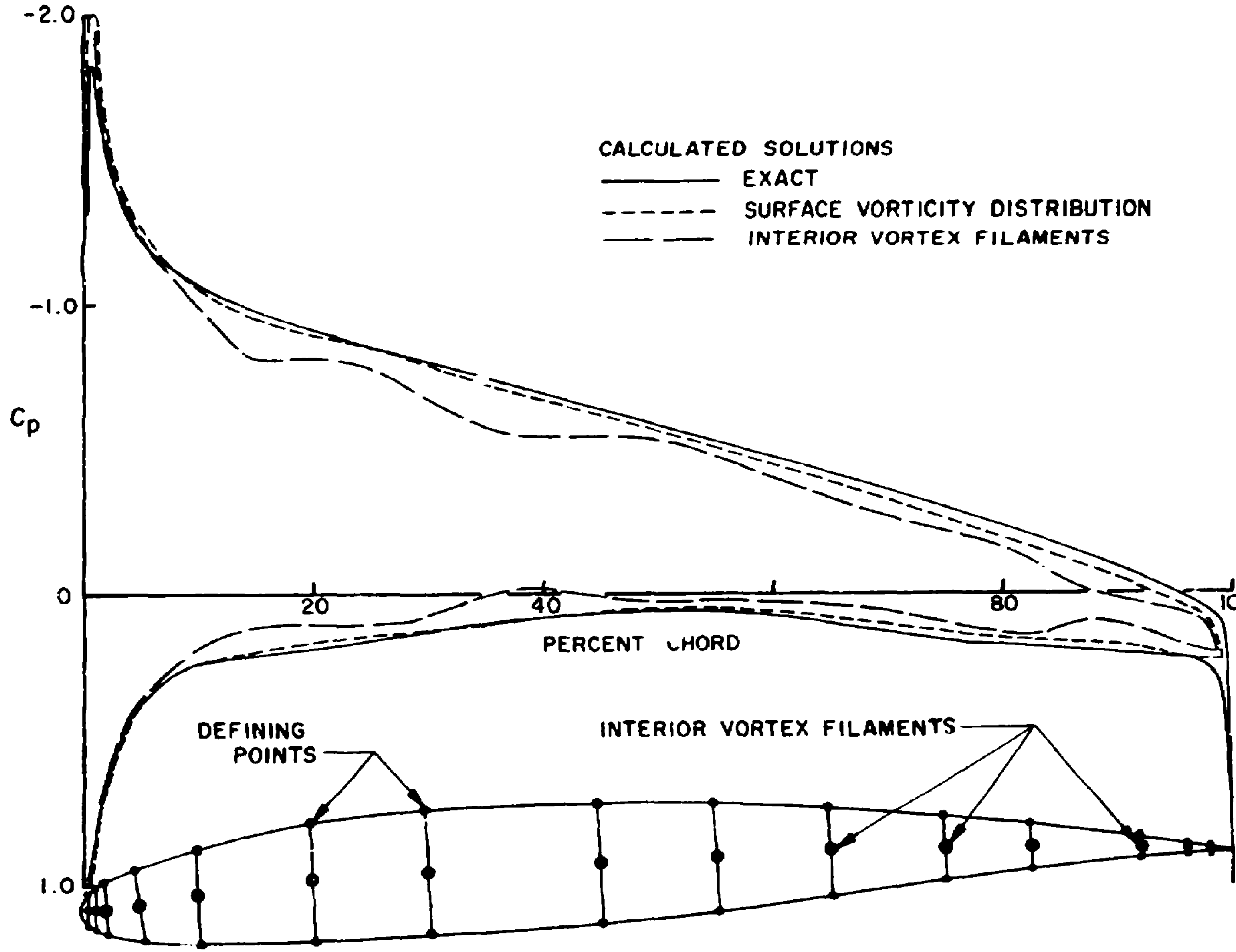

Figure 12. Surface pressure distributions on a conventional airfoil section at 6.9 degrees angle of attack.

The second case is the conventional airfoil section shown in figure 12. The coordinates of the points defining this airfoil were obtained by procedures usual in design applications, and the result is that the point distribution is not absolutely smooth but contains small irregularities. Calculations were performed with 32 surface elements. Figure 12 shows the points defining the airfoil and the locations of the 15 interior vortex filaments that were used in the calculations with strengths proportional to local thickness. Calculations were also performed using the constant-strength surface vorticity of the present method. Surface pressure distributions calculated by the two methods are compared with a very accurate conformal-mapping solution in figure 12. The surface vorticity approach is unaffected by any irregularities of the points and its results agree very well with the accurate solution. In fact the point distribution of figure 12 is the one used with the present method to produce the three-dimensional results of figure 42. The pressure distribution calculated by the approach based on interior vortex filaments has rather severe "wiggles" and also has a systematic error in pressure level so that the lift coefficient obtained by integrating the pressures differs from the exact value by 20 percent.

From these two examples and others that have been run, it is concluded that the representation of the bound vorticity by finite-strength surface vorticity is superior to the representation by interior vortex filaments. The former is far less sensitive to inaccuracy of the input data and tends to give a more accurate solution even when the data is smooth.

6.4 Use of a Dipole Distribution to Represent Vorticity

From the previous section it can be seen that in the present method the bound and trailing vorticity are represented by a general surface distribution of vorticity, possibly with concentrated vortex filaments at the edges. Formulas that express the velocity induced by such a vorticity distribution are required. Derivation of such expressions is complicated by the fact that the surface vorticity strength is a vector that varies in both magnitude and direction. Furthermore, care must be taken to insure that the vorticity distribution gives rise to a potential flow, i.e., that the individual infinitesimal vortex lines either form closed curves or go to infinity. Use of a surface dipole distribution circumvents these complications, because the dipole strength is a scalar and any arbitrary dipole distribution gives rise to a potential flow. A general result giving the relationship between dipole sheet and a vortex sheet is given in Appendix A. It may be summarized as follows: A variable-strength dipole sheet is equivalent to the sum of: (1) a variable-strength vortex sheet on the same surface as the dipole sheet whose vorticity has a direction at right angles to the gradient of the dipole strength and a magnitude equal to the magnitude of this gradient, and (2) a concentrated vortex filament around the edge of the sheet whose strength is everywhere equal to the local edge value of dipole strength. This relation, which is a straightforward generalization of the well-known two-dimensional result, does not appear explicitly in the literature. Its plausibility was discussed early in the present work by the author, A.M.O. Smith, and P.B.S. Lissaman. The proof of this relation in Appendix A, which was originally outlined by the author in reference 9, is apparently the first. A later derivation is contained in reference 10. In the present method all formulas are derived in terms of dipole distributions and the above relationship is used to interpret this situation in terms of the more physically significant vorticity. In particular "chordwise" dipole variation is equivalent to "spanwise" vorticity and "spanwise" dipole variation to "chordwise" vorticity. Also, if a dipole sheet terminates with a nonzero strength, it results in a concentrated vortex filament.

6.5 The Kutta Condition

It is an interesting and important fact that the "physical" Kutta condition of finite velocity at the trailing edge cannot be applied in a general numerical procedure for calculating flow. This is true in both two dimensions and three dimensions. If the general solution could be written down in explicit analytic form, as is possible in a few simple two-dimensional cases, then the appropriate parameters could be adjusted to eliminate the singular terms in the expression for surface velocity. However, in a numerical solution there is no true singularity, and a condition of finiteness without specifying a definite value cannot determine specific values of a parameter. Accordingly, the Kutta condition is applied by indirect means. What is done is to deduce another property of the flow at the trailing edge that is a direct consequence of the finiteness of velocity and to use this related property as "the Kutta condition." Various properties may be derived. Some are strictly valid only for the true flow (limit of infinite number of elements) and are applied to a case of finite element number as an approximation. Others happen to be true for finite element number, and still others have different forms in cases of infinite and of finite element numbers. In general, conditions cannot be applied exactly at the trailing edge if a finite number of elements is used (except in the sense that quantities can be extrapolated to the trailing edge). Thus, "the Kutta condition" is applied a small distance away from the trailing edge, and determining an appropriate value for this distance and its effect on the solution is part of the problem. The situation can be affected by the fact that some flow conditions at the trailing edge are extremely local, and their values are quite different even a small distance away. Such very local conditions cannot be applied to cases of reasonable element numbers.

Some related properties that may be deduced from the Kutta condition are as follows:

Two-Dimensions:

(a) A streamline of the flow leaves the trailing edge with a direction along the bisector of the trailing-edge angle.

(b) As the trailing edge is approached the surface pressures (velocity magnitudes) on the upper and lower surfaces have a common limit, which equals stagnation pressure (zero velocity) if the trailing-edge angle is nonzero.

(c) The source density at the trailing edge is zero.

Three-Dimensions:

(a) A stream surface of the flow leaves the trailing edge with a direction that is known, or at least can be approximated (see below).

(b) As the trailing edge is approached, the surface pressures (velocity magnitudes) on the upper and lower surfaces have a common limit.

(c) The source density at the trailing edge is zero.

The example properties above can be used to apply the Kutta condition in cases of finite element number. Property (a) in either dimensionality differs from the others in that it must be applied off the body surface.

Points downstream of the trailing edge are selected to be on the stream surface or streamline and directions normal to the stream surface or streamline are prescribed. Then a flow tangency condition of zero normal velocity is applied at these points just as if they were control points of rface elements. Selection of distances from the trailing edge at which to apply the flow tangency condition is part of the problem. Properties (b) and (c) are applied on the body surface. Since the flow on the body has meaning only at the control points, these conditions are applied to flow quantities at the control points of the elements adjacent to the trailing edge on the upper and lower surfaces. In two dimensions there are just two such elements, while in three dimensions there are two elements on each lifting strip. It might be supposed that property (c) is applied by requiring source densities on elements adjacent to the trailing edge to be zero. This amounts to two conditions per lifting strip and thus overdetermines the problem. The best that can be done is to require that for each lifting strip the values of source density on the two elements adjacent to the trailing edge be equal in magnitude and of opposite sign. Similarly, condition (b) is applied by requiring that for each lifting strip the magnitudes of the velocity at the control points of the two elements adjacent to the trailing edge be equal. This is done even in two dimensions where the theoretical velocity of zero is so local that the velocity is an appreciable fraction of freestream velocity at the control point adjacent to the trailing edge.

In applications, property (c) has not been used. The methods of references 4, 5, 6 and 7 use property (a). The present method has the option of using either property (a) or property (b) as "the Kutta condition." If property (a) is used the points where it is to be applied and the normal vectors at these points must be furnished to the program as input. Flow velocities are computed at all control points due to the bound vorticity distribution associated with each lifting strip. Each of these flows is considered as an onset flow to the body. Let the total number of quadrilateral source elements be N and the number of lifting strips be L. Then there are L vorticity onset flows, each of which consists of velocity components at: the N control points, the L points where property (a) is to be applied (if that option is used), and any other off-body point where flow is to be computed. For each onset flow a set of N values of source density on the elements is obtained that gives zero normal velocities at the N control points. The same is done for the uniform onset flow that represents the freestream. As described in section 6.1, the values of source density are obtained as solutions of a set of linear algebraic equations whose N x N coefficient matrix is the same for all L + 1 onset flows. The onset flows simply yield L + 1 right sides for the equations. Using a direct matrix solution all L + 1 sets of source density are obtained simultaneously. The desired source density distribution is a linear combination of these individual distributions. The constants in this linear combination are the L values of bound vorticity associated with the various lifting strips, and these are determined from the Kutta condition. (The solution corresponding to the uniform stream enters with unit coefficient.) Flow velocities for the individual solutions are computed only for the points used to apply the Kutta condition — either the control points of the elements adjacent to the trailing edge if property (b) is used, or the additional input points downstream of the trailing edge if property (a) is used. The Kutta condition results in L simultaneous equations whose solution yields the desired L values of bound vorticity. In typical cases the number of lifting strips L is 10 to 30, as contrasted with the number of surface elements N, which is 300 to 1000. Thus, solution of the equations expressing the Kutta condition is a negligible computation compared to solution of the equations for the values of source density. The values of bound vorticity are used to compute a single set of N values of source density — the "combined" values — that are used to compute velocities at the control points of the elements.

An alternative numerical procedure for implementing the application of the Kutta condition is employed in references 6 and 7. As mentioned above, the bound vorticity associated with each lifting strip induces a velocity at each control point. These may be treated exactly the same as the velocities induced by the individual source quadrilaterals (section 6.1), i.e., the L values of bound vorticity may be treated as additional unknowns in the equations expressing the normal velocity boundary condition. This yields N linear equations in N + L unknowns. The Kutta condition supplies the additional L equations. If the Kutta condition is expressed as property (a), as is done in references 6 and 7, the additional L equations are linear.

As discussed in references 1, 2, and 3, the N x N coefficient matrix due to the source quadrilaterals has a dominant main diagonal and is well suited to numerical solution either by direct solution or by iterative solution. The additional L equations from the Kutta condition do not have dominant diagonal terms so that the (N + L) x (N + L) matrix used in references 6 and 7 is not well-conditioned. However, suitable partitioning of this matrix (the partitioning is different in reference 6 from that of reference 7) yields rapidly convergent iterative solutions. If the property (b) is used to express the Kutta condition, the additional L equations are quadratic because they are applied to a vector magnitude. (In two dimensions the surface velocity has only one component, and the equations derived from property (b) are linear.) This might not be a serious handicap in an iterative procedure, but it has never been tried.

The relative advantage or disadvantage of an iterative solution, like that of references 6 and 7, compared to a direct solution, like that of the present method, is primarily a matter of computing time. The situation is affected by the particular computer being used and by the accounting algorithm for multiple-user machines. However, by far the most important considerations are the element number N and the type of body about which flow is to be computed. A direct solution for a set of linear equations requires a computing time proportional to N^3, and this time is independent of the body. An iterative solution requires a computing time proportional to the product IN^2, where I is the number of iterations needed for convergence. It is clear then that for sufficiently large N, the iterative solution is quicker (assuming that I is independent of N, which appears to be the case in the present application). Similarly, for sufficiently small N the direct solution is quicker. The "crossover" value of N, where the two methods are equal is directly proportional to I. For simple bodies, such as wing-fuselages, I is approximately 15 and the crossover value for N is perhaps 800 for an IBM 370-165. In any event, the iterative solution is clearly superior for N = 1000, and the direct solution is clearly superior for N = 500. For more complicated bodies, and particularly for situations involving interior flows, I is considerably larger, and thus so is the crossover value of N. Such situations arise, for example, with nacelles (reference 1) and with bodies in a wind tunnel (section 9.4). If the estimated computing times are not too different, the direct solution is to be preferred, because the time required is predictable. It appears that the most efficient procedure is one containing both direct and iterative solutions of the linear equations as options. Inclusion of an iterative solution in the present method is a desirable future extension.

In the present method, application of property (b) is straightforward and requires no additional input. Its effectiveness can be judged simply by the accuracy of the resulting calculation, as discussed below. Application of property (a) (either in the present method or in the methods of references 6 and 7) requires the answer to two questions: How far from the trailing edge should it be applied? In what direction with respect to the trailing edge should the point of application be situated? The answer to the second question which will be considered first, appears to be related to the direction by which the stream surface leaves the trailing edge of the wing. However, this last turns out to be false in many applications.

The behavior of the vortex wake in the neighborhood of the trailing edge of a three-dimensional lifting body has been worked out from basic principles in reference 11 under the assumption of inviscid potential flow. The results are easy to state. The only two quantities that affect the situation are the local section lift coefficient and the local value of the average component of velocity along the trailing edge (averaged between upper and lower surfaces). Theoretically, the magnitudes of these two quantities are not important – only their signs. Consider the usual case when the local section lift coefficient is positive. Then reference 11 states that if the component of velocity along the trailing edge is outboard, the vortex wake leaves the trailing edge tangent to the upper surface. If this velocity component is inboard, the sheet leaves tangent to the lower surface. The situation is illustrated in figure 13. If the local section lift coefficient is negative, the situation is reversed.

The above results mean that the way in which the vortex wake leaves the trailing edge depends on the final flow solution and is thus not known ahead of time. On the face of it this is a problem. However, in many practical cases it is obvious which way the flow at the trailing edge goes. In regions

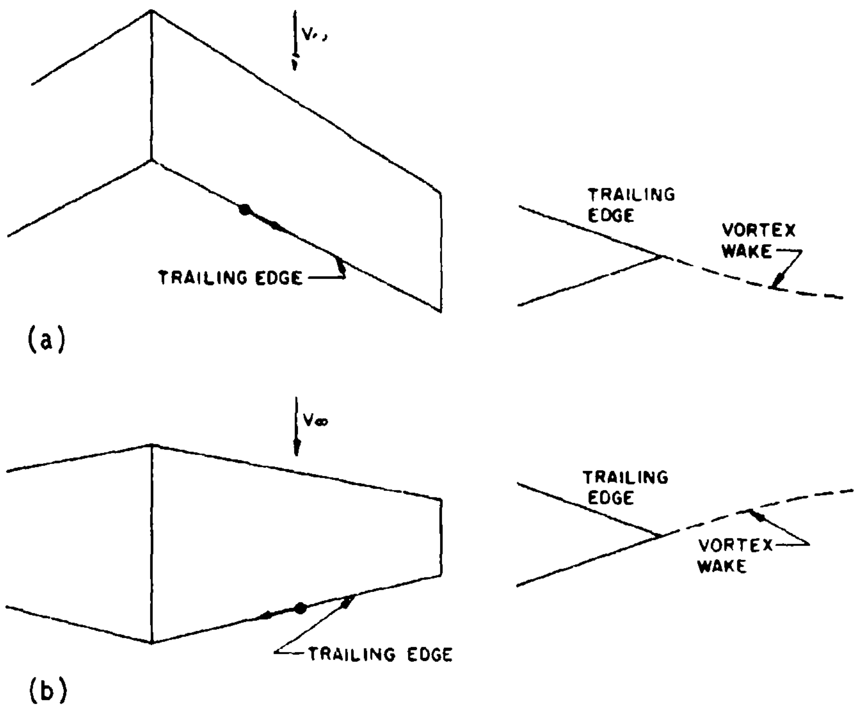

Figure 13. Theoretical behavior of the vortex wake at the trailing edge of a wing. (a) Outboard trailing edge velocity. (b) Inboard trailing edge velocity.

where there is some doubt the flow component along the trailing edge is probably small compared to freestream. This situation, which occurs rather often in applications, has an important effect on the application of the Kutta condition.

Reference 11 proves that for any outboard trailing-edge velocity, no matter how small, the wake is tangent to the upper surface as shown in figure 13a. Similarly, for any inboard velocity, no matter how small, the wake is tangent to the lower surface, as shown in figure 13b. On the other hand, it is physically evident that a small change in conditions at the trailing edge gives a small change in the wake position a finite distance away. That is, as the trailing-edge velocity changes from small and outboard to small and inboard the wake position a finite distance downstream does not "flip flop," but changes only slightly. The question is how can this be resolved with results of reference 11.

The only explanation appears to be that as the trailing-edge velocity component becomes small — either inboard or outboard — the wake approaches the trailing edge bisector at small finite distances from the trailing edge. That is, the curvature of the wake at the trailing edge becomes large as the velocity becomes small and in a very small distance the wake "curves around" and approaches the trailing-edge bisector. The situation is sketched in figure 14. The wake approaches the trailing-edge bisector more and more rapidly as the velocity component along the trailing edge approaches zero. The above argument requires only continuity and symmetry.

Thus, if the Kutta condition in the form of property (a) is applied, a finite distance from the trailing edge (as it must be in the present method and those of references 4, 5, 6 and 7) and if the sweep angle of the trailing edge is such that the component of velocity along the trailing edge is not large, then the point must lie along the trailing-edge bisector. For example, the method of reference 6 applies property (a) a distance of 3 percent of local airfoil chord downstream from the trailing edge and states that the point should lie along the bisector of the trailing edge rather than the tangent to the upper surface as required by reference 11. On the other hand,

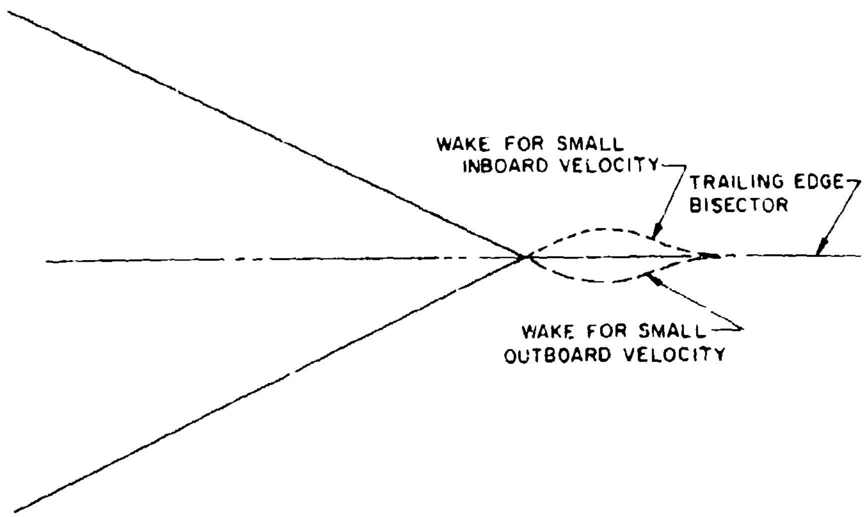

Figure 14. Behavior of the vortex wake near the trailing edge for small values of the trailing edge velocity component.

it is clear that for large positive sweep angles, the component of velocity along the trailing edge becomes the same order of magnitude as freestream velocity. Presumably, the Kutta condition should then be applied along the tangent to the upper surface. At what value of trailing-edge velocity it becomes necessary to change from one scheme to the other is not known, but it certainly must be dependent on the distance of the point of application from the trailing edge. Numerical experiments presented in reference 6 and similar experiments performed by the present author show that the calculated results are rather sensitive to the direction of the point of application of the Kutta condition. For a typical trailing-edge angle the calculated lift coefficient obtained from an application point on the trailing-edge bisector can easily differ by 20 percent from the lift coefficient obtained from an application point on the upper-surface tangent.

Even when the direction from the trailing edge of the point of application of the Kutta condition is not a problem, calculations using property (a) (wake tangency) are affected by the distance of the point of application from the trailing edge. This is to be expected. What is not expected, however, is that if property (b) (pressure equality) is used in the manner described above, the calculated results are not sensitive to distance from the trailing edge. A study was made in two-dimensional flow, where the streamline is known to leave the trailing edge along its bisector. The airfoil selected was a symmetric 10-percent thick RAE 101 airfoil at 10 degrees angle of attack. Bound vorticity was provided by a constant-strength sheet of vorticity coincident with the airfoil surface as described in section 6.3. Cases were run with 27, 53, and 103 surface elements. The results were also extrapolated to infinite element number. Calculated lift coefficients are shown in figure 15. Since property (b) (pressure equality) is applied at the control points of the two elements adjacent to the trailing edge, there is just one lift coefficient for each element number. These are plotted at the chordwise distance of the nearest control point from the trailing edge, which ranges from 1.75 percent chord for the 27 element case to 0.25 percent chord for the 103 element case. Remarkably, the calculated lift coefficients are almost constant at a value of about 0.944, and the extrapolation to the trailing edge itself (infinite element number) yields a value of 0.943. For each element number property (a) (wake tangency) was applied along the trailing-edge bisector at distances from the trailing edge ranging from 0.25 percent

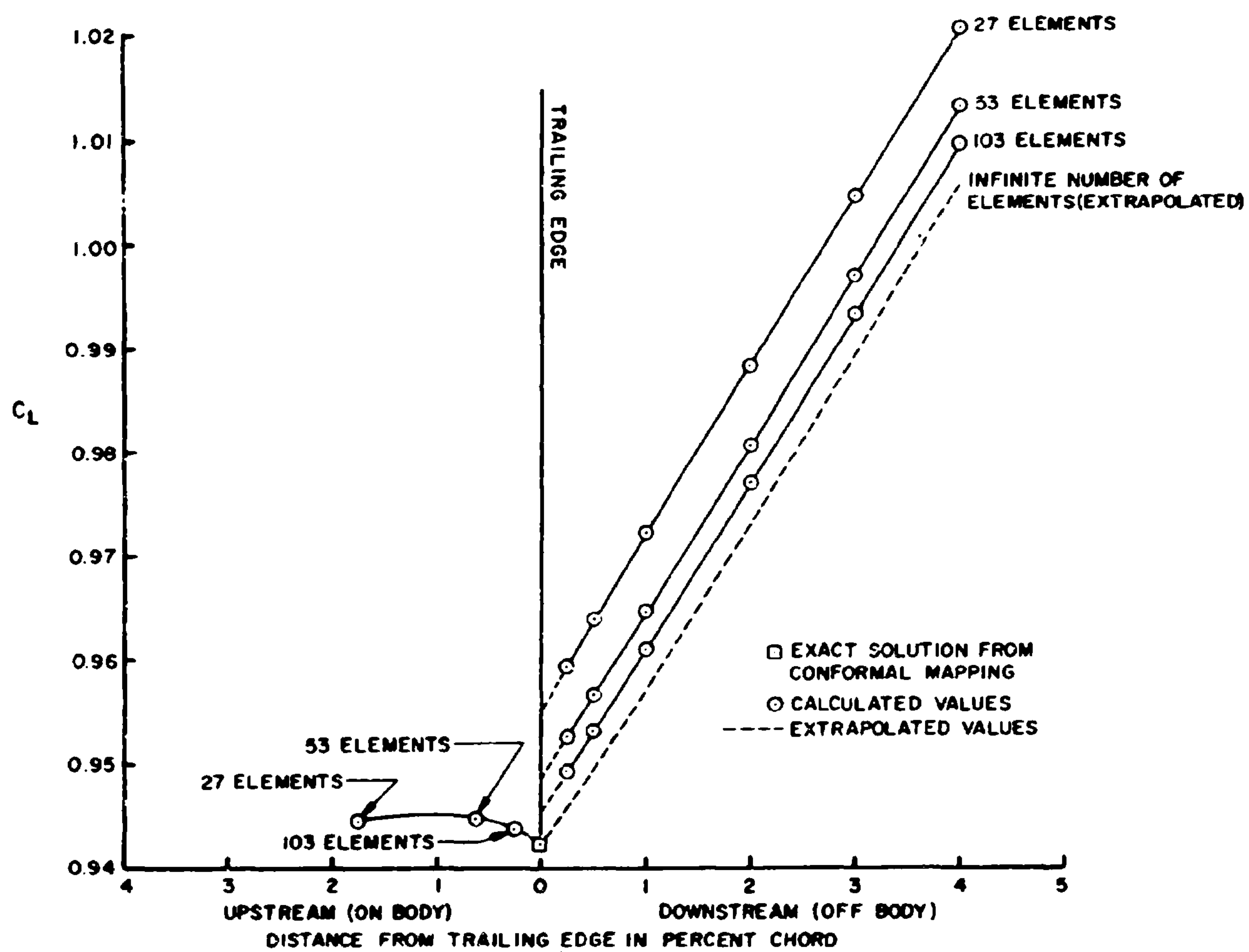

Figure 15. Calculated lift coefficients for a two-dimensional airfoil as functions of the distance from the trailing edge of the point of application of the Kutta condition. Airfoil is 10 percent thick symmetric section at 10 degrees angle of attack.

chord to 4.0 percent chord. The calculated lift varies significantly with both element number and distance of the application point from the trailing edge. It appears that results are more sensitive to distance from the trailing edge than to element number. If results are extrapolated both to infinite element number and to zero distance from the trailing edge, the lift coefficient is given as 0.942. This agrees with the value obtained by extrapolating property (b) and with the value of 0.9423 obtained by a high-accuracy conformal mapping solution. However, for the 27 element case (a reasonable number in three dimensions) the extrapolated lift coefficient for zero distance is 0.955, which is reasonably close to the correct value, but use of a point of application at 3 percent chord, as called for in reference 6, gives a lift coefficient of 1.005, which is considerably in error. Even for the extrapolation to infinite element number, a point of application at 3-percent chord gives a lift coefficient of 0.989. Thus, it appears that use of a pressure-equality Kutta condition applied on the body (property (b)) is more accurate and less sensitive than the flow-tangency Kutta condition applied in the wake (property (a)), which is used in references 4, 5, 6 and 7 even if the direction by which the wake leaves the trailing edge is not a problem.

6.6 Symmetry Planes

To conserve computing time and reduce the required input, the method is equipped to take advantage of any planes of symmetry the flow may possess. Either one or two symmetry planes may be accounted for. The xz-plane is denoted the first symmetry plane. If there is one plane of symmetry, it must be the xz-plane, and the points defining the nonredundant portion of the body must be input accordingly. The xy-plane is denoted the second symmetry plane. If there are two symmetry planes, they must be the xz- and xy-planes, and the input points must reflect this. Each symmetry plane is designated either "plus" or "minus". A plus symmetry plane has zero normal velocity at all points of the plane, i.e., it behaves as a solid wall. A minus symmetry plane has zero velocity potential at all points of the plane. The usual application in aerodynamics consists solely of plus symmetry planes. An example of a negative symmetry plane is a free surface for the condition of infinite Froude number. Thus, a hydrofoil traveling near the water surface has two symmetry planes — one plus and one minus.

Symmetry is accounted for in the part of the calculation devoted to the velocity induced by the quadrilateral surface elements. Recall that an element may have on it either a source or a dipole distribution or both. Velocities are computed at all control points due to the source and/or dipole distribution on a basic element defined by input points. Then this element is reflected successively in the symmetry planes, induced source and/or dipole velocities at the control points are computed for the reflected elements, and the induced velocities for the reflected elements are added to the corresponding quantities for the basic element. Reflection in a plus symmetry plane requires a source distribution of the same sign as the original but a dipole distribution of opposite sign. (All magnitudes of course are equal to the original.) A minus symmetry plane yields the opposite situation, i.e., source changes sign, dipole does not.

In symmetry cases it is assumed that the y-direction is essentially "spanwise" on the wing, so that the first symmetry plane is the midplane of the wing. The second symmetry plane (if any) is then available, for example, as a ground plane. Figure 16 shows a section of an element and its bordering N-lines, together with their reflections. The N-lines are labeled "first"

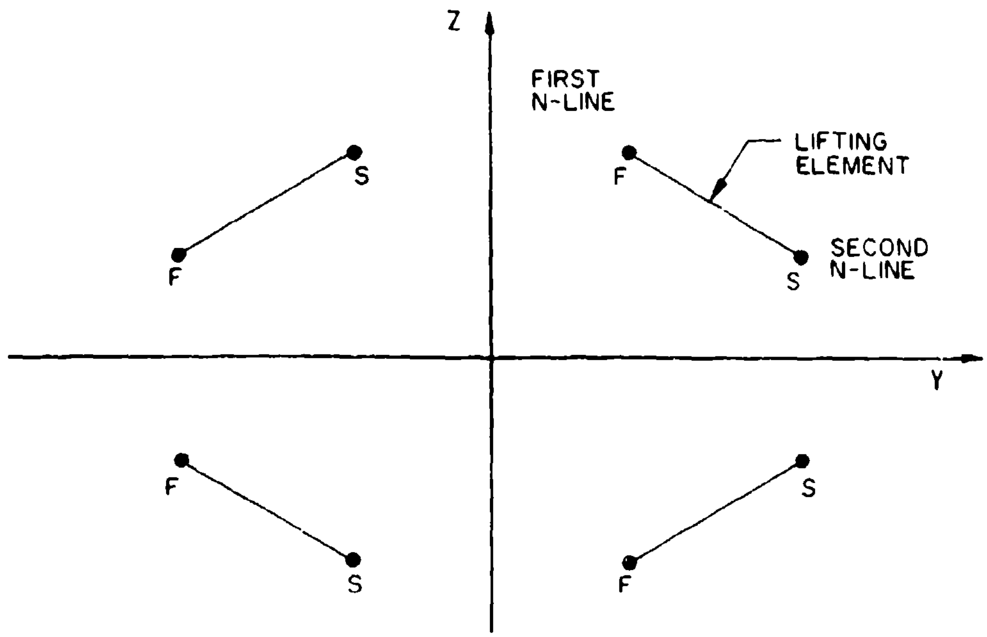

Figure 16. Reflection of an element and its associated N-lines in symmetry planes.

and "second", and in the case shown the "first" N-line is inboard from the "second" one with respect to the span direction on the basic element. It can be seen that reflection in the y-direction reverses this relationship while reflection in the z-direction does not. This condition affects the assembly of the dipole velocities, and thus the input points should be compatible with the above assumption.

6.7 Multiple Angles of Attack

The method can calculate flow about a lifting configuration for several angles of attack of the freestream in essentially the same computing time as that required for a single angle of attack. In the latter case, sets of source density are obtained for $L + 1$ onset flows — 1 uniform stream at angle of attack, and L bound vorticity onset flows. Here L is the number of lifting strips and is generally in the range 10 to 30. The Kutta condition then yields L combination constants for these vorticity flows. It is also possible to input several angles of attack, say F, and obtain $F + L$ basic source distributions for the F uniform flows and L vorticity flows. Then the Kutta condition is applied to each of the F uniform stream solutions separately to obtain a complete set of L combination constants for the vorticity flows. Using these constants, a "combined" source density distribution is obtained for each angle of attack in the manner described in section 6.5. The output consists of a complete set of surface pressures and off-body velocities for each angle of attack. For comparison purposes nonlifting solutions may also be obtained by computing strictly from the source densities obtained from the uniform onset flows.

When computed in the above manner, the solutions for all angles of attack have the same position for the trailing vortex wake. This is, of course, an approximation, because the true position of the wake changes with angle of attack. However, as will be discussed in section 8.5, the calculated surface pressures are very insensitive to angle of inclination of the wake with the range of practical interest. Thus, solutions obtained by the multiple angle-of-attack option are essentially as accurate as can be expected from potential flow.

6.8 Some Special Situations

The basic theoretical difficulties with the potential-flow model for lift (section 5.3) have their effect on the method of solution by necessitating special handling of certain frequently occurring situations. The special features that have been built into the method to handle these situations are discussed in this and in the following section. Other special situations may be discovered in the future.

Two special situations exist where elements must be placed inside the body surface. No normal-velocity boundary condition can be applied at such elements and no source density should be applied to them. Thus, these elements do not count as far as the matrix of induced velocities is concerned. However, they do have dipole distributions and these must be accounted for.

The first situation occurs when a nonlifting portion of the body intersects a lifting portion at a finite angle (often nearly normal) without breaking the continuity of the trailing edge. An example is provided by the wing-pylon intersection shown in figure 17. A certain portion of the

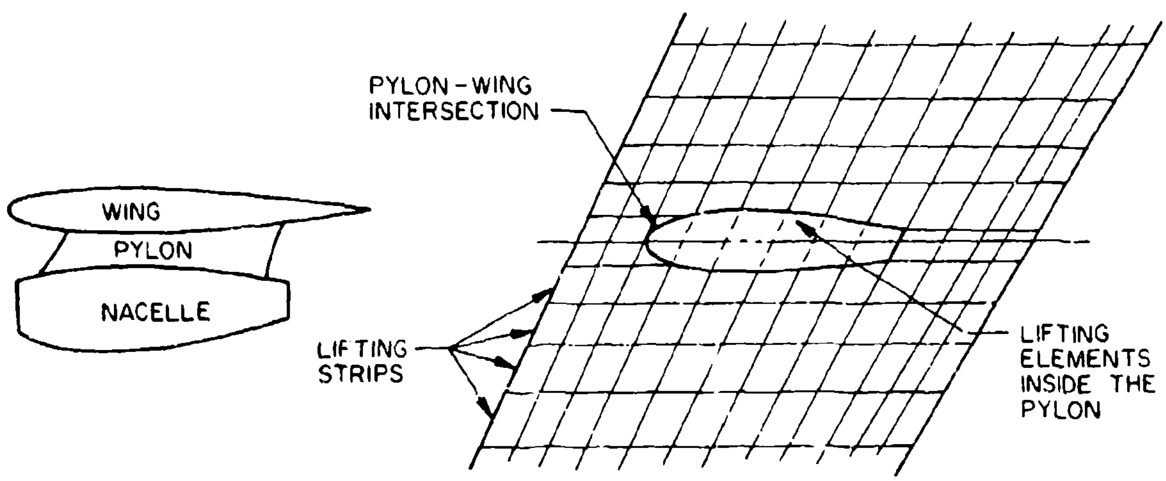

Figure 17. Handling of a wing-pylon intersection.

lifting body surface is "inside" the pylon. However, the dipole distribution should be continuous through this region to avoid numerical difficulties. Thus, as far as dipole calculations are concerned, the "inside" elements are normal members of the lifting strips to which they belong. But they are ignored as far as source calculations or boundary conditions are concerned. Such elements are designated "ignored elements." They usually comprise only part of a lifting strip.

The second situation occurs when a lifting portion of the body intersects a nonlifting portion at a finite angle (often nearly normal). The important case of this is the wing-fuselage intersection, as illustrated in figure 18. As is well-known, the local "section lift coefficient" on the wing does not

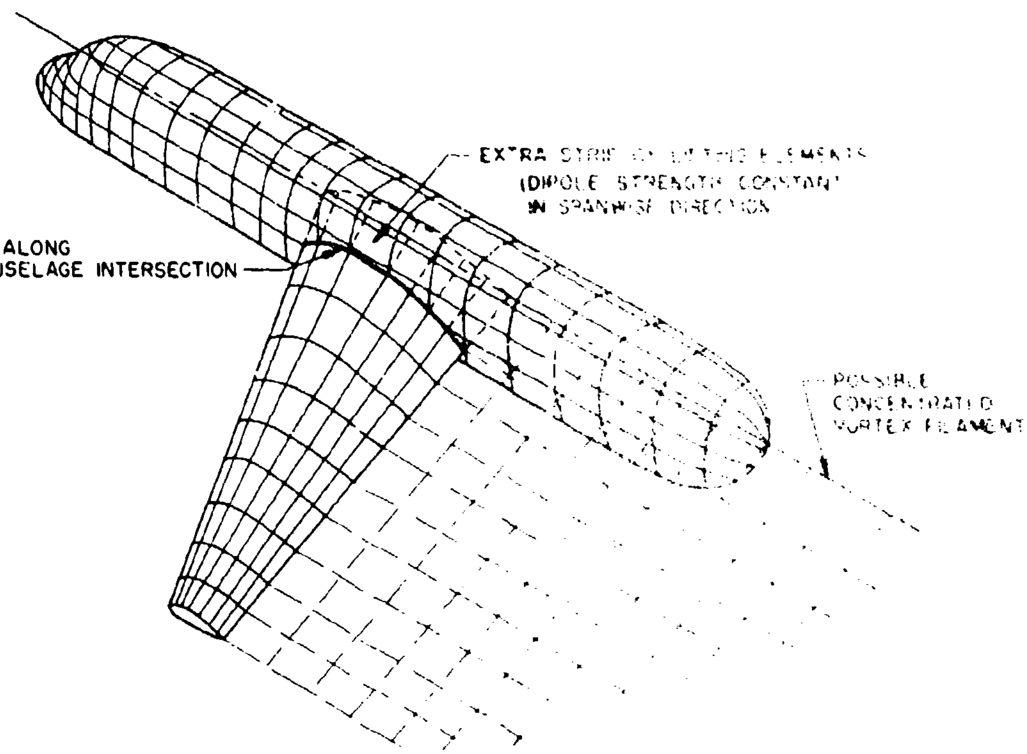

Figure 18. Handling of a wing-fuselage intersection.

fall to zero at the fuselage intersection. Thus the dipole strength on the N-line lying along the intersection is not zero. However, the lifting section cannot simply be terminated, because that would result in a concentrated vortex filament right on the surface. Accordingly, an additional or "extra" lifting strip is added to the lifting section (see figure 18). It is either the first or the last strip of the lifting section. The extra strip lies inside the nonlifting body and is a complete lifting strip including wake. No source densities or normal-velocity boundary conditions are applied to the elements of the extra strip. The dipole strength is taken constant in the "spanwise" direction across the extra strip. The value of the dipole strength on the extra strip is such that the dipole strength is continuous across the N-line lying along the wing-fuselage intersection. The interior edge of the extra strip has nonzero dipole strength and may lead to a concentrated vortex in the streamwise direction. For example, as shown in figure 18, the vortex may lie along the fuselage centerline and its downstream extension. If the lifting configuration has a right-and-left symmetry, e.g., a fuselage with both wings, and if the flow is also symmetric, e.g., zero yaw, the extra strips for the right and left sides have the same strengths on their interior edges. Thus, in this case there is no discontinuity of dipole strength and no concentrated vortex. If, however, the lift is not symmetric, there will be a concentrated vortex. This is unavoidable because it is physically real. An example is the hub vortex of a propeller. This also occurs at a tip tank, which is essentially a small fuselage with only one wing. However, the case shown in section 10.1 exhibits no numerical difficulty.

6.9 Summary of the Logic of the Calculation

The overall logic of the method is rather similar to that of the method for nonlifting potential flow described in section 6.1. There are, of course, certain additions. The order of the various parts of the calculation and their functions are outlined below.

The geometry of the three-dimensional configuration is input to the program in the form of coordinates of a set of points. The points are input along N-lines, which are essentially coordinate curves in the body surface (figure 6). The configuration is divided into lifting and nonlifting portions as discussed in section 6.2. Each of these may be further divided into sections — lifting and nonlifting. The nonlifting sections are input first. The N-lines of the lifting section define both the body and the trailing vortex wake. Coordinates of points off the body in the flow field where flow calculations are desired are input after the points defining the body. If the Kutta condition is applied by a condition of flow tangency downstream of the trailing edge in the wake, coordinates of these points and the corresponding normal vectors are input between the on-body and the off-body points. The remaining input consists of control flags governing the logic of the calculation plus a few parameters, such as angle of attack.

Surface elements are formed from input points in the manner described in section 7.2 for lifting sections and in the manner of reference 3 for nonlifting sections. The "formation" of an element consists of the calculation of various geometric quantities associated with that element, including coordinates of the control point (centroid), components of unit vectors along the axes of a coordinate system based on the element, one of which is the unit normal vector to the element, and moments of the area of the element. Elements of lifting sections are logically associated into lifting strips of elements, which consist of those elements formed from the same two N-lines.

Every element has on it a constant source density. Lifting elements also have a dipole distribution. Formulas have been derived that enable velocities induced by the elements at points in space to be calculated (section 7.0 for lifting elements and reference 3 for nonlifting elements). For each element the velocities induced by its constant source density at all control points and off-body points are computed and saved in low-speed storage (tape or disk). If there are symmetry planes, velocities induced by the reflections of an element are added to the velocities due to the element itself. This is the vector matrix of induced velocities. For each element of a lifting section velocities induced by its dipole distribution at all control points and off-body points are computed. These, however, are not saved individually. Instead, dipole velocities for all elements of a lifting strip, including wake elements, are added to obtain velocities due to the entire strip. Thus, if there are N source elements, at whose control points the normal-velocity boundary condition is to be applied, 0 off-body points, and L lifting strips, there is a $(N + 0) \times N$ matrix of induced source velocities and a

$(N + O) \times L$ matrix of induced dipole velocities. For the "step function" bound vorticity option, the dipole (vorticity) velocities induced by a lifting strip are those due to a spanwise constant dipole distribution and they can be computed in a straightforward manner. For the "piecewise linear" bound vorticity option, two sets of induced dipole velocities are computed for each lifting strip: one due to a spanwise constant dipole distribution and one due to a linear distribution with unit rate of change in the spanwise direction and zero value at the "midspan" of the strip. These are then combined using the mechanism of the parabolic fit and the conditions at the ends of the lifting sections to obtain L sets of induced dipole velocities, each of which is proportional to the midspan value of bound vorticity on one lifting strip. The calculations outlined in this paragraph comprise one of the two time-consuming parts of the method.

The first N rows of the induced source velocity matrix are the velocities at the control points. Components of these velocities along the local normal direction are computed to yield an $N \times N$ scalar matrix of induced normal velocities. This is the coefficient matrix of the linear equations for the source density. The right sides of the linear equations consist of components along the local normal direction of: F uniform onset flows at various angles of attack and the first N rows of the induced dipole velocity matrix. The linear equations are solved by direct elimination to yield $(F + L)$ sets of source densities on the N source elements. The matrix solution is the second time-consuming part of the method.

Flow velocities are computed for all $(F + L)$ sets of source density at the points used to establish the Kutta condition. These are the $2L$ control points adjacent to the trailing edge on all lifting strips if the condition of equal upper and lower surface pressure is used. If the condition of flow tangency in the wake downstream of the trailing edge is used, the points are L particular off-body points input to the program. The Kutta condition is formulated as L equations for the L values of bound vorticity on the lifting strips using each of the F uniform-stream flows in turn with the L vorticity flows. The result is F sets of L values of bound vorticity. For each uniform onset flow a "combined" set of source densities is obtained as a linear combination of the basic L sets of source densities corresponding to the vorticity flows and the set of source densities for the uniform flow itself. The combination constants for the vorticity flows are values of bound vorticity obtained from the Kutta condition. There are F sets of N values of the combined source densities. Similarly, the same values of bound vorticity are used as combination constants to obtain a "combined" onset flow at all N + 0 points where velocities are to be computed. There are, of course, F such "combined" onset flows.

A complete flow solution is computed using each set of combined source densities and its corresponding combined onset flow. Such a solution consists of: flow velocities and pressures at all control points, flow velocities at all off-body points, the bound vorticity values used to satisfy the Kutta condition, and integrated forces and moments on each lifting strip, on each lifting and nonlifting section, and on the entire configuration. An option also exists for computing a nonlifting solution at each angle of attack by setting all values of bound vorticity equal to zero.

7.0 DETAILS OF THE METHOD OF SOLUTION

7.1 Order of the Input Points

As mentioned previously, the points defining the body surface are input N-line by N-line, and the points on a given N-line are input consecutively. The order of the input determines the direction of the outer normal vectors to the elements, i.e., determines whether the case in question is an interior or an exterior flow. The rule for insuring that normal vectors point into the field of flow rather than into the interior of the body is the same as in reference 3: If an observer in the field of flow looking towards the body surface sees N-lines input from left to right, he should also see individual points on an N-line input from bottom to top. An example of correct input for the right wing of an airplane is as follows: The N-lines are input from tip to root. On each N-line the points are input beginning at the trailing edge, traversing the lower surface to the leading edge, returning to the trailing edge along the upper surface, and continuing into the wake. The alternate way of inputting a right wing is to input the N-lines from root to tip and on each N-line to input upper surface points first followed by the lower surface points and the wake points. Both of these input schemes produce identical surface elements. However, they lead to somewhat different implied surface dipole distributions. This matter is discussed in section 7.3. The conclusion is that the first of the two input schemes above is to be preferred. In any case, the logic of the program for determining which elements are on the surface and which are on the wake requires that the first point on an N-line of a lifting section be at the trailing edge.

7.2 Formation of the Elements from Input Points

This section outlines the way that the elements are actually formed from the input points. There are two principal differences between the formation of lifting elements and that of nonlifting elements. The first is the manner of adjusting the input points to make a plane quadrilateral. The second is the calculation of area moments up to fourth order. The procedure for forming nonlifting elements is given in reference 3 and will not be repeated in this section, which is concerned solely with lifting elements.

Let the coordinates of the input points that are used to form an element be denoted x_k^i, y_k^i, z_k^i, $k = 1, 2, 3, 4$. These coordinates are with respect to the reference coordinate system, the system in which the physical lifting configuration is defined. It simplifies the equations to use vector notation, so define

$$\vec{x}_k^i = x_k^i \vec{i} + y_k^i \vec{j} + z_k^i \vec{k} \tag{7.2.1}$$

where $\vec{i}$, $\vec{j}$, $\vec{k}$, are unit vectors along the axes of the reference coordinate system. Recall that an element is formed from points on two consecutive N-lines. The input points $k = 1$ and 2 are on one N-line, the "first" N-line, and the input points $k = 3$ and 4 are on the "second" N-line. In what follows, subscripts F and S are used to denote quantities associated with the first and second N-lines, respectively. The numbering $k = 1, 2, 3, 4$ is cyclic around the element to be consistent with reference 3. The adjustment of the input points, which is shown in figure 19, is as follows.

First form the N-line vectors

$$\vec{P}_F = \vec{x}_2^i - \vec{x}_1^i, \qquad \vec{P}_S = \vec{x}_3^i - \vec{x}_4^i \tag{7.2.2}$$

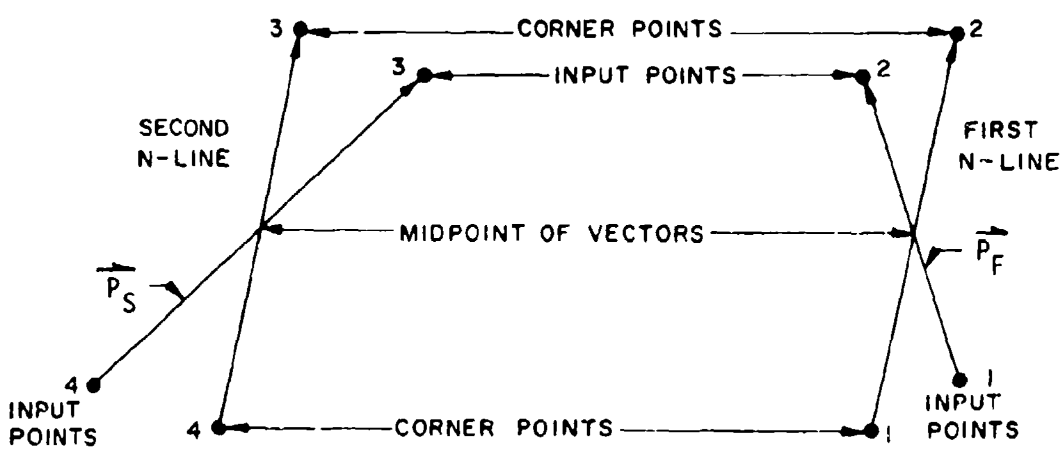

Figure 19. Adjustment of the input points to form a plane trapezoidal element.

The two parallel sides of the trapezoid are taken as parallel to the weighted average of these two vectors. In the coordinate system of the element this is also the direction of the x-axis. The unit vector parallel to the two parallel sides of the trapezoid is denoted $\vec{i}_E$ to show it is also the unit vector along the x or ξ axis of the element coordinate system. It is computed from

$$\vec{i}_E = \frac{\vec{P}_F + \vec{P}_S}{|\vec{P}_F + \vec{P}_S|} \tag{7.2.3}$$

where $|\vec{v}|$ means absolute magnitude of the vector $\vec{v}$, i.e., the square root of the sum of the squares of its components. The parallel sides have the direction of $\vec{i}_E$. The calculation insures that each parallel side has the same midpoint and the same length as the segment of N-line from which it is formed. In fact, once the elements are formed the original N-line segments are replaced by these parallel sides. The side lengths are

$$d_F = |\vec{P}_F| \qquad d_S = |\vec{P}_S| \tag{7.2.4}$$

The midpoints in vector form are

$$\vec{x}_F = \frac{1}{2}(\vec{x}_1^i + \vec{x}_2^i), \qquad \vec{x}_S = \frac{1}{2}(\vec{x}_3^i + \vec{x}_4^i) \tag{7.2.5}$$

The endpoints of the two parallel sides, which are thus the corner points of the trapezoidal element are, in vector form,

$$\begin{aligned} \vec{x}_1 &= \vec{x}_F - \frac{1}{2} d_F \vec{i}_E , & \vec{x}_2 &= \vec{x}_F + \frac{1}{2} d_F \vec{i}_E \\ \vec{x}_3 &= \vec{x}_S + \frac{1}{2} d_S \vec{i}_E , & \vec{x}_4 &= \vec{x}_S - \frac{1}{2} d_S \vec{i}_E \end{aligned} \tag{7.2.6}$$

The normal vector to the plane of the element is

$$\vec{N} = (\vec{x}_4 - \vec{x}_2) \times (\vec{x}_3 - \vec{x}_1) \tag{7.2.7}$$

The unit normal vector is

$$\vec{n} = \frac{\vec{N}}{|\vec{N}|} \tag{7.2.8}$$

This is also the unit vector along the z-axis of the element coordinate system. The unit vector along the y or η axis of the element coordinate system is

$$\vec{j}_E = \vec{n} \times \vec{i}_E \tag{7.2.9}$$

In component form the three unit vectors are

$$\begin{aligned} \vec{i}_E &= a_{11}\vec{i} + a_{12}\vec{j} + a_{13}\vec{k} \\ \vec{j}_E &= a_{21}\vec{i} + a_{22}\vec{j} + a_{23}\vec{k} \\ \vec{n} = \vec{k}_E &= a_{31}\vec{i} + a_{32}\vec{j} + a_{33}\vec{k} \end{aligned} \tag{7.2.10}$$

The 3 x 3 array of a's is the transformation matrix that is used to transform coordinates of points and components of vectors between the reference and element coordinate systems in the manner described in reference 3.

Temporarily the origin of the element coordinate system is taken as the point whose coordinates are the averages of those of the input points. (The same averages are obtained using the corner points.) In vector notation, the average point is

$$\vec{x}_{av} = \frac{1}{2}(\vec{x}_F + \vec{x}_S) \tag{7.2.11}$$

With this origin, the element coordinates of the corner points are

$$\begin{aligned} \xi_k^* &= a_{11}(x_k - x_{av}) + a_{12}(y_k - y_{av}) + a_{13}(z_k - z_{av}) \\ \eta_k^* &= a_{21}(x_k - x_{av}) + a_{22}(y_k - y_{av}) + a_{23}(z_k - z_{av}) \end{aligned} \tag{7.2.12}$$

$$k = 1,2,3,4$$

where in accordance with vector notation, x_k, y_k, z_k are the coordinates of $\vec{x}_k$ from (7.2.6). It will turn out that

$$\eta_1^* = \eta_2^* \qquad \text{and} \qquad \eta_3^* = \eta_4^* = -\eta_1^* \tag{7.2.13}$$

The width of the element is

$$w = \eta_1^* - \eta_3^* = 2\eta_1^* \qquad (7.2.14)$$

The slopes of the nonvertical sides of the element (figure 20) are

$$m_{32} = \frac{\xi_2^* - \xi_3^*}{w} \qquad m_{41} = \frac{\xi_1^* - \xi_4^*}{w} \qquad (7.2.15)$$

with respect to the η axis. The coordinates of the centroid are

$$\begin{aligned} \eta_o &= \frac{w^2}{6}\,\frac{m_{32} - m_{41}}{\xi_3^* + \xi_2^* - \xi_1^* - \xi_4^*} \\ \xi_o &= \frac{m_{32} + m_{41}}{2}\,\eta_o \end{aligned} \qquad (7.2.16)$$

The reference coordinates of the centroid are

$$\begin{aligned} x_o &= x_{av} + a_{11}\xi_o + a_{21}\eta_o \\ y_o &= y_{av} + a_{12}\xi_o + a_{22}\eta_o \\ z_o &= z_{av} + a_{13}\xi_o + a_{23}\eta_o \end{aligned} \qquad (7.2.17)$$

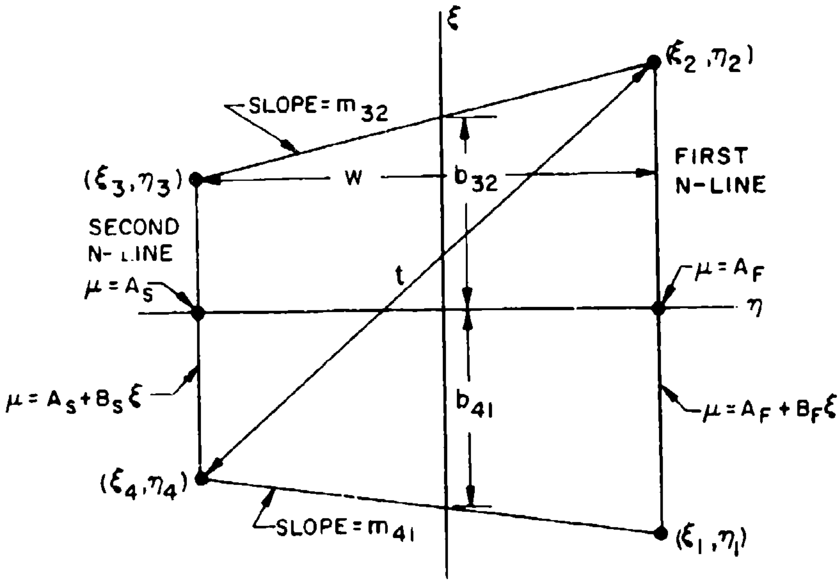

Figure 20. A plane trapezoidal element.

The centroid is now taken as the origin of the element coordinate system and replaces the average point in all subsequent calculations. With respect to the centroid as origin, the element coordinates of the corner points are

$$\xi_k = \xi_k^* - \xi_o$$
$$\eta_k = \eta_k^* - \eta_o \tag{7.2.18}$$

where

$$\eta_2 = \eta_1 \qquad \text{and} \qquad \eta_4 = \eta_3 \tag{7.2.19}$$

These are the corner point coordinates used in all subsequent calculations.

Several other geometric quantities are needed in future calculations. These are now computed. The intercepts where the sides intersect the x or ξ axis (figure 20) are

$$b_{32} = \frac{\xi_3\eta_2 - \xi_2\eta_3}{w} \qquad b_{41} = \frac{\xi_4\eta_1 - \xi_1\eta_4}{w} \tag{7.2.20}$$

The maximum diagonal of the element is

$$t = \text{Max} \begin{cases} \sqrt{(\xi_2 - \xi_4)^2 + (\eta_2 - \eta_4)^2} \\ \sqrt{(\xi_3 - \xi_1)^2 + (\eta_3 - \eta_1)^2} \end{cases} \tag{7.2.21}$$

The lengths of the sides are

$$d_{12} = d_F \qquad d_{34} = d_S$$
$$d_{32} = w\sqrt{1 + m_{32}^2} \qquad d_{41} = w\sqrt{1 + m_{41}^2} \tag{7.2.22}$$

Also needed are the total arc lengths along the N-lines from the trailing edge up to the element in question. These are

$$L_F = \sum d_F, \quad L_S = \sum d_S \tag{7.2.23}$$

where the sums are over previous elements of the lifting strip.

Finally the normalized moments of the area of the element are required. These are defined by

$$I_{nm} = \frac{1}{t^{n+m+2}} \iint_E \xi^n \eta^m \, d\xi d\eta \tag{7.2.24}$$

where the region of integration is the area of the element. For example, $t^2 I_{00}$ is the area of the element, $t^4 I_{20}$, $t^4 I_{11}$, $t^4 I_{02}$ are the moments of inertia or second moments. The first moments I_{10} and I_{01} are zero because the centroid is used as origin of coordinates. The order of a moment is the sum of its subscripts $n + m$. There are three second-order moments, four third-order, and five fourth-order. The present method uses up through fourth order. The moments are calculated by a straightforward but rather lengthy set of formulas which are given below.

First, normalize the corner point coordinates by the maximum diagonal,

$$\dot{\xi}_k = \xi_k/t, \qquad \dot{\eta}_k = \eta_k/t, \qquad k = 1, 2, 3, 4 \tag{7.2.25}$$

Now the normalized moment may be defined in terms of certain auxiliary functions

$$I_{nm} = -I_{nm}^{(32)} + I_{nm}^{(41)} + \frac{1}{(m+1)(n+1)} \left[\dot{\eta}_1^{m+1}(\dot{\xi}_2^{n+1} - \dot{\xi}_1^{n+1}) + \dot{\eta}_3^{m+1}(\dot{\xi}_4^{n+1} - \dot{\xi}_3^{n+1})\right] \tag{7.2.26}$$

The auxiliary function $I_{nm}^{(32)}$ is as follows:

If $|m_{32}| > 1$:

$$\begin{aligned} I_{nm}^{(32)} = {} & \frac{1}{(m+1)(n+1)} [\dot{\xi}^{n+1} \dot{\eta}^{m+1}]_3^2 \\ & - \frac{1}{(n+1)(n+2)} \frac{1}{m_{32}} [\dot{\xi}^{n+2} \dot{\eta}^{m}]_3^2 \\ & + \frac{m}{(n+1)(n+2)(n+3)} \frac{1}{m_{32}^2} [\dot{\xi}^{n+3} \dot{\eta}^{m-1}]_3^2 \\ & - \frac{m(m-1)}{(n+1)(n+2)(n+3)(n+4)} \frac{1}{m_{32}^3} [\dot{\xi}^{n+4} \dot{\eta}^{m-2}]_3^2 \\ & + \frac{m(m-1)(m-2)}{(n+1)(n+2)(n+3)(n+4)(n+5)} \frac{1}{m_{32}^4} [\dot{\xi}^{n+5} \dot{\eta}^{m-3}]_3^2 \\ & - \frac{m(m-1)(m-2)(m-3)}{(n+1)(n+2)(n+3)(n+4)(n+5)(n+6)} \frac{1}{m_{32}^5} [\dot{\xi}^{n+6} \dot{\eta}^{m-4}]_3^2 \end{aligned} \tag{7.2.27}$$

If $|m_{32}| \leq 1$:

$$
\begin{aligned}
I_{nm}^{(32)} = {} & \frac{1}{(m+1)(m+2)} m_{32} \left[\xi^{n} \eta^{m+2}\right]_3^2 \\
& - \frac{n}{(m+1)(m+2)(m+3)} m_{32}^2 \left[\xi^{n-1} \eta^{m+3}\right]_3^2 \\
& + \frac{n(n-1)}{(m+1)(m+2)(m+3)(m+4)} m_{32}^3 \left[\xi^{n-2} \eta^{m+4}\right]_3^2 \\
& - \frac{n(n-1)(n-2)}{(m+1)(m+2)(m+3)(m+4)(m+5)} m_{32}^4 \left[\xi^{n-3} \eta^{m+5}\right]_3^2 \\
& + \frac{n(n-1)(n-2)(n-3)}{(m+1)(m+2)(m+3)(m+4)(m+5)(m+6)} m_{32}^5 \left[\xi^{n-4} \eta^{m+6}\right]_3^2
\end{aligned}
\tag{7.2.28}
$$

where the bracketed symbols are defined by

$$
\left[\xi^{k} \eta^{p}\right]_3^2 = \xi_2^k \eta_2^p - \xi_3^k \eta_3^p \tag{7.2.29}
$$

(The superscripts in the above equations denote simple powers of the quantities except for the bracketed double superscript (32), which denotes the side of the quadrilateral.) It is clear from the above that the calculation of $I_{nm}^{(32)}$ requires $m + 2$ terms of (7.2.27) or $n + 1$ terms of (7.2.28). The calculation is simply terminated at this number of terms. The auxiliary function $I_{nm}^{(41)}$ is obtained from the above by an obvious substitution of subscripts.

All the above geometric quantities associated with a given element are saved and used as needed to calculate velocities induced by that element.

At this stage, some of the generated quantities are output, and the calculation may, if desired, be terminated. The purpose of this option is to provide an opportunity to discover errors in the input points before the execution of the lengthy calculations of the main part of the program.

7.3 Form of the Surface Dipole Distribution

7.3.1 General Form. Order of the Input Points

The surface of the lifting section is imagined covered with a dipole distribution that varies in the following manner. The dipole strength μ is fixed as zero at the first point of each N-line on the trailing edge. Along each N-line the dipole strength is proportional to distance along the section curve. This curve goes completely around the body and back to the trailing edge, at which point μ has some final nonzero value. Behind the trailing edge μ is constant and equal to its final trailing edge value. In the first input example of secton 7.1, a right wing is input from tip to root, and points on an N-line traverse the lower surface to the leading edge and return to the trailing edge along the upper surface. For this example the dipole variation is as shown in figure 21. The constant of proportionality that expresses the variation of μ along each N-line is initially unknown and its value is ultimately determined from the Kutta condition. Since the N-lines are roughly "chordwise" or "streamwise" on the lifting surface, this constant is the derivative of μ with respect to distance in the chordwise direction. Thus, according to the result of Appendix A, the proportionality constant that determines the growth of μ along each N-line is essentially the "spanwise" vorticity strength at that N-line, which is the bound vorticity that gives the lift.

As mentioned in section 7.1, points along an N-line of a lifting section are input beginning with the trailing edge, traversing the section curve of

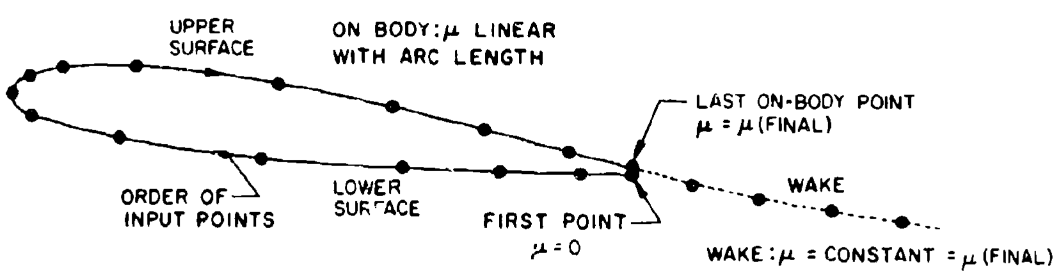

Figure 21. Variation of dipole strength along an N-line.

the wing and continuing into the wake. The order of input may be arranged so that either the lower surface is input first, as illustrated in figure 21, or else the upper surface is input first, in which case the section curve is traversed in the opposite sense to that shown in figure 21 (counterclockwise instead of clockwise). Thus, the positive direction of arc length along the section curve is opposite in the two input schemes. If the values of bound and trailing vorticity are to be identical, as they must be if the same body is input two ways, then the constants of proportionality that relate dipole strength to arc length along the N-line for each of the two input schemes must turn out to be equal in magnitude and opposite in sign. To illustrate the two cases, let the constant of proportionality be denoted B and arc length along the section curve be denoted s. Then $\mu = Bs$ if the input order is that of figure 21, and $\mu = -Bs$ if the order is opposite. The dipole strengths along the N-line for the two cases are illustrated in figures 22a and 22b. The dipole strengths in the wake are equal because the reversal of sign of the normal vector cancels out the apparent sign reversal

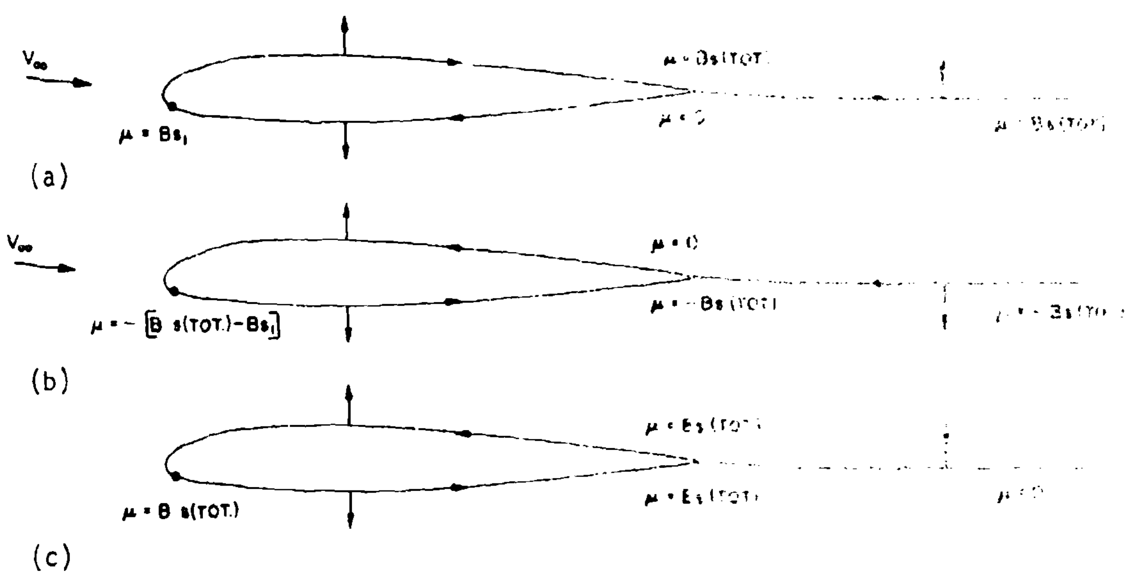

Figure 22. Three variations of dipole strength along a section curve (N-line). (a) Clockwise order of input points (lower surface input first). (b) Counterclockwise order of input points (upper surface input first). (c) Constant dipole strength on body obtained by subtracting cases (a) and (b).

of the dipole strength μ. The two solutions represented by figures 22a and 22b may be subtracted to give the solution illustrated in figure 22c, which has a constant dipole strength $B \cdot s(\text{tot.})$ all around the profile curve and zero strength in the wake. Since both the bound vorticity strength B and the total arc length around a section curve vary with "spanwise" location, the dipole strength of figure 22c varies in the "spanwise" direction but not in the "chordwise" direction. Thus, according to Appendix A, the related vorticity distribution consists of closed constant-strength filaments lying around the section curves. For the usual case of a wing with right and left symmetry at zero yaw, the symmetry insures a zero total strength for this vorticity distribution. Moreover, the flow solution of figure 22c has no uniform onset flow, which was canceled in the subtraction of the solutions corresponding to figures 22a and 22b. The solution corresponding to figure 22c is continuous, because the wake singularity is zero, and it satisfies the classical problem defined by equations (5.1.3), (5.1.5), and (5.1.4) with zero right side. This problem has a unique solution, namely the trivial solution. Thus, the solution of figure 22c represents zero flow, and the solutions of figures 22a and 22b are identical as they should be.

The theoretical considerations of the previous paragraph are strictly true for closed bodies in the limit of an infinite number of surface elements. An "open" wing tip of the type illustrated in figure 4c is excluded. For practical element numbers, numerical experiments must be performed. Results of such an experiment are presented in section 8.4 and are anticipated here. When a wing was input in the two ways discussed above, the resulting bound vorticity distributions were identical. The resulting surface pressure distributions were arly identical except near the wing tip where the input scheme illustrated in figures 21 and 22a seemed to give the more reasonable solution. Accordingly, it was concluded that points on N-lines of lifting sections should be input with the lower surface first, as shown in figure 21. However, two wing-fuselages input with the upper surface first have very reasonable surface pressures. The preceeding applies to positive angle of attack, for which the lower surface faces the onset flow. For more general flows the word "lower" in the above is replaced by "windward".

7.3.2 Variation Across the Span of a Lifting Strip

The variation of μ between the two N-lines used to form a lifting strip is assumed to be one of two forms that correspond to the "step function" and "piecewise linear" options for the spanwise bound vorticity variation, as discussed in section 6.3. For the "step function" option the proportionality constants on the two N-lines bounding the strip are set equal. This common value is essentially the bound vorticity on the strip and is determined directly by the Kutta condition. In general, the bound vorticity is different on adjacent lifting strips. Thus, there are really two values of "the" proportionality constant on an N-line, namely those corresponding to the two lifting strips on either side of the N-line. The dipole distribution is discontinuous across the N-line, which implies a discontinuity of bound vorticity and a concentrated trailing vortex filament along the N-line. The "piecewise linear" option essentially assumes a linear "spanwise" variation across a lifting strip for the "chordwise" proportionality constant of the dipole strength. The "spanwise" derivative is determined by the parabolic fit discussed in section 7.11. The discontinuity at the N-line is reduced to a higher order effect. As is shown below, this option requires an additional dipole term in the wake.

7.3.3 Variation Over a Trapezoidal Element

Consider now a typical trapezoidal lifting element, as shown in figure 20. As defined in section 7.2, the lifting strip to which the element belongs is bounded by two N-lines, which are designated the "first" N-line and the "second" N-line and which are represented by subscripts F and S, respectively. The constants of proportionality for the dipole strength along the N-lines are B_F and B_S, respectively. Thus, if s denotes arc length along an N-line:

$$\begin{aligned} \mu &= B_F s \quad \text{along the first N-line} \\ \mu &= B_S s \quad \text{along the second N-line} \end{aligned} \qquad (7.3.1)$$

On the element itself, the parallel side at $\eta = \eta_1$ is a segment of the first N-line, and the parallel side at $\eta = \eta_3$ is a segment of the second N-line (figure 20). The dipole strength varies linearly along each side, namely

$$\begin{aligned} \mu &= A_F + B_F\xi \qquad \text{on} \qquad \eta = \eta_1 \\ \mu &= A_S + B_S\xi \qquad \text{on} \qquad \eta = \eta_3 \end{aligned} \tag{7.3.2}$$

On the element the arc length along the N-lines is simply the coordinate ξ and the direction of increasing arc length is the positive ξ direction. On each side the constant A is the value of μ for $\xi = 0$. Thus,

$$\begin{aligned} A_F &= B_F \text{ (total arc length of } \xi\text{-axis from trailing edge)} \\ &= B_F h_F \end{aligned} \tag{7.3.3}$$

From figure 20 and equation (7.2.23)

$$h_F = L_F - \xi_1 \tag{7.3.4}$$

Similarly

$$A_S = B_S h_S \tag{7.3.5}$$

where

$$h_S = L_S - \xi_4 \tag{7.3.6}$$

Now the dipole distribution μ on the element is assumed in the form of a general two-variable second degree polynomial. When conditions (7.3.2) are applied, it turns out that μ must have the form

$$\mu = \frac{B_F - B_S}{W}\xi\eta + \frac{A_F - A_S}{W}\eta + \frac{B_S\eta_1 - B_F\eta_3}{W}\xi + \frac{A_S\eta_1 - A_F\eta_3}{W} + C(\eta - \eta_3)(\eta - \eta_1) \tag{7.3.7}$$

or, using (7.3.3) and (7.3.5)

$$\begin{aligned} \mu = &\frac{1}{W}[\xi\eta + h_F\eta - \eta_3\xi - \eta_3 h_F + cw(\eta - \eta_3)(\eta - \eta_1)]B_F \\ &- \frac{1}{W}[\xi\eta + h_S\eta - \eta_1\xi - \eta_1 h_S + cw(\eta - \eta_3)(\eta - \eta_1)]B_S \end{aligned} \tag{7.3.8}$$

where C and c are arbitrary constants. The absence of a term in ξ^2 is due to the orientation of the parallel sides along the ξ axis. All other terms of the general second degree polynomial are present in general. If, however, $B_F = B_S$, as is true in the "step function" option, then the quadratic terms vanish and μ is a linear function of ξ and η.

7.3.4 Variation Between Elements of a Lifting Strip

The variation of dipole strength across the N-lines, i.e., the variation from one lifting strip to the adjacent one, is discussed above. It remains to discuss the variation along a lifting strip, i.e., the variation from one lifting element to the next one of the strip. The dipole strength along the "top" side of the element between the points (ξ_3, η_3) and (ξ_2, η_2) (see figure 20) is obtained by setting $\xi = m_{32}\eta + b_{32}$ in (7.3.7). The result is

$$\mu(32) = \mu(\text{linear}) + (B_F - B_S)\{cw^2 + wm_{32}\}\left[\frac{s}{L}\left(\frac{s}{L} - 1\right)\right] \qquad (7.3.9)$$

In the square bracket s denotes arc length along the side and L the total length of the side ($L = d_{32}$ in the notation of seciton 7.2). The function μ(linear) is a linear function that varies from the value of μ at the point (ξ_3, η_3), which equals $B_S \cdot$ (arc length of the point from the trailing edge) to the value of μ at the point (ξ_2, η_2) which equals $B_F \cdot$ (arc length of the point from the trailing edge). On the adjacent element, the "bottom" side that lies between the points (ξ_4, η_4) and (ξ_1, η_1) is the one that lies along the side discussed above. The dipole strength along this side is

$$\mu(41) = \mu(\text{linear}) + (B_F - B_S)\{cw^2 + wm_{41}\}\left[\frac{s}{L}\left(\frac{s}{L} - 1\right)\right] \qquad (7.3.10)$$

Ignoring the small gaps between elements produced by the projection of the input points, the quantities μ(linear), s, and L are identical in equations (7.3.9) and (7.3.10), as are B_F and B_S. The only quantities that are different are those in the curly brackets. Here c and w correspond to different elements, while the slopes m_{32} and m_{41} correspond to different sides of different elements. It is clear from figure 20 that the products wm_{32} and wm_{41} are just the changes in the ξ-coordinate between the endpoints of the side question. These may be put in vector form. Let the vector between the endpoints of a side be denoted $\vec{m}$. Since a common side of two adjacent elements is being considered (ignoring any higher order gaps produced by the "adjustment" process of section 7.2), the same vector $\vec{m}$ applies to both elements. Then the change in ξ-coordinate over that side is $\vec{m} \cdot \vec{i}_E$ where as defined in section 7.2, $\vec{i}_E$ is the unit vector along the ξ-axis. Now the change in dipole strength across the side common to two elements is

$$\Delta\mu = (B_F - B_S)\{\Delta(w^2c) + \vec{m} \cdot (\Delta\vec{t}_E)\}[\frac{s}{L}(\frac{s}{L} - 1)] \qquad (7.3.11)$$

where any quantity preceeded by Δ represents a change in that quantity. If the N-lines are straight and the elements are coplanar, $\Delta\vec{t}_E = 0$. If the angle between two elements is small $\vec{t}_E$ is of the order of the square of the angle. Moreover, this angle is small if the slope of the surface is continuous and if enough elements are used to insure calculational accuracy. Thus, in the present method the parameter c is set equal to zero for all elements on the body surface. The resulting discontinuity in dipole strength between elements of an N-line is of higher order than the other approximations of the method if the slope of the body is continuous. At a slope discontinuity the dipole strength can be made continuous by having the N-lines intersect the line of discontinuity at right angles, so that $\vec{m} \cdot \vec{t}_E = 0$. However, this appears to be generally unnecessary for good accuracy.

One exception to the above rule is the trailing edge. The local slope discontinuity is quite severe, and requiring the N-lines to be perpendicular to the trailing edge is undesirable. Thus, if only the on-body dipole distribution is considered, there is a discontinuity of dipole strength at the trailing edge, having the parabolic variation of the square-bracketed term in (7.3.11) and thus a concentrated vortex filament of this form would lie along the trailing edge. This difficulty is disposed of by adding a dipole term of the correct form to the distribution in the wake. In the wake, the dipole strength is constant along N-lines and thus has the form of equation (7.3.7) with $B_F = B_S = 0$ (A_F and A_S are set equal to the actual values of B_F and B_S multiplied by the total on-body arc lengths of the respective N-lines). Thus, a value of C may be chosen which is proportional to $(B_F - B_S)$. That eliminates the discontinuity. By factoring out $(B_F - B_S)$ C may be replaced by c, in a manner analogous but not identical to the redefinition involved in going from equation (7.3.7) to (7.3.8). The resulting formulas are given in section 7.9, which deals with the wake elements.

The discontinuity discussed above, together with its remedy, occur only if the "piecewise linear" option is used for bound vorticity. If the "step function" option is used, then on an element $B_F - B_S = 0$, and the discontinuity disappears. This is another simplification connected with this option.

7.4 Overall Logic of the Calculation of the Velocity Induced by a Lifting Element at a Point in Space

The basic formulas of the present method are those giving the velocity induced by an element at points in space. These are applied to obtain the effects of the elements at each other's control points. For an element of a lifting section on the body surface there are two kinds of induced velocities, that due to the constant source density on the element and that due to the dipole distribution of the form (7.3.8). For different ranges of distance between the element centroid and the point where velocities are evaluated, different sets of formulas are used. The three ranges are denoted: (1) the far-field or point singularity regime, (2) the intermediate field or multipole regime, and (3) the near field or exact regime. The near-field formulas are obtained by an exact integration over the elements. Such formulas are necessary to obtain the desired accuracy at points near the element, but are quite time-consuming. At points further from the element approximate integration formulas are used to reduce computing time. When the distance between the element centroid and the point where velocities are being evaluated exceeds a certain multiple of the maximum diagonal of the element, approximate formulas are used. In the far field, velocities are calculated directly in the reference coordinate system. In the intermediate and near fields the field point where velocities are to be evaluated is transformed into the element coordinate system using the transformation matrix (7.2.10). Then velocities are computed in element coordinates, and finally the computed velocities are transformed back to reference coordinates using the transformation matrix. This procedure is well known and will not be discussed further here. A complete description is contained in reference 3.

Now notation will be introduced for the velocity calculation. It is assumed that the velocities that are being computed are due to the j-th element and are being evaluated at the control point (centroid) of the i-th element. Clearly, any point could be substituted for the i-th control point. The velocity due to the constant source density is denoted $\vec{V}_{ij}$. In element coordinates it has components V_x(source), V_y(source), and V_z(source), i.e.,

$$\vec{V}_{ij} = V_x(\text{source})\ \vec{i}_E + V_y(\text{source})\ \vec{j}_E + V_z(\text{source})\ \vec{k}_E \qquad (7.4.1)$$

For a general quadrilateral element of a nonlifting section, this source velocity is the only induced velocity, and it is computed by the formulas of reference 3 in all three ranges. For a trapezoidal element of a lifting section the calculation of source velocities is the same as for a nonlifting element in the far field and the intermediate field (a trivial difference is the use of normalized area moments). In the near field advantage can be taken of the fact that the element is a trapezoid to shorten the formulas and conserve computing time.

To develop formulas for the velocity induced by the dipole distribution on an element, some additional notation is required. Furthermore, it simplifies the development to consider the velocity potential initially rather than the velocity components. The potential due to the dipole distribution on the element at points of space is obtained by integrating over the element. Namely,

$$\phi = \iint_E \phi(\text{dipole})\ \mu(\xi,\eta)\ d\xi d\eta \tag{7.4.2}$$

where $\mu(\xi,\eta)$ is given by (7.3.8), where the integration is over the area of the element, and where $\phi(\text{dipole})$ is the potential of a unit point dipole with axis normal to the element, i.e.,

$$\phi(\text{dipole}) = \frac{z}{[(z-\xi)^2 + (y-\eta)^2 + z^2]^{3/2}} \tag{7.4.3}$$

Here (x, y, z) is the point where the potential and velocity are being evaluated expressed in the coordinate system of the element. Now define the auxiliary potentials

$$\phi_{pq} = \iint_E \phi(\text{dipole})\xi^p\eta^q\ d\xi d\eta \tag{7.4.4}$$

where p and q are integers. Now from (7.3.8), (7.4.2), and (7.4.4), the potential of the element is

$$\phi = \phi_F B_F - \phi_S B_S \tag{7.4.5}$$

where

$$\phi_F = \frac{1}{w}[\phi_{11} + h_F\phi_{01} - n_3\phi_{10} - n_3h_F\phi_{00} + cw\phi_c]$$

$$\phi_S = \frac{1}{w}[\phi_{11} + h_S\phi_{01} - n_1\phi_{10} - n_1h_S\phi_{00} + cw\phi_c] \qquad (7.4.6)$$

$$\phi_c = \phi_{02} - (n_1 + n_3)\phi_{01} + n_1n_3\phi_{00}$$

As stated in the previous section, the term ϕ_c is not currently used for lifting elements on the body. For completeness, it is included in the formulation, and equations are given in the subsequent sections. These last are needed for wake elements in any event. The velocity due to the dipole distribution is

$$\vec{V}_{ij}(\text{dipole}) = -\nabla\phi \qquad (7.4.7)$$

where ∇ denotes the gradient operator. In element coordinates this is

$$\nabla\phi = \frac{\partial\phi}{\partial x}\vec{i}_E + \frac{\partial\phi}{\partial y}\vec{j}_E + \frac{\partial\phi}{\partial z}\vec{k}_E \qquad (7.4.8)$$

From (7.4.5) and (7.4.7) it is clear that

$$\vec{V}_{ij}(\text{dipole}) = B_F\,\vec{V}_{ij}^{(F)} + B_S\,\vec{V}_{ij}^{(S)} \qquad (7.4.9)$$

where

$$\vec{V}_{ij}^{(F)} = -\nabla\phi_F, \qquad \vec{V}_{ij}^{(S)} = +\nabla\phi_S \qquad (7.4.10)$$

The desired velocities are these $\vec{V}_{ij}$, $\vec{V}_{ij}^{(F)}$, and $\vec{V}_{ij}^{(S)}$. In the far field these are calculated directly. In the near and intermediate field the source velocity is evaluated directly, but the dipole velocities are broken up into separate terms in the manner of (7.4.6). Thus to evaluate the dipole velocities, formulas are needed for the derivatives of ϕ_{00}, ϕ_{10}, ϕ_{01}, ϕ_{11}, and ϕ_{02}. These formulas are presented in the following sections.

As mentioned above, the integrals (7.4.4) can be evaluated analytically and the resulting expressions differentiated. This is what is done for the near field (section 7.7). The resulting expressions are quite involved and time-consuming to evaluate. To save computing time, approximate formulas are used when the field point is some distance from the element. This is accomplished by means of a multipole expansion. The basic idea is to expand ϕ(dipole) from (7.4.3) in a two-dimensional Taylor Series about $\xi = \eta = 0$. This process is a standard development in the textbooks. The result is

$$\phi(\text{dipole}) = F_{00}(x,y,z) + F_{10}(x,y,z)\xi + F_{01}(x,y,z)\eta + F_{00}(x,y,z)\xi^2 + F_{11}(x,y,z)\xi\eta + F_{02}(x,y,z)\eta^2 + \ldots + \sum_n \sum_m F_{nm}(x,y,z)\xi^n\eta^m + \ldots \tag{7.4.11}$$

where the F_{nm} are the derivatives of ϕ(dipole) at the origin of element coordinates and are independent of ξ and η. When (7.4.11) is inserted into (7.4.4), the $F_{nm}(x,y,z)$ are taken out of the integral, the remaining integrals are of the form (7.2.24) and are thus moments of the area of the element, which can be normalized by division by the appropriate powers of t.

In the intermediate field the expansion (7.4.11) is used through the second-order terms, F_{20}, F_{11}, F_{02}. In the far field only the initial, zero order, term is used. It is clear from the form of (7.4.11) that F_{00} is the potential of a unit point dipole at the origin of element coordinates (centroid). In the far field every auxiliary potential (7.4.4) is a multiple of the point dipole potential and thus so are the combined potentials (7.4.6). Thus, induced velocities in the far field may be expressed directly in reference coordinates using the well-known formulas for a point dipole.

The above discussed only the dipole velocity, but the same procedure is followed for the source velocity. In fact, the development for this case is given in detail in reference 3.

7.5 Far-Field Formulas for the Velocity Induced by a Lifting Element

First calculate the distance r_0 between the centroid of the element and the field point where velocities are to be calculated. If the reference coordinates of the centroid are x_0, y_0, z_0 and the reference coordinates of the field point are x', y', z', then

$$r_o = \sqrt{(x' - x_o)^2 + (y' - y_o)^2 + (z' - z_o)^2} \tag{7.5.1}$$

Now test r_o/t, where t is the maximum diagonal of the element. If

$$r_o/t > \rho_1 \tag{7.5.2}$$

where ρ_1 is a certain criterion, then the far-field formulas are used. Currently ρ_1 is set equal to 4.0. The far-field formulas calculate velocities directly in reference coordinates. First define the vector

$$\vec{r}_o = (x' - x_o)\vec{i} + (y' - y_o)\vec{j} + (z' - z_o)\vec{k} \tag{7.5.3}$$

The source velocity is

$$\vec{V}_{ij} = \frac{t^2 I_{00}}{r_o^2} \frac{\vec{r}_o}{r_o} \tag{7.5.4}$$

The dipole velocities are

$$\begin{aligned} \vec{V}_{ij}^{(F)} &= -Q_F \vec{D} \\ \vec{V}_{ij}^{(S)} &= Q_S \vec{D} \end{aligned} \tag{7.5.5}$$

where

$$\begin{aligned} Q_F &= \frac{t^2}{w} \frac{1}{r_o^3} [t^2 I_{11} - \eta_3 h_L I_{00} + cw(t^2 I_{02} + \eta_1 \eta_3 I_{00})] \\ Q_S &= \frac{t^2}{w} \frac{1}{r_o^3} [t^2 I_{11} - \eta_1 h_R I_{00} + cw(t^2 I_{02} + \eta_1 \eta_3 I_{00})] \end{aligned} \tag{7.5.6}$$

and where

$$\vec{D} = - \left[3\left(\frac{\vec{n} \cdot \vec{r}_o}{r_o}\right) \frac{\vec{r}_o}{r_o} - \vec{n} \right] \tag{7.5.7}$$

It will be recalled that $\vec{n}$ is the unit normal vector of the element ($\vec{n}$ is not connected with the field point) and that I_{nm} denotes normalized moments as given by (7.2.24). A comparison of (7.5.6) with (7.4.6) shows that the

ϕ_{01} and ϕ_{10} terms have dropped out because they are multiplied by the zero value moments I_{01} and I_{10}.

7.6 Intermediate-Field or Multipole Formulas for the Velocity Induced by a Lifting Element

If $r_0/t < \rho_1$, transform the reference coordinates x', y', z' of the field point by the transformation matrix to obtain element coordinates x, y, z of the field point. Now perform another test. If

$$r_0/t > \rho_2 \tag{7.6.1}$$

where ρ_2 is another input criterion, which is currently taken as $\rho_2 = 2.5$, then the multipole formulas are used. The dipole velocities are taken in the form (7.4.10), which means that derivatives of all quantities in (7.4.6) must be calculated.

First define direction cosines

$$\alpha = \frac{x}{r_o}, \qquad \beta = \frac{y}{r_o}, \qquad \gamma = \frac{z}{r_o} \tag{7.6.2}$$

Next define certain "derivative functions" as follows:

First Order

$$u_x = -\alpha, \qquad u_y = -\beta, \qquad u_z = -\gamma \tag{7.6.3}$$

Second Order

$$\begin{aligned} u_{xx} &= 3\alpha^2 - 1, & u_{xy} &= 3\alpha\beta, & u_{yy} &= 3\beta^2 - 1 \\ u_{xz} &= 3\alpha\gamma & u_{yz} &= 3\beta\gamma, & u_{zz} &= 3\gamma^2 - 1 \end{aligned} \tag{7.6.4}$$

Third Order

$$\begin{aligned} u_{xxx} &= 3\alpha(3 - 5\alpha^2), & u_{xxy} &= 3\beta(1 - 5\alpha^2), & u_{xxz} &= 3\gamma(1 - 5\alpha^2) \\ u_{xyy} &= 3\alpha(1 - 5\beta^2) & u_{xyz} &= -15\alpha\beta\gamma & u_{xzz} &= 3\alpha(1 - 5\gamma^2) \\ u_{yyy} &= 3\beta(3 - 5\beta^2) & u_{yyz} &= 3\gamma(1 - 5\beta^2) & u_{yzz} &= 3\beta(1 - 5\gamma^2) \end{aligned} \tag{7.6.5}$$

Fourth Order

$$
\begin{aligned}
u_{xxxx} &= 9 - 90\alpha^2 + 105\alpha^4 \\
u_{xxxy} &= 15\alpha\beta(7\alpha^2 - 3) \\
u_{xxxz} &= 15\alpha\gamma(7\alpha^2 - 3) \\
u_{xxyy} &= 3 - 15(\alpha^2 + \beta^2) + 105\alpha^2\beta^2 \\
u_{xxyz} &= 15\beta\gamma(7\alpha^2 - 1) \\
u_{xxzz} &= 3 - 15(\alpha^2 + \gamma^2) + 105\alpha^2\gamma^2 \qquad (7.6.6) \\
u_{xyyy} &= 15\alpha\beta(7\beta^2 - 3) \\
u_{xyyz} &= 15\alpha\gamma(7\beta^2 - 1) \\
u_{xyzz} &= 15\alpha\beta(7\gamma^2 - 1) \\
u_{yyyy} &= 9 - 90\beta^2 + 105\beta^4 \\
u_{yyyz} &= 15\beta\gamma(7\beta^2 - 3) \\
u_{yyzz} &= 3 - 15(\beta^2 + \gamma^2) + 105\beta^2\gamma^2
\end{aligned}
$$

Then the source velocity components are

$$
\begin{aligned}
V_x(\text{source}) &= \frac{t^2}{r_o^2}\left\{- I_{00}u_x - \frac{1}{2}\left(\frac{t}{r_o}\right)^2 [I_{20}u_{xxx} + 2I_{11}u_{xxy} + I_{02}u_{xyy}]\right\} \\
V_y(\text{source}) &= \frac{t^2}{r_o^2}\left\{- I_{00}u_y - \frac{1}{2}\left(\frac{t}{r_o}\right)^2 [I_{20}u_{xxy} + 2I_{11}u_{xyy} + I_{02}u_{yyy}]\right\} \qquad (7.6.7) \\
V_z(\text{source}) &= \frac{t^2}{r_o^2}\left\{- I_{00}u_z - \frac{1}{2}\left(\frac{t}{r_o}\right)^2 [I_{20}u_{xxz} + 2I_{11}u_{xyz} + I_{02}u_{yyz}]\right\}
\end{aligned}
$$

These are identical to the miltipole formulas of reference 3 with a slightly different notation.

Specific formulas for the derivatives of the various dipole potentials ϕ_{pq} appearing in (7.4.6) are given on the following page. To illustrate the

Dipole Derivatives for Multipole Expansion

Far-Field 1st Order 2nd Order

$$\frac{\partial \phi_{00}}{\partial x} = -\frac{t^2}{r_o^3}\left\{I_{00}u_{xz} - \cancel{\left(\frac{t}{r_o}\right)\left[I_{10}u_{xxz} + I_{01}u_{xyz}\right]} + \left(\frac{t}{r_o}\right)^2\left[I_{20}u_{xxxz} + 2I_{11}u_{xxyz} + I_{02}u_{xyyz}\right]\right\}$$

$$\frac{\partial \phi_{00}}{\partial y} = -\frac{t^2}{r_o^3}\left\{I_{00}u_{yz} - \cancel{\left(\frac{t}{r_o}\right)\left[I_{10}u_{xyz} + I_{01}u_{yyz}\right]} + \left(\frac{t}{r_o}\right)^2\left[I_{20}u_{xxyz} + 2I_{11}u_{xyyz} + I_{02}u_{yyyz}\right]\right\} \quad (7.6.8)$$

$$\frac{\partial \phi_{00}}{\partial z} = -\frac{t^2}{r_o^3}\left\{I_{00}u_{zz} - \cancel{\left(\frac{t}{r_o}\right)\left[I_{10}u_{xzz} + I_{01}u_{yzz}\right]} + \left(\frac{t}{r_o}\right)^2\left[I_{20}u_{xxzz} + 2I_{11}u_{xyzz} + I_{02}u_{yyzz}\right]\right\}$$

$$\frac{\partial \phi_{10}}{\partial x} = -\frac{t^3}{r_o^3}\left\{\cancel{I_{10}u_{xz}} - \left(\frac{t}{r_o}\right)\left[I_{20}u_{xxz} + I_{11}u_{xyz}\right] + \left(\frac{t}{r_o}\right)^2\left[I_{30}u_{xxxz} + 2I_{21}u_{xxyz} + I_{12}u_{xyyz}\right]\right\}$$

$$\frac{\partial \phi_{10}}{\partial y} = -\frac{t^3}{r_o^3}\left\{\cancel{I_{10}u_{yz}} - \left(\frac{t}{r_o}\right)\left[I_{20}u_{xyz} + I_{11}u_{yyz}\right] + \left(\frac{t}{r_o}\right)^2\left[I_{30}u_{xxyz} + 2I_{21}u_{xyyz} + I_{12}u_{yyyz}\right]\right\} \quad (7.6.9)$$

$$\frac{\partial \phi_{10}}{\partial z} = -\frac{t^3}{r_o^3}\left\{\cancel{I_{10}u_{zz}} - \left(\frac{t}{r_o}\right)\left[I_{20}u_{xzz} + I_{11}u_{yzz}\right] + \left(\frac{t}{r_o}\right)^2\left[I_{30}u_{xxzz} + 2I_{21}u_{xyzz} + I_{12}u_{yyzz}\right]\right\}$$

$$\frac{\partial \phi_{01}}{\partial x} = -\frac{t^3}{r_o^3}\left\{\cancel{I_{01}u_{xz}} - \left(\frac{t}{r_o}\right)\left[I_{11}u_{xxz} + I_{02}u_{xyz}\right] + \left(\frac{t}{r_o}\right)^2\left[I_{21}u_{xxxz} + 2I_{12}u_{xxyz} + I_{03}u_{xyyz}\right]\right\}$$

$$\frac{\partial \phi_{01}}{\partial y} = -\frac{t^3}{r_o^3}\left\{\cancel{I_{01}u_{yz}} - \left(\frac{t}{r_o}\right)\left[I_{11}u_{xyz} + I_{02}u_{yyz}\right] + \left(\frac{t}{r_o}\right)^2\left[I_{21}u_{xxyz} + 2I_{12}u_{xyyz} + I_{03}u_{yyyz}\right]\right\} \quad (7.6.10)$$

$$\frac{\partial \phi_{01}}{\partial z} = -\frac{t^3}{r_o^3}\left\{\cancel{I_{01}u_{zz}} - \left(\frac{t}{r_o}\right)\left[I_{11}u_{xzz} + I_{02}u_{yzz}\right] + \left(\frac{t}{r_o}\right)^2\left[I_{21}u_{xxzz} + 2I_{12}u_{xyzz} + I_{03}u_{yyzz}\right]\right\}$$

$$\frac{\partial \phi_{11}}{\partial x} = -\frac{t^4}{r_o^3}\left\{I_{11}u_{xz} - \left(\frac{t}{r_o}\right)\left[I_{21}u_{xxz} + I_{12}u_{xyz}\right] + \left(\frac{t}{r_o}\right)^2\left[I_{31}u_{xxxz} + 2I_{22}u_{xxyz} + I_{13}u_{xyyz}\right]\right\}$$

$$\frac{\partial \phi_{11}}{\partial y} = -\frac{t^4}{r_o^3}\left\{I_{11}u_{yz} - \left(\frac{t}{r_o}\right)\left[I_{21}u_{xyz} + I_{12}u_{yyz}\right] + \left(\frac{t}{r_o}\right)^2\left[I_{31}u_{xxyz} + 2I_{22}u_{xyyz} + I_{13}u_{yyyz}\right]\right\} \quad (7.6.11)$$

$$\frac{\partial \phi_{11}}{\partial z} = -\frac{t^4}{r_o^3}\left\{I_{11}u_{zz} - \left(\frac{t}{r_o}\right)\left[I_{21}u_{xzz} + I_{12}u_{yzz}\right] + \left(\frac{t}{r_o}\right)^2\left[I_{31}u_{xxzz} + 2I_{22}u_{xyzz} + I_{13}u_{yyzz}\right]\right\}$$

$$\frac{\partial \phi_{02}}{\partial x} = -\frac{t^4}{r_o^3}\left\{I_{02}u_{xz} - \left(\frac{t}{r_o}\right)\left[I_{12}u_{xxz} + I_{03}u_{xyz}\right] + \left(\frac{t}{r_o}\right)^2\left[I_{22}u_{xxxz} + 2I_{13}u_{xxyz} + I_{04}u_{xyyz}\right]\right\}$$

$$\frac{\partial \phi_{02}}{\partial y} = -\frac{t^4}{r_o^3}\left\{I_{02}u_{yz} - \left(\frac{t}{r_o}\right)\left[I_{12}u_{xyz} + I_{03}u_{yyz}\right] + \left(\frac{t}{r_o}\right)^2\left[I_{22}u_{xxyz} + 2I_{13}u_{xyyz} + I_{04}u_{yyyz}\right]\right\} \quad (7.6.12)$$

$$\frac{\partial \phi_{02}}{\partial z} = -\frac{t^4}{r_o^3}\left\{I_{02}u_{zz} - \left(\frac{t}{r_o}\right)\left[I_{12}u_{xzz} + I_{03}u_{yzz}\right] + \left(\frac{t}{r_o}\right)^2\left[I_{22}u_{xxzz} + 2I_{13}u_{xyzz} + I_{04}u_{yyzz}\right]\right\}$$

development, the terms containing the moments I_{10} and I_{01} are written down. They are then crossed out to show that such terms need not be calculated because $I_{10} = I_{01} = 0$. (Inclusion of these terms generalizes the formulas to the case where the centroid is not used as origin.)

7.7 Near-Field Formulas for the Velocity Induced by a Lifting Element

If $r_0/t < \rho_2$, the near-field or exact formulas are used to compute induced velocities. The calculation starts with the element coordinates x, y, z of the field point and the geometric quantities associated with the element that are discussed in section 7.2. In particular, the corner point coordinates ξ_k, η_k, $k = 1, 2, 3, 4$ are needed, together with the width w from (7.2.14), the slopes m_{32} and m_{41} from (7.2.15), the intercepts b_{32} and b_{41} from (7.2.20), the maximum diagonal t from (7.2.21), and the side lengths $d_{12}, d_{32}, d_{34}, d_{41}$, from (7.2.22). These quantities are illustrated in figure 20. In addition to the basic near-field equation, there are special limiting formulas for small values of r_0 and z. However, the basic near-field formulas are used in the large majority of cases.

Preliminary quantities to be calculated are:

$$r_k = \sqrt{(x-\xi_k)^2 + (y-\eta_k)^2 + z^2}, \qquad k = 1, 2, 3, 4$$

$$\alpha_k = \frac{x-\xi_k}{r_k}, \qquad \beta_k = \frac{y-\eta_k}{r_k}, \qquad \gamma_k = \frac{z}{r_k} \qquad k = 1, 2, 3, 4 \tag{7.7.1}$$

$$p_k^{(32)} = m_{32}[z^2 + (y-\eta_k)^2] - (x-\xi_k)(y-\eta_k), \qquad k = 3 \text{ or } 2$$

$$p_k^{(41)} = m_{41}[z^2 + (y-\eta_k)^2] - (x-\xi_k)(y-\eta_k), \qquad k = 4 \text{ or } 1 \tag{7.7.2}$$

The basic functions are

$$L^{(mn)} = \log \frac{r_m + r_n - d_{mn}}{r_m + r_n + d_{mn}}, \qquad m, n \text{ consecutive, i.e., } mn = 12, 23, 34, \text{ or } 41 \tag{7.7.3}$$

and

$$T_k^{(32)} = \tan^{-1}\left[\frac{p_k^{(32)}}{zr_k}\right], \qquad k = 3 \text{ or } 2$$

$$T_k^{(41)} = \tan^{-1}\left[\frac{p_k^{(41)}}{zr_k}\right], \qquad k = 4 \text{ or } 1 \qquad (7.7.4)$$

Also needed are derivatives of the T's and L's. The derivatives of $T_k^{(32)}$ are

$$\left.\begin{aligned}
\frac{\partial T_k^{(32)}}{\partial x} &= -\frac{z(r_k^2\beta_k + p_k^{(32)}\alpha_k)}{D_k^{(32)}} \\
\frac{\partial T_k^{(32)}}{\partial y} &= \frac{z[(2m_{32}\beta_k - \alpha_k)r_k^2 - p_k^{(32)}\beta_k]}{D_k^{(32)}} \\
\frac{\partial T_k^{(32)}}{\partial z} &= \frac{2m_{32}z^2r_k - p_k^{(32)}(r_k + z\gamma_k)}{D_k^{(32)}} \\
D_k^{(32)} &= z^2r_k^2 + [p_k^{(32)}]^2
\end{aligned}\right\} \quad k = 3 \text{ or } 2 \qquad (7.7.5)$$

There is an analagous set of formulas for the derivatives of $T_k^{(41)}$.

The derivatives of $L^{(mn)}$ are

$$\frac{\partial L^{(mn)}}{\partial x} = D_{mn}(\alpha_m + \alpha_n), \qquad \frac{\partial L^{(mn)}}{\partial y} = D_{mn}(\beta_m + \beta_n), \qquad \frac{\partial L^{(mn)}}{\partial z} = D_{mn}(\gamma_m + \gamma_n)$$

$$D_{mn} = \frac{2d_{mn}}{(r_m + r_n)^2 - d_{mn}^2} \qquad (7.7.6)$$

$$mn = 12,\ 23,\ 34,\ 41$$

Now in terms of the above functions the source velocities and dipole potential derivatives needed in (7.4.6) can be written.

The source velocities are

$$V_x(\text{source}) = -\frac{1}{\sqrt{1+m_{32}^2}} L^{(32)} + \frac{1}{\sqrt{1+m_{41}^2}} L^{(41)}$$

$$V_y(\text{source}) = - L^{(12)} + L^{(34)} + \frac{m_{32}}{\sqrt{1+m_{32}^2}} L^{(32)} - \frac{m_{41}}{\sqrt{1+m_{41}^2}} L^{(41)} \tag{7.7.7}$$

$$V_z(\text{source}) = - T_2^{(32)} + T_3^{(32)} + T_1^{(41)} - T_4^{(41)}$$

To evaluate the dipole potential derivatives, the derivatives of V_x and V_y are needed (since $V_z = \phi_{00}$, its derivatives are exactly a potential derivative). The derivatives of V_x and V_y are

$$\frac{\partial V_x(\text{source})}{\partial x} = -\frac{1}{\sqrt{1+m_{32}^2}} \frac{\partial L^{(32)}}{\partial x} + \frac{1}{\sqrt{1+m_{41}^2}} \frac{\partial L^{(41)}}{\partial x}$$

$$\frac{\partial V_x(\text{source})}{\partial y} = -\frac{1}{\sqrt{1+m_{32}^2}} \frac{\partial L^{(32)}}{\partial y} + \frac{1}{\sqrt{1+m_{41}^2}} \frac{\partial L^{(41)}}{\partial y}$$

$$\frac{\partial V_x(\text{source})}{\partial z} = -\frac{1}{\sqrt{1+m_{32}^2}} \frac{\partial L^{(32)}}{\partial z} + \frac{1}{\sqrt{1+m_{41}^2}} \frac{\partial L^{(41)}}{\partial z} \tag{7.7.8}$$

$$\frac{\partial V_y(\text{source})}{\partial x} = -\frac{\partial L^{(12)}}{\partial x} + \frac{\partial L^{(34)}}{\partial x} + \frac{m_{32}}{\sqrt{1+m_{32}^2}} \frac{\partial L^{(32)}}{\partial x} - \frac{m_{41}}{\sqrt{1+m_{41}^2}} \frac{\partial L^{(41)}}{\partial x}$$

$$\frac{\partial V_y(\text{source})}{\partial y} = -\frac{\partial L^{(12)}}{\partial y} + \frac{\partial L^{(34)}}{\partial y} + \frac{m_{32}}{\sqrt{1+m_{32}^2}} \frac{\partial L^{(32)}}{\partial y} - \frac{m_{41}}{\sqrt{1+m_{41}^2}} \frac{\partial L^{(41)}}{\partial y}$$

$$\frac{\partial V_y(\text{source})}{\partial z} = -\frac{\partial L^{(12)}}{\partial z} + \frac{\partial L^{(34)}}{\partial z} + \frac{m_{32}}{\sqrt{1+m_{32}^2}} \frac{\partial L^{(32)}}{\partial z} - \frac{m_{41}}{\sqrt{1+m_{41}^2}} \frac{\partial L^{(41)}}{\partial z}$$

Now the potential derivatives are as follows.

$$\frac{\partial\phi_{00}}{\partial x} = -\frac{\partial T_2^{(32)}}{\partial x} + \frac{\partial T_3^{(32)}}{\partial x} + \frac{\partial T_1^{(41)}}{\partial x} - \frac{\partial T_4^{(41)}}{\partial x}$$

$$\frac{\partial\phi_{00}}{\partial y} = -\frac{\partial T_2^{(32)}}{\partial y} + \frac{\partial T_3^{(32)}}{\partial y} + \frac{\partial T_1^{(41)}}{\partial y} - \frac{\partial T_4^{(41)}}{\partial y} \qquad (7.7.9)$$

$$\frac{\partial\phi_{00}}{\partial z} = -\frac{\partial T_2^{(32)}}{\partial z} + \frac{\partial T_3^{(32)}}{\partial z} + \frac{\partial T_1^{(41)}}{\partial z} - \frac{\partial T_4^{(41)}}{\partial z}$$

$$\frac{\partial\phi_{01}}{\partial x} = -z\,\frac{\partial V_y(\text{source})}{\partial x} + y\,\frac{\partial\phi_{00}}{\partial x}$$

$$\frac{\partial\phi_{01}}{\partial y} = -z\,\frac{\partial V_y(\text{source})}{\partial y} + y\,\frac{\partial\phi_{00}}{\partial y} + V_z(\text{source}) \qquad (7.7.10)$$

$$\frac{\partial\phi_{01}}{\partial z} = -z\,\frac{\partial V_y(\text{source})}{\partial z} + y\,\frac{\partial\phi_{00}}{\partial z} - V_y(\text{source})$$

$$\frac{\partial\phi_{10}}{\partial x} = -z\,\frac{\partial V_x(\text{source})}{\partial x} + x\,\frac{\partial\phi_{00}}{\partial x} + V_z(\text{source})$$

$$\frac{\partial\phi_{10}}{\partial y} = -z\,\frac{\partial V_x(\text{source})}{\partial y} + x\,\frac{\partial\phi_{00}}{\partial y} \qquad (7.7.11)$$

$$\frac{\partial\phi_{10}}{\partial z} = -z\,\frac{\partial V_x(\text{source})}{\partial z} + x\,\frac{\partial\phi_{00}}{\partial z} - V_x(\text{source})$$

Evaluation of the derivatives of ϕ_{11} and ϕ_{02} requires certain auxiliary quantities J_{11} and H_{02} and their derivatives. Thus define

$$\begin{aligned} J_{11} &= \frac{r_3 - r_2}{1 + m_{32}^2} + \frac{r_1 - r_4}{1 + m_{41}^2} \\ &+ \frac{m_{32}}{(1 + m_{32}^2)^{3/2}}\,(x - m_{32}y - b_{32})L^{(32)} \qquad (7.7.12) \\ &- \frac{m_{41}}{(1 + m_{41}^2)^{3/2}}\,(x - m_{41}y - b_{41})L^{(41)} \end{aligned}$$

$$\frac{\partial J_{11}}{\partial x} = \frac{\alpha_3 - \alpha_2}{1 + m_{32}^2} + \frac{m_{32}}{(1 + m_{32}^2)^{3/2}} L^{(32)} + \frac{m_{32}}{(1 + m_{32}^2)^{3/2}} (x - m_{32}y - b_{32}) \frac{\partial L^{(32)}}{\partial x}$$

$$+ \frac{\alpha_1 - \alpha_4}{1 + m_{41}^2} - \frac{m_{41}}{(1 + m_{41}^2)^{3/2}} L^{(41)} - \frac{m_{41}}{(1 + m_{41}^2)^{3/2}} (x - m_{41}y - b_{41}) \frac{\partial L^{(41)}}{\partial x}$$

$$\frac{\partial J_{11}}{\partial y} = \frac{\beta_3 - \beta_2}{1 + m_{32}^2} - \frac{m_{32}^2}{(1 + m_{32}^2)^{3/2}} L^{(32)} + \frac{m_{32}}{(1 + m_{32}^2)^{3/2}} (x - m_{32}y - b_{32}) \frac{\partial L^{(32)}}{\partial y}$$

$$+ \frac{\beta_1 - \beta_4}{1 + m_{41}^2} + \frac{m_{41}^2}{(1 + m_{41}^2)^{3/2}} L^{(41)} - \frac{m_{41}}{(1 + m_{41}^2)^{3/2}} (x - m_{41}y - b_{41}) \frac{\partial L^{(41)}}{\partial y}$$

$$\frac{\partial J_{11}}{\partial z} = \frac{\gamma_3 - \gamma_2}{1 + m_{32}^2} + \frac{m_{32}}{(1 + m_{32}^2)^{3/2}} (x - m_{32}y - b_{32}) \frac{\partial L^{(32)}}{\partial z}$$

$$+ \frac{\gamma_1 - \gamma_4}{1 + m_{41}^2} - \frac{m_{41}}{(1 + m_{41}^2)^{3/2}} (x - m_{41}y - b_{41}) \frac{\partial L^{(41)}}{\partial z}$$

(7.7.13)

Using the above

$$\frac{\partial \phi_{11}}{\partial x} = z \frac{\partial J_{11}}{\partial x} + x \frac{\partial \phi_{01}}{\partial x} + y \frac{\partial \phi_{10}}{\partial x} - xy \frac{\partial \phi_{00}}{\partial x} - zV_y \text{ (source)}$$

$$\frac{\partial \phi_{11}}{\partial y} = z \frac{\partial J_{11}}{\partial y} + x \frac{\partial \phi_{01}}{\partial y} + y \frac{\partial \phi_{10}}{\partial y} - xy \frac{\partial \phi_{00}}{\partial y} - zV_x \text{ (source)} \qquad (7.7.14)$$

$$\frac{\partial \phi_{11}}{\partial z} = z \frac{\partial J_{11}}{\partial z} + x \frac{\partial \phi_{01}}{\partial z} + y \frac{\partial \phi_{10}}{\partial z} - xy \frac{\partial \phi_{00}}{\partial z} + J_{11}$$

Also define

$$H_{02} = m_{32} \frac{r_2 - r_3}{1 + m_{32}^2} + m_{41} \frac{r_4 - r_1}{1 + m_{41}^2}$$

$$+ \frac{1}{(1 + m_{32}^2)^{3/2}} (x - m_{32}y - b_{32}) L^{(32)} \qquad (7.7.15)$$

$$- \frac{1}{(1 + m_{41}^2)^{3/2}} (x - m_{41}y - b_{41}) L^{(41)}$$

$$\frac{\partial H_{02}}{\partial x} = \frac{m_{32}}{1 + m_{32}^2}(\alpha_2 - \alpha_3) + \frac{1}{(1 + m_{32}^2)^{3/2}} L^{(32)} + \frac{(x - m_{32}y - b_{32})}{(1 + m_{32}^2)^{3/2}} \frac{\partial L^{(32)}}{\partial x}$$

$$+ \frac{m_{41}}{1 + m_{41}^2}(\alpha_4 - \alpha_1) - \frac{1}{(1 + m_{41}^2)^{3/2}} L^{(41)} - \frac{(x - m_{41}y - b_{41})}{(1 + m_{41}^2)^{3/2}} \frac{\partial L^{(41)}}{\partial x}$$

$$\frac{\partial H_{02}}{\partial y} = \frac{m_{32}}{1 + m_{32}^2}(\beta_2 - \beta_3) - \frac{m_{32}}{(1 + m_{32}^2)^{3/2}} L^{(32)} + \frac{(x - m_{32}y - b_{32})}{(1 + m_{32}^2)^{3/2}} \frac{\partial L^{(32)}}{\partial y}$$

$$+ \frac{m_{41}}{1 + m_{41}^2}(\beta_4 - \beta_1) + \frac{m_{41}}{(1 + m_{41}^2)^{3/2}} L^{(41)} - \frac{(x - m_{41}y - b_{41})}{(1 + m_{41}^2)^{3/2}} \frac{\partial L^{(41)}}{\partial y}$$

$$\frac{\partial H_{02}}{\partial z} = \frac{m_{32}}{1 + m_{32}^2}(\gamma_2 - \gamma_3) + \frac{(x - m_{32}y - b_{32})}{(1 + m_{32}^2)^{3/2}} \frac{\partial L^{(32)}}{\partial z}$$

$$+ \frac{m_{41}}{1 + m_{41}^2}(\gamma_4 - \gamma_1) - \frac{(x - m_{41}y - b_{41})}{(1 + m_{41}^2)^{3/2}} \frac{\partial L^{(41)}}{\partial z} \qquad (7.7.16)$$

Using the above

$$\frac{\partial \phi_{02}}{\partial x} = z \frac{\partial H_{02}}{\partial x} + 2y \frac{\partial \phi_{01}}{\partial x} - (y^2 + z^2) \frac{\partial \phi_{00}}{\partial x}$$

$$\frac{\partial \phi_{02}}{\partial y} = z \frac{\partial H_{02}}{\partial y} + 2y \frac{\partial \phi_{01}}{\partial y} - (y^2 + z^2) \frac{\partial \phi_{00}}{\partial y} - 2zV_y(\text{source}) \qquad (7.7.17)$$

$$\frac{\partial \phi_{02}}{\partial z} = z \frac{\partial H_{02}}{\partial z} + 2y \frac{\partial \phi_{01}}{\partial z} - (y^2 + z^2) \frac{\partial \phi_{00}}{\partial z} + H_{02} - 2z\phi_{00}$$

7.8 Some Alternate Near-Field Formulas for Use in the Plane of the Element

If the point where the velocity induced by an element is being calculated lies in the plane of the element, i.e., if $z = 0$, there may be numerical difficulties in the evaluation of the formulas of section 7.7 for $\phi_{00} = V_z(\text{source})$ and its z-derivative. To avoid possible difficulty special formulas have been derived for this case.

If

$$|z/t| < 0.001 \tag{7.8.1}$$

the point (x,y,z) is considered to be in the plane of the element and z is set equal to zero. Now $V_z(\text{source})$ is 2π for points inside the element and zero for points outside. Some tests for this condition have encountered problems of numerical significance. The following tests are currently used. First define

$$\begin{aligned} h_{32} &= m_{32}(y - \eta_3) - (x - \xi_3) \\ h_{41} &= m_{41}(y - \eta_1) - (x - \xi_1) \end{aligned} \tag{7.8.2}$$

Then a point is inside the element if all three of the following tests are satisfied and outside if any one is not satisfied.

$$\begin{aligned} r_0/t &< 1/2 \\ h_{32}h_{41} &< 0 \\ (y - \eta_1)(y - \eta_3) &< 0 \end{aligned} \tag{7.8.3}$$

The velocity $V_z(\text{source})$ is simply set equal to 2π or to zero as appropriate.

Numerical difficulty can be encountered in the evaluation of the z-derivative of ϕ_{00} when the point $(x,y,0)$ is on an extension of a side of an element. This condition can be determined by testing the above-defined h's and the $y - \eta$. Specifically, the point is considered to be on a side if any of the following tests are satisfied (refer to figure 20 for element geometry):

$$
\begin{array}{ll}
\text{Point on Side 12 if} & |y - \eta_1|/t < 0.001 \\
\text{Point on Side 23 if} & |h_{32}|/t < 0.001 \\
\text{Point on Side 34 if} & |y - \eta_3|/t < 0.001 \\
\text{Point on Side 41 if} & |h_{41}|/t < 0.001
\end{array} \tag{7.8.4}
$$

If none of the above tests are satisfied, the formulas of section 7.7 are used for the z-derivative of ϕ_{00}. Only one of the conditions (7.8.4) can be true. If this occurs, then the following substitution is made in equation (7.7.9).

$$
\begin{array}{ll}
\text{Side 12:} & -\dfrac{\partial T_2^{(32)}}{\partial z} + \dfrac{\partial T_1^{(41)}}{\partial z} = \dfrac{m_{41}}{|x - \xi_1|} - \dfrac{m_{32}}{|x - \xi_2|} \\[2ex]
\text{Side 23:} & -\dfrac{\partial T_2^{(32)}}{\partial z} + \dfrac{\partial T_3^{(32)}}{\partial z} = \dfrac{m_{32}}{\sqrt{1 + m_{32}^2}}\left(\dfrac{1}{|y - \eta_3|} - \dfrac{1}{|y - \eta_1|}\right) \\[2ex]
\text{Side 34:} & \dfrac{\partial T_3^{(32)}}{\partial z} - \dfrac{\partial T_4^{(41)}}{\partial z} = \dfrac{m_{32}}{|x - \xi_3|} - \dfrac{m_{41}}{|x - \xi_4|} \\[2ex]
\text{Side 41:} & \dfrac{\partial T_1^{(41)}}{\partial z} - \dfrac{\partial T_4^{(41)}}{\partial z} = \dfrac{m_{41}}{\sqrt{1 + m_{41}^2}}\left(\dfrac{1}{|y - \eta_1|} - \dfrac{1}{|y - \eta_3|}\right)
\end{array} \tag{7.8.5}
$$

The remaining two T derivatives of equation (7.7.9) are evaluated by the formulas of section 7.7.

7.9 The Velocity Induced by a Wake Element

In the wake the dipole strength is constant along N-lines, as illustrated in figure 21. The form of the dipole distribution on a wake element is obtained by setting $B_F = B_S = 0$ in equation (7.3.7). Specifically,

$$
\mu = \frac{1}{W}\left[(A_F - A_S)\eta + A_S\eta_1 - A_F\eta_3\right] + C(\eta - \eta_3)(\eta - \eta_1) \tag{7.9.1}
$$

Denote by L (total) the total arc length along an N-line from the trailing edge around the section curve of the body and back to the trailing edge. This arc length is computed in a manner similar to (7.2.23), namely

$$\begin{aligned} L_F \text{ (total)} &= \sum d_F \\ L_S \text{ (total)} &= \sum d_S \end{aligned} \tag{7.9.2}$$

where the sums are over all on-body lifting elements of the strip lying between the two N-lines. Now from the form of the dipole distribution shown in figure 21 it is clear that the constant values A_F and A_S assumed along the N-lines in the wake are equal to

$$\begin{aligned} A_F &= B_F L_F \text{ (total)} \\ A_S &= B_S L_S \text{ (total)} \end{aligned} \tag{7.9.3}$$

Thus, velocity potential due to a wake element has the form

$$\phi = \phi_F B_F - \phi_S B_S \tag{7.9.4}$$

just as in equation (7.4.5). Here, however,

$$\begin{aligned} \phi_F &= \frac{1}{w} [\phi_{01} - \eta_3 \phi_{00}] L_F \text{ (total)} + c\phi_c \\ \phi_S &= \frac{1}{w} [\phi_{01} - \eta_1 \phi_{00}] L_S \text{ (total)} + c\phi_c \\ \phi_c &= \phi_{02} - (\eta_1 + \eta_3)\phi_{01} + \eta_1 \eta_3 \phi_{00} \end{aligned} \tag{7.9.5}$$

These replace (7.4.6). The dipole velocity is given as before (see (7.4.7), (7.4.9), and (7.4.10) by

$$\vec{V}_{ij} = -\nabla\phi = B_F \vec{V}_{ij}^{(F)} + B_S \vec{V}_{ij}^{(S)} \tag{7.9.6}$$

where

$$\vec{V}_{ij}^{(F)} = -\nabla\phi_F, \qquad \vec{V}_{ij}^{(S)} = +\nabla\phi_S \tag{7.9.7}$$

To evaluate (7.9.6) in the near and intermediate field, the derivatives of ϕ_{02}, ϕ_{01}, and ϕ_{00} are evaluated by the formulas of sections 7.7 and 7.8.

In the far field the formulas for the dipole velocities due to a wake element are

$$\vec{V}_{ij}^{(F)} = -Q_F \vec{D} \qquad \vec{V}_{ij}^{(S)} = Q_S \vec{D} \tag{7.9.8}$$

where

$$Q_F = -\frac{t^2}{w}\frac{I_{00}}{r_o^3} n_3 L_F(\text{tot}) \qquad Q_S = -\frac{t^2}{w}\frac{I_{00}}{r_o^3} n_1 L_S(\text{tot}) \tag{7.9.9}$$

and where as before (see (7.5.7))

$$\vec{D} = -\left[3\left(\frac{\vec{n}\cdot\vec{r}_o}{r_o}\right)\frac{\vec{r}_o}{r_o} - \vec{n}\right] \tag{7.9.10}$$

There is no source density on wake elements and no source velocities are computed.

As discussed in section 7.3.4, the values of c on wake elements are not zero if the "piecewise linear" option for bound vorticity is used. Instead, the value of c on the first wake element is determined to avoid a discontinuity in dipole strength at the trailing edge. Values of c on the remaining wake elements are chosen to eliminate discontinuities between adjacent wake elements along the lifting strip. Let superscript (1) denote quantities associated with the first on-body element of a lifting strip and superscript u denote quantities associated with the last on-body element of the strip. Similarly, the superscripts w1, w2, etc. denote the first wake element, second wake element, etc. of the same lifting strip. The important value of c is $c^{(w1)}$, i.e., the one for the first wake element. It is computed from

$$c^{(w1)} = \frac{w^{(u)}[w^{(u)}c^{(u)} + m_{32}^{(u)}] - w^{(1)}[w^{(1)}c^{(1)} + m_{41}^{(1)}]}{[w^{(w1)}]^2} \tag{7.9.11}$$

where the quantities w, m_{32}, m_{41} have their usual meaning. Values of c for the remaining wake elements are obtained from

$$c^{(w1)}[w^{(w1)}]^2 = c^{(w2)}[w^{(w2)}]^2 = c^{(w3)}[w^{(w3)}]^2 = \quad . \; . \; . \tag{7.9.12}$$

7.10 Option for a Semi-Infinite Last Wake Element

In most cases of interest the trailing vortex wake extends to infinity. To facilitate accounting for this condition, provision has been made for considering the last element of the wake to be semi-infinite. A finite element of the sort shown in figure 20 is formed at the end of the wake, including all the geometric quantities of section 7.2. The induced velocity calculation for this element is performed using the origin of coordinates appropriate to the finite element, but the formulas used to calculate induced velocities are appropriate for the semi-infinite element. Naturally, all points in space are in the "near field" with respect to a semi-infinite element, so it is the formulas of section 7.7 that apply. These formulas are modified by setting

$$m_{32} = 0 \tag{7.10.1}$$

$$\xi_2 \to \infty \qquad\qquad \xi_3 \to \infty$$

This yields immediately

$$\alpha_1,\ \beta_1,\ \gamma_1,\ \alpha_4,\ \beta_4,\ \gamma_4 \text{ unchanged} \tag{7.10.2}$$

$$\alpha_3 = \alpha_2 = -1, \qquad\qquad \beta_3 = \beta_2 = \gamma_3 = \gamma_2 = 0$$

The log functions (7.7.3) and their derivatives (7.7.6) are replaced by

$$L^{(41)} = \text{unchanged, all derivatives unchanged} \tag{7.10.3}$$

$$L^{(32)} = 0, \quad \text{all derivatives equal zero}$$

$$-L^{(12)} + L^{(34)} = \log \frac{r_4 - (x - \xi_4)}{r_1 - (x - \xi_1)} \tag{7.10.4}$$

$$\frac{\partial L^{(34)}}{\partial x} = \frac{\alpha_4 - 1}{r_4 - (x - \xi_4)} \qquad \frac{\partial L^{(12)}}{\partial x} = \frac{\alpha_1 - 1}{r_1 - (x - \xi_1)}$$

$$\frac{\partial L^{(34)}}{\partial y} = \frac{\beta_4}{r_4 - (x - \xi_4)} \qquad \frac{\partial L^{(12)}}{\partial y} = \frac{\beta_1}{r_1 - (x - \xi_1)} \tag{7.10.5}$$

$$\frac{\partial L^{(34)}}{\partial z} = \frac{\gamma_4}{r_4 - (x - \xi_4)} \qquad \frac{\partial L^{(12)}}{\partial z} = \frac{\gamma_1}{r_1 - (x - \xi_1)}$$

[illegible]

$$[illegible] = \text{unchanged}$$

$$[illegible]$$

$$[illegible]$$

$$[illegible]$$

$$\frac{\partial \phi_s^{(41)}}{\partial x} = \text{unchanged}$$

$$\frac{\partial \phi_s^{(41)}}{\partial y} = \text{unchanged}$$

$$\frac{\partial \phi_s^{(41)}}{\partial z} = \text{unchanged}$$

All of the quantities of section [illegible] are now recalculated using these modified values, except that M_{02} is replaced by

$$M_{02} = m_{41}\,\frac{r_4 - r_1}{1 + m_{41}^2} \quad [illegible] \quad \frac{[illegible]\; m_{41}y - b_{41}}{(1 + m_{41}^2)^{1/2}} \quad [illegible]$$

The induced velocities from the last wake element are added to the other [illegible] velocities of the lifting strip in the ordinary way.

7.11 Formation of the Vorticity Onset Flows

As described in section 7.4 the induced velocity calculation for each lifting element produces three vector velocities at each on-body control point and at each off-body point. These are the source velocity $\vec{V}_{ij}$ and the dipole velocities $\vec{V}_{ij}^{(F)}$ and $\vec{V}_{ij}^{(S)}$. Nonlifting elements have only the first of these. Wake elements, "ignored" elements and elements of "extra strips" have only the second and third. In symmetry cases all three velocities consist of the sum of the effects of the basic element and the elements obtained by reflecting the basic one in the symmetry planes (section [illegible]).

The source velocities are stored individually to yield an $N \times N$ matrix and and $O \times N$ matrix, where N is the number of on-body control points at which the normal-velocity boundary condition is applied and O is the number of off-body points. The dipole velocities, however, are not saved individually but are summed over each lifting strip. Specifically,

$$
\left.
\begin{aligned}
\vec{V}_{ik}^{(F)} &= \sum_{j}^{\text{strip } k} \vec{V}_{ij}^{(F)} \\
\vec{V}_{ik}^{(S)} &= \sum_{j}^{\text{strip } k} \vec{V}_{ij}^{(S)}
\end{aligned}
\right\}
\quad k = 1, 2, \ldots, L
\qquad (7.11.1)
$$

where L is the number of lifting strips. The summations of (7.11.1) are over a complete lifting strip including the wake elements. If a lifting section begins with an "extra strip" (section 6.8), both velocities $\vec{V}_{ik}^{(F)}$ and $\vec{V}_{ik}^{(S)}$ for the extra strip are added to the velocity $\vec{V}_{ik}^{(F)}$ corresponding to the first ordinary lifting strip of the section. Similarly, if the last strip of a lifting section is an extra strip, both velocities for the extra strip are added to the $\vec{V}_{ik}^{(S)}$ of the last ordinary lifting strip of the section. (This gives a dipole strength on the lifting strip that is constant at a value equal to that attained on the adjacent lifting strip along the common N-line of the two strips.) Thus, the calculation of (7.11.1) gives an $N \times L$ matrix of on-body velocities at the control points and an $O \times L$ matrix of velocities at off-body points, where L refers to ordinary lifting strips only. Since L is small compared to N, these matrices are small compared to the source-velocity matrices. Each of the velocities (7.11.1) represents the velocity due to a dipole distribution on the strip that is unity on one N-line and zero on the other with a linear "spanwise" variation in between.

The characteristic onset flow velocities due to a strip are

$$\vec{V}_{ik}^{(0)} = \vec{V}_{ik}^{(S)} + \vec{V}_{ik}^{(F)}$$

$$\vec{V}_{ik}^{(1)} = \frac{1}{2}\,[\vec{V}_{ik}^{(S)} - \vec{V}_{ik}^{(F)}] \qquad (7.11.2)$$

The first velocity of (7.11.2) is that due a dipole distribution on the strip that is constant in the "spanwise" direction. The second velocity is that due to a dipole distribution that varies linearlly in the "spanwise" direction and has zero value at "midspan ". These velocities are used to form the basic circulatory onset flows $\vec{V}_i^{(k)}$.

If the "step function" option for bound vorticity is used (section 6.3), the proper form of the dipole distribution is simply constant in the "spanwise" direction over a lifting strip, and the velocity $\vec{V}_{ik}^{(0)}$ is precisely the onset flow. Thus, for this option, the vorticity onset flows are

$$\vec{V}_i^{(k)} = \vec{V}_{ik}^{(0)}\,, \qquad k = 1,\ 2,\ \ldots,\ L \qquad (7.11.3)$$

The above yields L onset flows, each of which corresponds to a unit value of the "streamwise" dipole derivative B on one lifting strip and zero values of B on all other lifting strips. (Recall that the "streamwise" derivative of dipole strength is essentially the value of the bound vorticity.) No special handling is required at the ends of the lifting section.

The machinery for the "piecewise linear" option for bound vorticity is somewhat more complicated. The "spanwise" variation of the "streamwise" dipole derivative B (bound vorticity) is linear in the "spanwise" direction across a lifting strip. Thus, the velocity at the i-th point (control point or off-body point) due to the k-th strip is

$$\vec{V}_i\ (\text{strip } k) = \vec{V}_{ik}^{(0)}\ B_k + w_k \vec{V}_{ik}^{(1)}\ B_k' \qquad (7.11.4)$$

where w_k is the "spanwise" width of the strip, B' is the "spanwise" derivative of B, and subscripts k denote quantities associated with the k-th lifting strip. The derivative B_k' is evaluated by a parabolic fit through B_{k-1}, B_k, and B_{k+1}. Specifically, define

$$D_k = -\frac{w_k}{w_k + 1/2(w_{k-1} + w_{k+1})}\left[\frac{w_k + w_{k+1}}{w_k + w_{k-1}}\right]$$

$$E_k = \frac{w_k}{w_k + 1/2(w_{k-1} + w_{k+1})}\left[\frac{w_k + w_{k+1}}{w_k + w_{k-1}} - \frac{w_k + w_{k-1}}{w_k + w_{k+1}}\right] \qquad (7\ 11.5)$$

$$F_k = \frac{w_k}{w_k + 1/2(w_{k-1} + w_{k+1})}\left[\frac{w_k + w_{k-1}}{w_k + w_{k+1}}\right]$$

Then (7.11.4) is approximated numerically by

$$\bar{V}_i\ (\text{strip } k) = \bar{V}_{ik}^{(0)}B_k + \bar{V}_{ik}^{(1)}\ [D_kB_{k-1} + E_kB_k + F_kB_{k+1}] \qquad (7.11.6)$$

The velocity (7.11.6) contains values of the "streamwise" dipole derivative B for three consecutive strips. However, a proper circulatory onset flow is proportional to the value of B on a single strip. Since each B_k enters $\bar{V}_i$ (strip k) for three consecutive strips, its three contributions may be summed to give the basic vorticity onset flow.

$$\bar{V}_i^{(k)} = \bar{V}_{ik}^{(0)} + \bar{V}_{i,k-1}^{(1)}F_{k-1} + \bar{V}_{ik}^{(1)}E_k + \bar{V}_{i,k+1}^{(1)}D_{k+1} \qquad (7.11.7)$$

In performing the above parabolic fit (7.1..6), the values of the function B to be fit are of course the values of bound vorticity on the strips. Each of these has been associated with an abscissa or "independent variable" that expresses the spanwise position of each strip. Differences of these abscissas appear as combinations of the widths w_k. Calculation of the w_k is not obvious, because in general the "span" or width of each strip is not constant but varies in the "chordwise" direction. Accordingly, it was decided to input the quantities necessary to deduce the spanwise positions of the lifting strips. The input quantities consist of a set of widths w_k for all lifting strips. If a strip is truly of constant width, it is natural to input that width. If the strip varies in width, some average value must be input as where w_k is the "spanwise" width of the strip, B' is the "spanwise" derivative of B, and subscripts k denote quantities associated with the k-th lifting strip. The derivative B'_k is evaluated by a parabolic fit through B_{k-1}, B_k, and B_{k+1}. Specifically, define

$$D_k = -\frac{w_k}{w_k + 1/2(w_{k-1} + w_{k+1})}\left[\frac{w_k + w_{k+1}}{w_k + w_{k-1}}\right]$$

$$E_k = \frac{w_k}{w_k + 1/2(w_{k-1} + w_{k+1})}\left[\frac{w_k + w_{k+1}}{w_k + w_{k-1}} - \frac{w_k + w_{k-1}}{w_k + w_{k+1}}\right] \tag{7.11.5}$$

$$F_k = \frac{w_k}{w_k + 1/2(w_{k-1} + w_{k+1})}\left[\frac{w_k + w_{k-1}}{w_k + w_{k+1}}\right]$$

Then (7.11.4) is approximated numerically by

$$\vec{V}_i \text{ (strip } k) = \vec{V}_{ik}^{(0)} B_k + \vec{V}_{ik}^{(1)} [D_k B_{k-1} + E_k B_k + F_k B_{k+1}] \tag{7.11.6}$$

The velocity (7.11.6) contains values of the "streamwise" dipole derivative B for three consecutive strips. However, a proper circulatory onset flow is proportional to the value of B on a single strip. Since each B_k enters $\vec{V}_i$ (strip k) for three consecutive strips, its three contributions may be summed to give the basic vorticity onset flow.

$$\vec{V}_i^{(k)} = \vec{V}_{ik}^{(0)} + \vec{V}_{i,k-1}^{(1)} F_{k-1} + \vec{V}_{ik}^{(1)} E_k + \vec{V}_{i,k+1}^{(1)} D_{k+1} \tag{7.11.7}$$

In performing the above parabolic fit (7.11.6), the values of the function B to be fit are of course the values of bound vorticity on the strips. Each of these has been associated with an abscissa or "independent variable" that expresses the spanwise position of each strip. Differences of these abscissas appear as combinations of the widths w_k. Calculation of the w_k is not obvious, because in general the "span" or width of each strip is not constant but varies in the "chordwise" direction. Accordingly, it was decided to input the quantities necessary to deduce the spanwise positions of the lifting strips. The input quantities consist of a set of widths w_k for all lifting strips. If a strip is truly of constant width, it is natural to input that width. If the strip varies in width, some average value must be input as the w_k for that strip, and this average is decided upon by the user. These w_k are used only in performing the parabolic fit. To facilitate fitting at the first and last strips of a lifting section, it was decided originally to input widths for ficticious strips adjacent to the first and last strips of the section. Thus, if the strips of a lifting section were input from left to right, the table of w_k would consist of the following sequence: a value of w_k for a ficticious strip to the left of the first lifting strip, the values of w_k for the lifting strips of the section in order from left to right, and finally a value of w_k for a ficticious strip to the right of the last strip of the section. Thus, if the section has L lifting strips, $L + 2$ values of w_k are input. This is still the format of the input. However, for certain frequently-occurring situations, the program overrides the input and puts in a predetermined value of w_k. In fact, it is only for the "extra strip" condition described below that input values of w_k corresponding to ficticious strips are actually used in the calculations.

Physically, a lifting section may end in various ways, some of which involve logical difficulties in the basic potential-flow model (section 5.3). The various ways a lifting section may end require various procedures for performing the parabolic fit of the piecewise-linear vorticity option. These procedures are outlined below. In future work perhaps still other procedures will be required for situations that are unanticipated at present.

Sometimes a single lifting portion of a three-dimensional configuration is divided into two or more lifting sections. This may be done to concentrate elements in a certain region, as shown in figure 23, or it may be done simply for convenience. In this case the division into sections is purely logical rather than physical, and the bound vorticity distribution should vary smoothly from one section to another. As regards the parabolic fit, the last lifting strip of the first section and first lifting strip of the second should be regarded as adjacent strips of a single lifting section and the fit performed accordingly. This situation has been designated "continue" in the method.

If the lifting section has a physical ending in the fluid, such as a wing tip, the bound vorticity strength must fall to zero. A ficticious logical

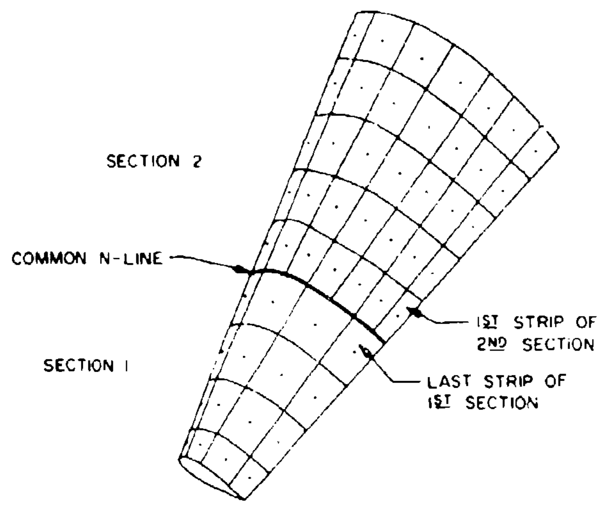

Figure 23. An example of division of a single physical lifting portion of a body into two lifting sections.

strip is imagined adjacent to the tip in the fluid (figure 24a). The bound vorticity slope at the midspan of the strip of elements adjacent to the tip (figure 24) is obtained by fitting a parabola through the value on the strip itself, the value on the next strip inboard, and a zero value at the midspan of the ficticious logical strip. Various assumptions about the width of the ficticious logical strip were tried, and it was concluded that taking its width equal to that of the lifting strip adjacent to the tip is about as good a choice as any, and this has been built into the program as an override to any input value. A zero width of the ficticious strip has a certain appeal, because in the limit of infinite element number the bound vorticity must be zero right at the tip. However, this choice leads to poor results. This type of end to a lifting section is denoted "normal."

If a lifting section ends at a positive symmetry plane of the flow (figure 24b), the proper procedure is obvious. Physically, there is a strip adjacent to the last strip of the section on the other side of the symmetry plane, and these two strips have equal widths and equal values of bound vorticity. The parabolic fit is performed accordingly.

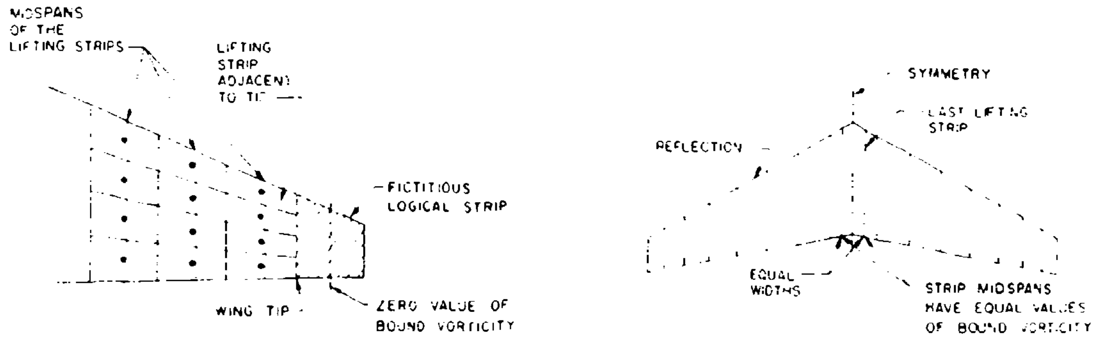

(a) (b)

Figure 24. Special procedures at the ends of a lifting section for the parabolic fit used with the piecewise linear vorticity option. (a) Wing tip. (b) Positive symmetry plane.

If there is an extra strip of elements adjacent to the end of a lifting section, as described in section 6.4, the width of the extra strip is input as the last (or first) w_k of that section and used in the parabolic fit. For purposes of determining the parabola, the value of bound vorticity on the extra strip is taken as equal to the value at the midspan of the last ordinary lifting strip of the section, even though this is not strictly true unless the slope of the bound vorticity on the last ordinary strip is zero.

7.12 The Linear Equations for the Values of Surface Source Density

A dot product is taken of each source velocity $\vec{V}_{ij}$ at each on-body control point, $i = 1, 2, \ldots, N$, with the unit normal vector of the surface element containing the control point. Specifically,

$$A_{ij} = \vec{n}_i \cdot \vec{V}_{ij} \qquad \begin{array}{l} i = 1, 2, \ldots, N \\ j = 1, 2, \ldots, N \end{array} \qquad (7.12.1)$$

The scalar $N \times N$ matrix A_{ij} represents the normal velocities at the control points due to unit values of source density σ on the elements.

The quantities

$$\sum_{j=1}^{N} A_{ij}\sigma_j \qquad i = 1, 2, \ldots, N \qquad (7.12.2)$$

where the source densities σ_j are as yet unknown, are the normal velocities at the control points due to the entire surface source distribution. For the usual condition of zero normal velocity at the control points (7.12.2) must be set equal to the negative of the normal velocities due to the onset flow. This is done for each onset flow. Normal components of the basic circulatory onset flows (7.11.3) or (7.11.7) are obtained by taking dot products with the unit normal vectors in a manner similar to (7.12.1), i.e.,

$$N_i^{(k)} = \bar{n}_i \cdot \bar{V}_i^{(k)} \qquad k = 1, 2, \ldots, L \qquad (7.12.3)$$

where L is the number of lifting strips. The same is done for the uniform onset flow $\bar{V}_\infty$, i.e.,

$$N_i^{(\infty)} = \bar{n}_i \cdot \bar{V}_\infty \qquad (7.12.4)$$

As discussed in section 6.7 more than one uniform onset flow may be considered simultaneously, in which case there is an $N_i^{(\infty)}$ for each of them.

The linear equations that yield the values of source density on the elements are

$$\sum_{j=1}^{N} A_{ij}\sigma_j^{(k)} = -N_i^{(k)} \qquad \begin{array}{l} i = 1, 2, \ldots, N \\ k = 1, 2, \ldots, L, \infty \end{array} \qquad (7.12.5)$$

These are solved by a direct elimination procedure. There is a set of N values of σ_j for each onset flow, including all uniform onset flows.

7.13 Application of the Kutta Condition

For each uniform onset flow a single combined set of source densities is calculated from

$$\sigma_j = \sigma_j^{(\infty)} + \sum_{k=1}^{L} B^{(k)}\sigma_j^{(k)} \qquad j = 1, 2, \ldots, N \qquad (7.13.1)$$

where L is the number of lifting strips and where the $B^{(k)}$ are as yet unknown. The combination constants $B^{(k)}$ are the values of the streamwise dipole derivative (bound vorticity) on the lifting strips. Similarly there is a single combined onset flow

$$\vec{V}_i^{(0)} = \vec{V}_i^{(\infty)} + \sum_{k=1}^{L} B^{(k)}\vec{V}_i^{(k)} \qquad i = 1, 2, \ldots, N + 0 \qquad (7.13.2)$$

The total velocity at any point is

$$\begin{aligned} \vec{V}_i &= \sum_{j=1}^{N} \vec{V}_{ij}\sigma_j + \vec{V}_i^{(0)} \\ &= \vec{v}_i^{(\infty)} + \sum_{k=1}^{L} B^{(k)}\vec{v}_i^{(k)} \end{aligned} \qquad i = 1, 2, \ldots, N + 0 \qquad (7.13.3)$$

where the velocities

$$\begin{aligned} \vec{v}_i^{(\infty)} &= \sum_{j=1}^{N} \vec{V}_{ij}\sigma_j^{(\infty)} + \vec{V}_\infty \\ \vec{v}_i^{(k)} &= \sum_{j=1}^{N} \vec{V}_{ij}\sigma_j^{(k)} + \vec{V}_i^{(k)} \qquad k = 1, 2, \ldots, L \end{aligned} \qquad (7.13.4)$$

are the velocities at the control points for the individual onset flows. It is important to point out that velocities (7.13.4) are calculated only for the points where the Kutta condition is to be applied. Only the velocity (7.13.3) is evaluated at all points.

As mentioned in section 6.5, there are two rather different means of applying the Kutta condition.

7.13.1 Flow Tangency in the Wake

The first method for applying the Kutta condition is based on property (a) of section 6.5, i.e., the condition that a stream surface of the flow leave the body at the trailing edge. This is implemented by inputting L

points and L normal vectors. The points are considered to be the first L off-body points, and both points and normal vectors are designated by subscripts $i = N + 1, N + 2, \ldots, N + L$. The total velocity at these points is given by (7.13.3) for these values of i. The dot product of each velocity is taken with the corresponding input normal vector, which is presumed to be the unit normal vector to the stream surface. The results are set equal to zero, i.e.,

$$\vec{n}_i \cdot \vec{V}_i = \vec{n}_i \cdot \vec{v}_i^{(\infty)} + \sum_{k=1}^{L} B^{(k)} \vec{n}_i \cdot \vec{v}_i^{(k)} = 0$$

$$i = N + 1, \ldots, N + L \qquad (7.13.5)$$

Thus, there are L linear equations for the L unknown values $B^{(k)}$, namely

$$\sum_{k=1}^{L} D_{ik} B^{(k)} = -D_{i\infty} \qquad i = N + 1, \ldots, N + L \qquad (7.13.6)$$

where

$$\begin{aligned} D_{ik} &= \vec{n}_i \cdot \vec{v}_i^{(k)} \qquad & k = 1, 2, \ldots, L \\ D_{i\infty} &= \vec{n}_i \cdot \vec{v}_i^{(\infty)} \qquad & i = N + 1, \ldots, N + L \end{aligned} \qquad (7.13.7)$$

If more than one uniform onset flow is considered, the same matrix D_{ik} applies to all of them. Only the $D_{i\infty}$ are different.

7.13.2 Pressure Equality on Upper and Lower Surface at the Trailing Edge

The second method of applying the Kutta condition is based on property (b) of section 6.5, i.e., the condition that the pressures be equal at the two control points of each strip that are adjacent to the trailing edge. The pressure at any point is uniquely determined by the square of the velocity magnitude, which is

$$\begin{aligned} V_i^2 = \vec{V}_i \cdot \vec{V}_i &= (\vec{v}_i^{(\infty)} \cdot \vec{v}_i^{(\infty)}) + 2 \sum_{k=1}^{L} (\vec{v}_i^{(\infty)} \cdot \vec{v}_i^{(k)}) B^{(k)} \\ &+ \sum_{k=1}^{L} \sum_{m=1}^{L} (\vec{v}_i^{(k)} \cdot \vec{v}_i^{(m)}) B^{(k)} B^{(m)} = M_i^2 + 2 \sum_{k=1}^{L} M_{ik} B^{(k)} \\ &+ \sum_{k=1}^{L} \sum_{m=1}^{L} M_{ikm} B^{(k)} B^{(m)} \end{aligned} \qquad (7.13.8)$$

where the M's are defined by equation (7.13.8). Now let the integer q denote the lifting strip, i.e., $q = 1, 2, \ldots, L$, and define

$$H_{qkm} = M_{ikm} \quad \text{(at control point adjacent to trailing edge of q-th strip on upper surface)}$$
$$\qquad\qquad -M_{ikm} \quad \text{(at control point adjacent to trailing edge of q-th strip on lower surface)} \tag{7.13.9}$$

Similarly define

$$\begin{aligned} H_{q\infty k} &= M_{i\infty k} \text{ (upper q-th)} - M_{i\infty k} \text{ (lower q-th)} \\ H_{q\infty} &= M_{i\infty}^2 \text{ (upper q-th)} - M_{i\infty}^2 \text{ (lower q-th)} \end{aligned} \tag{7.13.10}$$

where the expressions in parentheses in (7.13.10) are intended to be abbreviations of the parentheses in (7.13.9). With this notation, the equal-pressure condition is

$$P_q = \sum_{k=1}^{L} \sum_{m=1}^{L} H_{qkm} B^{(k)} B^{(m)} + 2 \sum_{k=1}^{L} H_{q\infty k} B^{(k)} + H_{q\infty} = 0 \qquad q = 1, 2, \ldots, L \tag{7.13.11}$$

This represents L quadratic equations in the L unknown values of $B^{(k)}$. The method of solution is a Newton-Raphson iterative procedure. Define the derivative

$$G_{qk} = \frac{\partial P_q}{\partial B^{(k)}} = 2 \sum_{m=1}^{L} H_{qkm} B^{(m)} + 2H_{q\infty k} \qquad \begin{matrix} q = 1, 2, \ldots, L \\ k = 1, 2, \ldots, L \end{matrix} \tag{7.13.12}$$

Then (7.13.11) is solved iteratively by solving successive sets of linear equations for the changes $\Delta B^{(k)}$ in the values of $B^{(k)}$. Namely,

$$\sum_{k=1}^{L} G_{qk} \Delta B^{(k)} = -P_q \qquad q = 1, 2, \ldots, L \tag{7.13.13}$$

At any stage G_{qk} and P_q are evaluated using the $B^{(k)}$ from the previous iteration. Then (7.13.13) is solved and new $B^{(k)}$ computed by adding $\Delta B^{(k)}$ to the previous values. The rate of convergence of this process or even the existence of convergence, cannot be proven on theoretical grounds. However, in virtually all cases convergence of this iterative process has been very rapid. There can be difficulties, however, in extreme cases (see section 8.8). If difficulties should arise in the future perhaps (7.13.11) should be solved by a different iterative procedure than that represented by (7.13.13). In any event the procedure of section 7.13.1 can be used with confidence since no iteration is involved.

If several uniform onset flows are considered, the same H_{qkm} applies to all of them.

7.14 Final Flow Computation

Once the $B^{(k)}$ are known, a single set of source densities (for each uniform onset flow) is computed from (7.13.1) and a single onset flow from (7.13.2). Then flow velocities at the on-body control points and off-body points are computed from (7.13.3). Pressure coefficients at control points are computed from

$$C_{pi} = 1 - V_i^2 \tag{7.14.1}$$

Forces and moments are computed by assuming the pressure to be constant over each element. If S_i denotes the area of the i-th element, the force on this element is

$$\vec{F}_i = -\vec{n}_i C_{pi} S_i \tag{7.14.2}$$

and the moment of the force on the element is

$$\vec{M}_i = \vec{r}_i \times \vec{F}_i \tag{7.14.3}$$

where $\vec{r}_i$ represents the vector displacement of the control point of the element from an input moment reference point. With the above assumption forces and moments on the body are obtained by simple summation

$$\begin{aligned} \vec{F} &= \sum_i \vec{F}_i \\ \vec{M} &= \sum_i \vec{M}_i \end{aligned} \tag{7.14.4}$$

Various ranges of summation are used in (7.14.4) so that forces and moments on different parts of the configuration may be calculated. In particular (7.14.4) is performed for: each nonlifting section; each lifting strip; each lifting section; and all elements of the entire case.

7.15 Computation Time, Effort, and Cost

In the past when computing machines executed one program at a time, computation time, effort, and cost had definite and agreed-upon meanings. The total elapsed time necessary to execute the program was measured, and this was charged to the user at a rate of a certain amount of money per hour. Thus, computation time and cost were simply proportional. Computational effort was slightly less direct, since elapsed time included all necessary inputs and outputs and certain other operations in addition to straightforward arithmetic and logic. Nevertheless, it was customary simply to define computational effort as the time required to execute. Thus, program descriptions customarily reported computing times, but by implicit assumption they were also defining computational effort and cost.

The situation was changed considerably by the widespread use of computer systems that process several unrelated programs simultaneously. Computing time, effort, and cost are no longer essentially identical; and indeed their precise relationship cannot be specified, except possibly in terms of a particular computing facility. Generally, the time the so-called central processing unit spends on a particular program is recorded. This "CPU time" is that required for the arithmetic and logic of the program. From CPU time an imaginary "computing time" is calculated by an arbitrary formula that accounts for the number of inputs and outputs. Finally, cost is determined by multiplying "computing time" by a rate that depends in a complicated way upon the fraction of the total capacity of the computer that is engaged on that particular problem, i.e., how much high-speed core storage is required, how many low-speed tape or disk units are used, etc. The relationship between CPU time and "computing time" varies from facility to facility, as does the formula for computing cost from "computing time." Thus, no general statements can be made. A change in the accounting procedure can significantly alter the cost of a computer run. A program that is optimized for one accounting procedure may perform poorly on another. Often the use of less high-speed storage will result in increases in computing time and effort but a decrease in cost.

While nothing definite can be said, still there is a need for some simple, commonly-accepted measure of the size of a program. It has become fairly common to use CPU time for this measure. There are many valid objections to this, but no other quantity is more acceptable. It should always be remembered that CPU time is merely a rough guide to the order of magnitude of the program. For the present application CPU times are given for the IBM 370-165 computer.

Below are CPU times obtained for typical cases, all of which had one plane of symmetry, which was accounted for in the calculations. The element number N refers to those describing one half of the body.

Element Number N	CPU Time in Minutes
250	1.7
500	6
650	12
950	30

The times for the lower element numbers are quite acceptable. The rapid increase in CPU time with element number for the larger cases is presumably due to the use of a direct solution for solving the simultaneous equations. Clearly an iterative solution should be used for $N > 1000$, and probably for $N > 800$. On the other hand, the direct solution is seen to be very efficient for $N < 500$ and probably should be used for $N < 700$.

8.0 NUMERICAL EXPERIMENTS TO ILLUSTRATE VARIOUS ASPECTS OF THE METHOD

8.1 Element Number on an Isolated Lifting Wing

It is important in three-dimensional problems to be able to estimate element numbers that make the error in the potential flow calculation consistent with the errors inherent in the approximation of a real flow by a potential flow, e.g., errors due to neglect of compressibility or viscosity. Too small an element number may give useless results, while too large an element number leads to a needlessly large computing time. For good accuracy, complicated three-dimensional geometries require more elements than any program makes available and would require very long computation times. For such cases the decision regarding element number is an easy one; simply use the maximum permissible number of elements and accept a lesser accuracy. For simpler cases a study of the matter may prove worthwhile. In the course of developing the present method some studies of this type were conducted. The results are included here in the hope that they will be of value to future users. Obviously, only a few cases could be studied in detail. If a design application involves many cases of similar geometry, an element-number study for that particular geometry should be conducted by the user before proceeding.

The simplest case is that of an isolated wing. Two questions must be answered. How many lifting strips should be placed across the span of the wing? How many lifting elements should lie on each strip? The second of these questions can be answered by running two-dimensional cases using the method of reference 1. These cases are, of course, very fast and cheap compared to the three-dimensional cases that must be run to answer the first question. For this investigation, as well as some others to be discussed below, the geometry chosen was an untwisted wing, which is described fully in reference 12. The planform is shown in figure 25, and the airfoil shape in sections parallel to the symmetry plane of the wing is symmetric and is 7.6 percent thick. Two-dimensional considerations lead to the use of 30 lifting elements on each strip – 15 on each of the upper and lower surfaces. This appears to be about a minimum number for acceptable accuracy, but on the other hand it appears sufficient for most applications.

Calculations were performed for this wing with various numbers of lifting strips. Four of the cases are shown in figure 25. They range from 6 to 20 lifting strips on the right half of the wing. In comparing solutions the quantity used is the local section lift coefficient as a function of spanwise location. This quantity is obtained from a numerical integration of the calculated pressure, which is assumed to be constant over each surface element. As explained in section 9.1, this quantity is considerably more sensitive than pressure distribution in the sense that two pressure distributions that appear nearly identical may have section lift coefficients that are noticeably different, but the reverse is never true. The cases run to investigate the effect on accuracy of the number of lifting strips used the "step function" bound vorticity option (section 6.3) and applied the Kutta condition by means of the condition of equal-pressure at the first and last control points of each lifting strip (section 7.13.2). Calculated section lift coefficients at eight degrees angle of attack are shown in figure 26 for cases of 8, 13, and 20 strips (figure 25). The results for 13 and 20 strips are nearly identical except for a small region near 90 percent semispan, and the 20-strip results are thus taken as correct. The values of lift calculated for 8 strips are somewhat too large but may be close enough for many purposes. However, it appears that if 13 strips are used, accurate results are obtained, and this is thus the recommended neighborhood for the number of lifting strips. Thus, in the present example a total of 30 times 13 or 390 lifting elements are desirable.

8.2 Two Forms of the Kutta Condition

In section 6.5 two forms of the Kutta condition are described. They may be denoted the wake-tangency condition (property (a) of section 6.5) and the equal-pressure condition (property (b) of section 6.5). In figure 15 calculated results are compared for a two-dimensional case where the stream surface leaving the body is known to lie along the trailing-edge bisector. For a wing of the type shown in figure 25, the theory of reference 11 (section 6.5 and figure 13) states that the stream surface leaves the wing along the tangent to the upper surface. However, as discussed in section 6.5 and reference 6, it is often more accurate to apply the wake-tangency condition along the trailing-edge bisector. The 8-strip case of figure 25 was run at 8 degree angle of attack using the "step function" option for bound vorticity with a wake-tangency condition applied at a distance of 2 percent of local chord from the trailing edge. Calculated section lift coefficients are shown in figure 26 for points of application of the wake-tangency condition lying on the trailing-edge bisector and also on the upper-surface tangent. For the 8-strip case the error for the case where the trailing-edge bisector is used is seen to be about twice as large as that obtained with the equal-pressure condition out to about 80-percent semispan. Application of the wake-tangency condition at a point on the tangent to the upper surface gives results that are very seriously in error.

Based on the above results the equal pressure condition appears superior to the wake tangency condition, for ordinary cases. Unless otherwise indicated, it is used for all cases presented in this report.

8.3 Step Function and Piecewise Linear Bound Vorticity

As discussed in section 6.3, the present method has two options for treating the variation of the bound vorticity over the small but finite "span" of a lifting strip. The bound vorticity may be taken either constant or linearally varying over the "span" of each strip to yield an overall spanwise variation over the wing that is, respectively, a step function or a piecewise linear function (figure 10). To investigate the differences between these two representations of the bound vorticity, the 13-strip wing of figure 25 was run at 8 degrees angle of attack with an equal-pressure Kutta condition using each of the bound-vorticity options. For each case the bound vorticity as a function of "spanwise" location on the wing was obtained by fairing a smooth curve through the computed values of bound vorticity at the "midspans" of the lifting strips. Thus, in comparing the bound vorticity functions computed by the two options, the detailed variation over the individual strips is ignored. The calculated results are shown in figure 27. (Because of the sign convention adopted, bound vorticity leading to a positive lift has a negative value of the proportionality constant B, if the N-line is input with the lower surface first as recommended in sections 7.31 and 8.4.) The results are seen to be virtually identical. Surprisingly, agreement is best in the region of rapid variation near the tip and worst in the region of relatively slow variation near the plane of symmetry of the wing.

To further compare the two bound-vorticity options, section lift coefficients were computed by numerical integration of the surface pressures. The results are shown in figure 28. Agreement of the two calculations is good except for the region near the tip. A comparison with the presumably more accurate results from the 20-strip case (figure 26) indicates that the section lift coefficients calculated by the step function option are more accurate than those calculated by the piecewise linear option. The values of pressure near the tip are affected by the spanwise velocity component, which is sensitive to the details of the parabolic fit used at the wing tip to extrapolate the piecewise linear bound vorticity to a zero value in the fluid (sections 6.3 and 7.11). However, a limited amount of experimentation with the parabolic fit failed to improve the calculated distribution of section lift coefficient near the tip.

Based on the above results it is concluded that there is no apparent advantage to using the more complicated piecewise linear form of the bound vorticity, at least for simple cases. Accordingly, the simpler step function form of the bound vorticity has been used for all cases presented in this report. However, further experimentation with the piecewise linear form of the bound vorticity seems to be desirable, particularly for more complicated geometries. Evidently, an improved wing tip condition would be desirable.

8.4 Order of the Input Points

As discussed in section 7.3.1 the input can be arranged so that the points on an N-line are input in one of two orders. In any case the first point input is at the trailing edge. Then the points may be input along the lower surface of the wing to the leading edge and back along the upper surface to the trailing edge. Alternatively, the points may be input along the upper surface to the leading edge and back to the trailing edge along the lower surface. (Recall that a different order for the N-lines is required in each case.) The distinction between these two cases is illustrated in figure 22. It is concluded in section 7.3.1 that the calculated values of bound vorticity should be equal (corresponding proportionality constants B equal in magnitude and of opposite sign) in the two cases and that the difference between the two calculated results (figure 22c) should vanish in the limit of infinite element number.

The situation described above was investigated by calculating flow about the 8-strip wing of figure 25 at 8 degrees angle of attack using both possible orders for the input points. Both cases used the step function option for bound vorticity and applied the Kutta condition by means of the equal-pressure condition. Calculations were performed using an "open" wing tip of finite thickness and repeated using a "closed" wing tip, for which the section curve at the tip was arbitrarily given zero thickness. There was no essential difference between results for the open and closed tips, so only the former case is presented here. Figure 29 compares calculated spanwise bound vorticity distributions obtained for the two orders of input points. The two distributions are seen to be virtually identical, as predicted. Figure 30 compares calculated spanwise distributions of section lift coefficient, which are obtained by integrating surface pressures. Agreement is good except near the wing tip where the solution obtained by inputting the lower surface first is clearly to be preferred. What has occurred is that the difference of the two solutions, represented by the solution of figure 22c, does not vanish near the tip because of the finite element number.

On the other hand, effects like that of figure 30 do not always occur. Two of the wing-fuselages of section 9.3 were computed using an order of input points such that the upper surface of each section curve of the wing was input before the lower surface. Moreover, the wing tips in both cases were of the "open" type. The calculated spanwise distributions of section lift coefficient (figures 40a and 42a) appear reasonable. Of possible importance is the fact that the strip of elements adjacent to the wing tip is considerably wider in both wing-fuselage cases than in the 8-strip wing of figure 25. Evidently this matter deserves further study. However, inputting the lower surface first has never led to trouble.

It is concluded that ordering the input so that the lower surface of a lifting section is input before the upper surface is a desirable procedure, and it is followed in all cases presented in this report unless otherwise stated. The terms "lower" and "upper" refer to the usual case of a wing at positive angle of attack. The essential condition is the orientation of the surface to the direction of the onset flow. Thus, for a general flow the term "lower" should be replaced by "windward" and the term "upper" by "leeward." If in any application there is difficulty deciding which side of a lifting body is leeward and which windward, then almost certainly it will make little difference which is chosen. Finally, the differences in the calculated results for the two orders of input are small except near a wing tip.

8.5 Location of the Trailing Vortex Wake

As discussed in section 6.3, the location of the trailing vortex wake must be furnished as input to the program. In practical applications the exact location is not known, but an approximation may be estimated from experience. To determine the sensitivity of the calculated results to wake location, several geometries were calculated with different wake locations. Among the geometries considered was the wing described in section 8.1 and another wing of identical planform with camber and twist. Wakes were assumed that left the trailing edge along the bisector and also along the tangent to the upper surface. Straight wakes were used and also wakes that curved and became parallel to the direction of the uniform onset flow. None of these permutations gave any significant change in the surface pressures or lift distributions on the wing. It is thus concluded that for ordinary moderate values of angle of attack, trailing edge angle, and degree of camber any reasonable wake location gives a satisfactory solution.

It may be recalled that the two solutions of figure 26 obtained for a wake-tangency type of Kutta condition differed very markedly from each other. This was due to the locations of the point of application of the wake-tangency condition not to the assumed wake location.

As part of the present study, a review of the literature on wake location was carried out. In view of the above, the results of the review do not appear to be of paramount importance to the present method. This is fortunate because the amount of published information on this subject is not very large. The literature review is summarized in Appendix B.

It should be emphasized that what was proved in the above study is that the flow on a lifting body is insensitive to the position of its own wake.

Obviously if the wake from one lifting body passes near another body, the flow on the second body is sensitive to the location of this wake. This occurs, for example, in problems of wing-tail interference.

8.6 A Wing in a Wall. Fuselage Effects

A very common application of the present method is a wing-fuselage. For an isolated fuselage much larger surface elements can be used to obtain good accuracy than can be used for a wing. The question then arises as to whether this same rather sparse element distribution can be used for a fuselage on which a wing is mounted. To investigate this point, calculations were performed for a straight wing protruding from a plane wall. The basic geometry is shown in figure 31a. The wing has a rectangular planform with span equal to five times chord. The airfoil section is a symmetric one with a thickness of 10-percent chord. The plane wall extends a distance of five airfoil chords from the airfoil in both fore-and-aft and sideways directions.

Two studies were performed. In both of them the uniform onset flow is parallel to the plane of the wall and is at 10-degrees angle of attack with respect to the wing. In the first study the width of the "extra strip" of elements that lies on the opposite side of the wall from the wing was given a fixed span equal to one airfoil chord as shown in figure 31a. Three element distributions on the wall were used, as shown in figures 31b, 31c, and 31d. The dense element distribution of figure 31b has wall elements of the same chordwise extent as the elements on the wing, while the sparse distribution of figure 31d has only two wall elements over the span of the wing. Section lift coefficients on the wing calculated with the three different wall element distributions differ by one unit in the fourth decimal place, which is utterly negligible.

The second study used the wall element distribution shown in figure 31d and considered three different spanwise extents for the "extra strip:" one chord, as shown in figure 31a, three chords, and one-third chord. Calculated values of section lift coefficients on the wing differ by one unit in the second decimal place. This is of some importance but a very large range of spans is being considered. Certainly it can be concluded that the span of the extra strip is not crucial.

The spanwise variation of section lift coefficient at 10 degrees angle of attack for the case with a one-chord extra strip is compared in figure 32 with that obtained at the same angle of attack for the isolated wing of aspect ratio 5, and that for the aspect ratio 10 wing obtained by reflecting the wing in the plane of the wall. This last case corresponds to use of an infinite plane wall. It can be seen that the wall of figure 31 has almost the same effect as the infinite wall. The difference lies not in the finite element size but in the finite extent (5 chords) of the wall.

8.7 A Sudden Change in Element Shape

Section 9.3 presents results for a wing of rectangular planform mounted as a midwing on a rectangular fuselage. Section 10.1 investigates the effects of external stores mounted on this wing-fuselage. As part of this latter study, two different element distributions were used on the wing. These distributions are shown in figure 33. In both cases the spanwise distribution of lifting strips is identical. In the first case the distribution of elements is identical at all spanwise locations (input point distribution identical on all N-lines) so that the elements are all rectangular and are distributed "straight" across the wing. In the second case "slanted" elements are used on four consecutive strips near midsemispan (point distribution changed on three consecutive N-lines). In both cases all input points are exactly on the wing surface. The freestream was taken at 6 degrees angle of attack. Calculated spanwise variations of section lift coefficient are shown in figure 34a. The sudden change in element shape causes a noticable "wiggle" in the calculated spanwise lift distribution. In a more complicated application, such an effect might be taken as physically real. Accordingly, if element distributions must change over a body, it is preferable that they do so gradually.

Figure 34b compares calculated chordwise pressure distributions at the midspan of one of the two central strips of the slanted-element region. It appears that differences in lift are due almost entirely to differences in pressure in the neighborhood of the upper-surface pressure peak. Elsewhere the two calculated pressure distributions agree very well.

8.8 An Extreme Geometry

The numerical experiments of the previous sections provide guidelines on the use of the method for ordinary design applications. To delineate limits of validity of the method, calculations were performed for a case having a highly deflected flap (figure 35). As may be inferred from the figure, the geometry shown is a partial-span flap on a complete wing-fuselage configuration (reference 13). This portion of the configuration contains the essential difficulty, and it was selected for study rather than the complete wing-fuselage to save computing time. This geometry was selected as an extreme example. Real flow about such a body is not even approximately a potential flow. In the tests of reference 13 the flow over the geometry of figure 35 was separated even if area suction was used on the body surface.

When calculations were performed at zero angle of attack with the equal-pressure Kutta condition, the iterative procedure of section 7.13.2 diverged strongly. This is the only case to date where this failure occurred.* The wake-tangency Kutta condition of section 7.13.1 was applied and gave a reasonable spanwise distribution of bound vorticity. However, the pressures at the two control points of each strip adjacent to the trailing edge were not approximately equal. In a case such as this the proper location for the trailing vortex wake cannot be approximated well by intuition. Calculations were performed with different assumed wake locations, and significant differences in the calculated flow were obtained.

Thus, it appears that the present method can calculate flow about "normal" configurations in a routine fashion but that there are limits beyond which some care is required.

---

*However, see section 10.4

9.0 COMPARISON OF CALCULATED RESULTS WITH EXPERIMENTAL DATA

9.1 General Remarks

In the following sections, flow quantities calculated by the present method are compared with experimental data. All computations follow the recommendations of section 8.0. In particular, the step function option for bound vorticity and the equal-pressure Kutta condition are used.

Two flow quantities are compared: the section lift coefficient as a function of spanwise location and the chordwise pressure distribution at fixed spanwise location. The former of these is much more sensitive than the latter. As will be seen, the usual situation is one in which the calculated and experimental pressure distributions agree fairly well but the section lift coefficients are noticeably different because the difference between the two pressure distributions is of constant sign and its integrated effect is significant.

It is well known that for unseparated flow the effect of viscosity is small in nonlifting flow but is quite significant in flows with lift. While the exact magnitude of the effect depends on the Reynolds number, the general effect of viscosity is to reduce the lift about 10 percent from its inviscid value. In two dimensions calculated inviscid and experimental pressure distributions on an airfoil are quite different if they correspond to equal angles of attack but agree very well if they correspond to equal lift coefficients. That is, the principal effect of viscosity is on the lift rather than on the details of the pressure distribution. This last is probably true in three dimensions also. However, a condition of equal lift is difficult to arrange if there is a spanwise variation of the lift coefficient and of the corresponding viscous effect. In any case it is desireable to calculate the lift, not to accept it as given. Thus, the proper aim is to calculate correct flow quantities at a given angle of attack. Accordingly, comparisons of calculated and experimental results are given here at equal angles of attack. It is believed that most, if not all, of the differences between the calculated and experimental quantities are due to the effects of viscosity (and compressibility in some of the tests). Some preliminary work on this matter has been done and confirms this opinion (See the following section).

9.2 An Isolated Wing

An untwisted swept wing with a symmetric airfoil section is described in section 8.1. Low speed wind tunnel data are available for this wing in reference 12. At a Reynolds number of 18 million the results indicate that no separation occurs at an angle of attack of 8 degrees, and calculations and experiment are compared for this flow condition. Results are shown in figure 36. It can be seen that calculated and experimental pressures agree rather well at all chordwise and spanwise locations, except possibly near the trailing edge near the tip (figure 36d). Calculated and experimental distributions of section lift coefficient are quite similar in shape, but the calculated inviscid values are too high by 10-15 percent.

To test the hypothesis that viscous effects are primarily responsible for the disagreement between calculation and experiment, a crude estimate of the distribution of boundary-layer displacement thickness was added to the wing. Flow about the altered body was calculated by the present method, and the results are also shown in figure 36. A dramatic improvement in the spanwise lift distribution is evident in figure 36a. Thus, the hypothesis concerning viscous effects appears valid. Changes in the pressure distributions are less spectacular, but as mentioned above, these are relatively insensitive.

9.3 Wing-Fuselages

Reference 14 presents experimental data for a simplified wing-fuselage that consists of an uncambered wing of rectangular planform mounted as a midwing on a round fuselage. Low-speed tests were conducted at the very low Reynolds number of 0.31 million. Thus, viscous effects are rather large for this experiment. This is not a very suitable case for comparison with a potential flow method. It was selected because calculated and experimental results for a very similar geometry are presented in reference 6, and it seemed interesting to compare the predictions of the present method with that of reference 6. The situation is complicated by the fact that the data of reference 6 were taken at a higher Reynolds number of 0.66 million, so that viscous effects are reduced.

Figure 37 shows the geometry of the configuration. Figure 38 compares calculated and experimental results on the wing for an angle of attack of 6 degrees. The two spanwise lift distributions are of similar shape with the calculated values about 20 percent higher than the experimental. The pressure distributions are in better agreement, but the differences in lift are so great that the pressures on the upper surface are affected. No conclusions can be drawn regarding the relative effectiveness of the present method and that of reference 6. The agreement of calculation and experiment presented in reference 6 is much the same as that shown in figure 38.

A configuration of current interest is a wing with a so-called "supercritical" airfoil section mounted as a high wing on a fuselage. The configuration and the surface elements used in the calculation are shown in figure 39. The "supercritical" airfoil section, which is also shown in figure 39 is very thin in the neighborhood of the trailing edge and carries a relatively large percentage of its lift in this region. As can be seen in figure 39, the fuselage represents an attempt at realism with low element numbers. The cockpit canopy and the wing-tunnel sting are both accounted for. Figure 40 compares calculated results on the wing at 7 degrees angle of attack with experimental data from a low-speed wind-tunnel test conducted by Douglas personnel. The comparison of the section lift coefficient distributions exhibits the by-now-familiar behavior of similar-shaped curves with experimental values lower than calculated ones due to viscous effects. The agreement of the pressure distributions is quite good, especially at the leading-edge peak. Also, the characteristic "supercritical" type pressure distribution aft of midchord is predicted fairly well by the calculations. The pressure distributions of figure 40b at 15 percent semispan are at a location quite near the wing-fuselage junction, which is at 13.3 percent semispan. Thus, three-dimensional interference effects are relatively large at this location and are predicted fairly well.

A comparison configuration to the one of the previous paragraph consists of a wing with a conventional airfoil section mounted as a low wing on a fuselage. The body and the surface elements used to represent it are shown in figure 41. Once again the cockpit canopy and the wind tunnel sting are accounted for in the calculations. Wind tunnel tests of this configuration at 6.9 degrees angle of attack were conducted by Douglas personnel at a freestream Mach number of 0.5. These test results are compared with the incompressible calculations of the present method in figure 42. At first sight the results appear quite gratifying. The agreement of calculation and experiment is much better for this case than for the supercritical wing-fuselage, whose results are shown in figure 40. Agreement is especially good for the pressures at 25-percent semispan, figure 42c, but the spanwise distribution of section lift coefficient (figure 42a) is also in fairly good agreement. Unfortunately, part of the reason for this agreement is that the errors in the calculation due to neglect of viscosity and the errors due to neglect of compressibility are of opposite sign and tend to cancel each other. To illustrate the magnitude of the compressibility effect, the calculated results have been divided by the quantity $\sqrt{1 - M^2}$, where M denotes freestream Mach number (figure 42). This type of correction has validity in two-dimensions within the limits of small perturbation theory, but it has no justification in three-dimensions. The curves with this divisor in figure 42 are not attempts to quantitatively predict compressibility effects but are supposed to illustrate their general magnitude. It appears that when compressibility is accounted for the agreement of calculation and experiment for the configuration of figure 41 is about the same as for the configuration of figure 39.

The discussion of the previous paragraph also points out the need for a compressibility correction to be added to the present method. Based on previous two-dimensional experience, this should prove to be much easier than accounting for viscous effects. The classical procedure is based on the Göethert transformation. However, this is not very satisfactory. Its accuracy is poor in regions such as wing leading edges where the surface slope is not approximately parallel to freestream velocity. Moreover, a complete calculation must be performed from the beginning for each Mach number. What is needed is a procedure that obtains compressible results directly from an incompressible solution, so that only one lengthy flow calculation need be performed by the present method. An example of such a method is presented in reference 6, but the results are not entirely satisfactory. Evidently further investigation is required.

The wings of the configurations of figures 39 and 41 were input with the upper surface first. The calculated distributions of section lift coefficient that are given in figures 40 and 42 do not show unusual behavior near the wing tip, as was exhibited in figure 30. These are the cases referred to in section 8.4.

9.4 A Wing-Fuselage in a Wind Tunnel

A rather extensive study was performed for the somewhat unusual configuration shown in figure 43. Agreement of calculation and experiment was never obtained, but the results are a good illustration of the versatility of the method and the uncertainty connected with much wind tunnel data. The basic configuration is a W-wing mounted on a round fuselage. In the wind tunnel the model was mounted on a support strut, as shown in figures 43a and 43b. The data were supposedly corrected for all tunnel interference effects (reference 15). Thus the initial calculation was for the isolated wing-body (no strut or tunnel walls) at a corrected free-air angle of attack of 4.4°, which supposedly corresponds to a tunnel angle of attack of 4°. A comparison of calculated and experimental section lift coefficients across the span are shown in figure 44a. Agreement is good except at the kink and near the tip, where viscous effects are important. The lack of response of the calculations to the kink was surprising. However, an approximate potential flow calculation gives results that agree in general character, but not in precise value, with the calculations of the present method. This also indicates that viscosity is responsible for the dip at the kink in the experimental curve of lift coefficient. However, the agreement of calculated and experimental pressure distributions is not good, as is shown in figures 44b and 44c for two spanwise locations. A check on the blockage and upwash corrections that were applied to the data raised some questions. Accordingly, calculations were performed for the strut-mounted body in the tunnel, which is shown in figure 43. The actual wind tunnel angle of attack of 4° was used. The results of this calculation are included in figure 44. Figures 44b and 44c show a rather large effect of the strut on the lower surface pressures, particularly at the inboard location. The strut effect is mainly to increase blockage below the wing but not above. Thus, lower-surface pressures are lowered (higher velocity) and the result is the loss of lift shown in figure 44a. The effect shown is much larger than the nominal upwash and blockage corrections, and thus some doubt exists as to the validity of the data. This is an interesting application of the program. No conventional correction could account for the strut effect, but the program obtains it rather easily. However, the experimental pressures are still more negative than the calculated in a way that cannot be explained on physical grounds. A difference in reference static pressure possibly could cause this discrepancy.

10.0 INTERFERENCE STUDIES

Presented below are three examples of the use of the present method to predict the three-dimensional intereference effects on lifting wings of other bodies in close proximity - both lifting and nonlifting. The cases discussed in section 10.1 are generated geometries that have all the essential properties of actual designs. However, they are not themselves designs of interest, but serve to illustrate the capability of the present method. On the other hand, the cases of sections 10.2, 10.3, and 10.4 were generated by outside users and the results themselves were of interest. These cases thus represent the first use of the method as an analysis tool.

10.1 Wing-Fuselage with External Stores

For this example of an interference study, the basic geometry is a rectangular wing mounted as a midwing on a round fuselage. This geometry is shown in figure 37 and is discussed in section 9.3 and reference 14. Two external-store configurations are considered. The first consists of a tip tank. The geometry and element distribution for this case are shown in figure 45a. The second configuration consists of the same external store mounted beneath the wing on a short pylon centered at 60-percent semispan. The geometry and element distribution for this case are shown in figure 45b.

Figure 45a also shows the "extra strip" of elements inside the tip tank. As discussed in section 5.8, there will be a "hub vortex" trailing downstream from the tip tank. However, this does not appear to cause any numerical problem, and calculated surface velocities near the downstream end of the tip tank seem entirely reasonable. Figure 45b shows that the trailing edge of the wing is continuous across the span. Accordingly, the "ignored element" procedure of section 5.8 is used for the elements on the lower surface of the wing that are covered or partially covered by the pylon, as illustrated by the dotted planform of the pylon in figure 45b.

Calculations were performed at 6 degrees angle of attack for the three configurations: the clean wing, the wing with tip tank, and the wing with pylon-mounted external store. The round fuselage was present in all cases.

Calculated results on the wing are compared in figure 46. Figure 46a compares spanwise distributions of section lift coefficient. The addition of the tip tank to the wing prevents the lift from falling to zero at the tip, so there is a large increase in lift coefficient in this region. Moreover, as predicted by various theories, the addition of a tip tank increases the effective aspect ratio of the wing and thus increases the section lift coefficient all the way to the fuselage. The effect of the pylon-mounted external store falls to zero at the wing tip, but at the fuselage this effect is about the same size as that of the tip tank but in the opposite direction. The major effect of the pylon is to reduce lift in its vicinity by increasing lower-surface velocities and thus reducing lower-surface pressures (figure 46c). Notice that lift on the wing cannot be meaningfully computed at the spanwise location of the pylon because the lower surface is not exposed to the flow. Of course, there is a force on the external store, but it cannot be meaningfully associated with a particular location on the wing. The bound vorticity distribution is continuous across the span. The general form of this function is quite similar to that of the section lift coefficient. Indeed, it looks as if a human had faired a plausible joining curve between the disjoint portions of the curve of figure 46a.

Chordwise pressure distributions for the clean wing and for the wing with the tank are compared in figure 46b for a spanwise location close to the tip tank. The increase in lift due to the tip tank is seen to be primarily due to increased velocity on the upper surface of the wing. Figures 46c and 46d compare chordwise pressure distributions for the clean wing and for the wing with pylon-mounted external store. The spanwise location of figure 46c represents the strip of elements immediately adjacent to the pylon location. The considerable reduction in lower surface pressures due to the presence of the pylon and store is evident. Upper surface pressures are scarcely affected. Figure 46d compares pressure distributions on the upper surface of the wing corresponding to a strip of elements that lies directly above the location of the pylon. The pressure distribution computed for the wing with pylon-mounted external store is quite reasonable except for a "hump" between 65-percent chord and 90-percent chord. Examination of the side view of figure 45b shows that in this region the surface elements on the pylon and wing have dimensions that are considerably larger than the local thickness of the wing. Thus, the presence of pylon is sensed "through" the wing on the upper surface. An increase in element number could remove this pressure "hump" but this seems unnecessary. The proper way to fair the upper surface pressure distribution is quite obvious. It is felt that the computed results of figure 46 represent a very successful application of the present method.

10.2 Wing with Endplates

A case in which the calculated results were of interest to a user concerned the effect of endplates on a wing. The wing in question has a rectangular planform of aspect ratio 1.4 and an NACA 4415 airfoil section. The endplate has a planform consisting of a semicircular forward section and a rectangular rear section. The entire configuration is shown in figure 47. Three-dimensional calculations were performed at 10 degrees angle of attack with and without the endplates. A two-dimensional calculation was also obtained for comparison. This last corresponds to a case of endplates of infinite extent.

Calculated results are compared in figure 48. It can be seen from figure 48a that the addition of the endplates produces a lift distribution that is virtually independent of spanwise location. (The slight drop at the last spanwise location is probably a numerical error and should be faired out.) However, the level of the lift is much closer to that of the isolated three-dimensional wing than it is to the two-dimensional value. The chordwise pressure distributions in the symmetry plane (figure 48b) also exhibit this behavior.

In performing the above calculations the endplates were taken as simple symmetric airfoils 4-percent thick and, of course, had sharp trailing edges. If an endplate were present without the wing, it would be nonlifting. In the presence of the wing the endplate has an inward lift above the wing and an outward lift below it. The level of lift on the endplate above the wing is considerably larger than that on the endplate below the wing (about three times) and is about one-fourth the level of lift on the wing.

This case differs from previous cases in that it represents an intersection of two lifting portions of a configuration. The "ignore" option of section 6.8 was used on certain strips of the endplate to accommodate the wing intersection.

10.3 Wing in a Wind Tunnel

The wing of aspect ratio 1.4 described in section 10.2 was considered to be in a wind tunnel at 10 degrees angle of attack, as shown in figure 49. If the wing completely spans the tunnel, the theoretical inviscid result is the two-dimensional flow about the airfoil section in the presence of the upper and lower walls, i.e., about the sideview of figure 49 considered as a two-dimensional flow. However, the presence of the gaps between the wing tips and the tunnel sidewalls allows the bound vorticity on the wing to fall to zero at the tips and introduces significant three-dimensional effects. The purpose of the calculation was to evaluate these three-dimensional effects.

Figure 50 compares calculated results for the above-described two-dimensional case with those for the three-dimensional wing with and without the wind tunnel sidewalls. All cases include the effects of the top and bottom walls of the wind tunnel. In the three-dimensional case without side-walls, the top and bottom walls have been extended horizontally a distance of several wing spans. The importance of the gaps is quite evident in figure 50. Results for the case of the small but finite gaps are much closer to those for infinite gaps (sidewalls removed) than to those for zero gaps (two-dimensional case).

10.4 Wing With Endplates in a Wind Tunnel

As a final example, the wing with endplates (figure 47) was inserted in the wind tunnel shown in figure 49 to obtain the configuration shown in figure 51. When calculations were performed for this case with the equal-pressure Kutta condition, the iterative procedure of section 7.13.2 appeared to be neutrally convergent and the iterations never fully "settled down". This may have been caused by the close proximity of the elements on the wind tunnel wall to the trailing edges of the endplates. In all cases except this one and the strongly divergent case of section 8.8 the iterative procedure of section 7.13.2 converged very rapidly.

Because of the above situation, calculations were performed for the configuration of figure 51 using the wake-tangency Kutta condition. Figure 52 compares the results obtained with those for the isolated wing in free air. To evaluate the effect on the results of the form of the Kutta condition, calculations were performed for the wing in free air using both forms of the Kutta condition. As can be seen in figure 52, the effect of the form of the Kutta condition is not large, and most of the differences between the calculations for the wing with endplates in the tunnel and the various other results shown in figures 48, 50, and 52 are due to differences between the geometries. It is evident from figure 52a that the effects of endplates and wind tunnel walls together give a lift distribution independent of spanwise location. (Again, the drop in lift at the spanwise location adjacent to the endplate is probably a numerical inaccuracy and should be faired out). Moreover, the level of the lift is much closer to the two-dimensional value than were those obtained using endplates or tunnel walls separately (figures 48a and 50a).

The chordwise pressure distributions of figure 52b also show the interference effects described above. Also shown are the small but noticeable differences between upper and lower-surface trailing-edge pressures in the cases that used the wake-tangency Kutta condition. For the wing in free air the pressure distributions calculated using the two forms of the Kutta condition differ from each other only in the vicinity of the trailing edge and are essentially identical over most of the surface.

11.0 ACKNOWLEDGEMENT

The author was very fortunate to have had the assistance of two extremely capable and conscientious associates. Mrs. Sue Schimke made significant contributions at all stages of the work, including several analytical derivations and the running of all the cases, and her contributions in preparing the present report were invaluable. All computing analysis, coding, and program documentation was performed by Mr. Dun Mack, whose ability to put together all the many options and alternatives of the present method with a minimum of supervision is greatly appreciated.

12.0 REFERENCES

1. Hess, J. L., and Smith, A.M.O.: Calculation of Potential Flow about Arbitrary Bodies. Progress in Aeronautical Sciences, Vol. 8, Pergammon Press, New York (1966).

2. Hess, J. L.: Numerical Solution of the Integral Equation for the Neumann Problem with Application to Aircraft and Ships. Douglas Aircraft Company Engineering Paper No. 5987 (October 1971).

3. Hess, J. L., and Smith, A.M.O.: Calculation of Nonlifting Potential Flow about Arbitrary Three-Dimensional Bodies. Douglas Aircraft Company Report No. ES 40622 (March 1962). (An abbreviated version appeared in Journal of Ship Research, Vol. 8, No. 2 (September 1964).)

4. Rubbert, P. E., et al: A General Method for Determining the Aerodynamic Characteristics of Fan-in-Wing Configurations. Vol. I, Theory and Application. USAAVLABS Technical Report No. 67-61A (December 1967).

5. Rubbert, P. E., and Saaris, G. R.: Review and Evaluation of a Three-Dimensional Lifting Potential Flow Analysis Method for Arbitrary Configurations. AIAA Paper No. 72-188 (January 1972).

6. Labrujere, Th.E., Loeve, W., and Sloof, J. W.: An Approximate Method for the Calculation of the Pressure Distribution on Wing-Body Combinations at Subcritical Speeds. AGARD Conference Proceedings No. 71, Aerodynamic Interference (September 1970).

7. Kraus, W.: Das MBB-UFE Unterschall-Panelverfahren, Teil 2: Das Auftriebsbehaftete Verdrängungsproblem in Kompressibler Strömung. UFE 633-70 (1970).

8. Hess, J. L.: Calculation of Potential Flow about Arbitrary Three-Dimensional Lifting Bodies. Phase II, Final Report. McDonnell Douglas Report No. MDC J0971-01 (October 1970).

9. Hess, J. L.: Calculation of Potential Flow about Arbitrary Three-Dimensional Lifting Bodies. Phase I, Final Report. McDonnell Douglas Report No. MDC J0545 (December 1969).

10. Ebihara, M.: A Method for the Calculation of Lifting Potential Flow Problems. National Aerospace Laboratory (Japan) Technical Report No. TR-240T (July 1971).

11. Mangler, K. W., and Smith, J. H. B.: Behavior of the Vortex Sheet at the Trailing Edge of a Lifting Wing. Royal Aircraft Establishment Technical Report No. 69049 (March 1969).

12. Kolbe, C. D., and Boltz, F. W.: The Forces and Pressure Distributions at Subsonic Speeds on a Plane Wing Having 45° of Sweepback, and Aspect Ratio of 3, and a Taper Ratio of 0.5. NACA RM A51G31 (October 1951).

13. Griffin, R. N., Jr., and Hickey, D. H.: Investigation of the Use of Area Suction to Increase the Effectiveness of Trailing-Edge Flaps of Various Spans on a Wing of 45° Sweepback and Aspect Ratio 6. NACA RM A56B27 (June 1956).

14. Körner, H.: Untersuchungen zur Bestimmung der Druckverteilung an Flügel-Rumpf-Kombinationen. Teil I: Messergebnisse für Mittledecker-anordnung aus dem 1, 3 m-Windkanal. Bericht 69/21 Braunschweig (1969). (DFVLR - Bericht Nr. 0562.)

15. Polhamus, E. C., and Few, A. G., Jr.: Pressure Distribution at Low Speed on a Model Incorporating a W-Wing with Aspect Ratio 6, 45° Sweep, Taper Ratio 0.6, and an NACA 65A009 Airfoil Section. NACA RM L52F11, (August 1952).

16. Milne-Thomson, L. M.: Theoretical Hydrodynamics. MacMillan, New York (1950) p. 49.

17. McCormick, B. W., Tangler, J. L., and Sherrieb, H. E.: Structure of Trailing Vortices. Journal of Aircraft, Vol. 5, No. 3 (May-June 1968).

18. Tolhurst, W. H.: Downwash Characteristics and Vortex-Sheet Shape Behind a 63° Swept-Back-Wing-Fuselage Combination at a Reynolds Number of 6.1×10^6. NACA TN 3175 (May 1954).

19. Hackett, J. E., and Evans, M. R.: Vortex Wakes Behind High-Lift Wings. AIAA Paper No. 69-740.(July 1969).

20. Hoggard, H. P., and Hagerman, J. P.: Downwash and Wake Behind Untapered Wings of Various Aspect Ratios and Angles of Sweep. NACA TN 1703 (October 1948).

APPENDIX A

RELATION BETWEEN DIPOLE AND VORTEX SHEETS OF VARIABLE STRENGTH

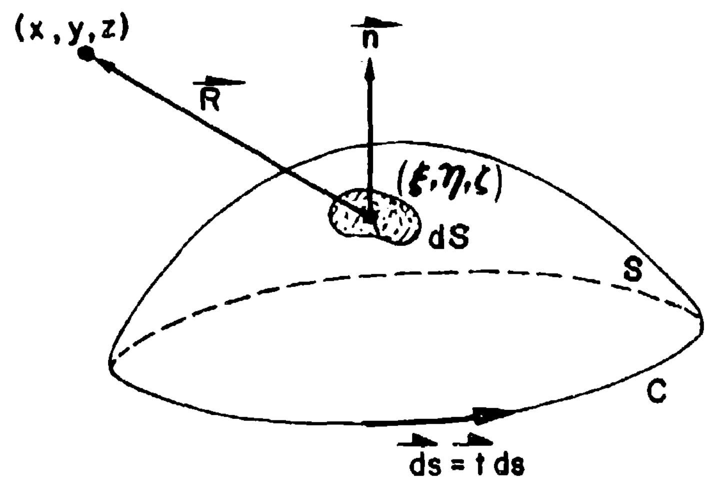

Figure A1. Notation for a general surface.

Consider a surface S in space bounded by a closed curve c. (If S is a closed surface, c vanishes.) At any point (ξ, η, ζ) on S the unit normal vector is $\vec{n}$, and at any point on c the unit tangent vector is $\vec{t}$. The vector between the point (ξ, η, ζ) and a general point (x, y, z) in space is denoted $\vec{R}$, and the length of this vector is denoted R. Specifically,

$$\begin{aligned} \vec{R} &= (x-\xi)\vec{i} + (y-\eta)\vec{j} + (z-\zeta)\vec{k} \\ R &= \sqrt{(x-\xi)^2 + (y-\eta)^2 + (z-\zeta)^2} \end{aligned} \tag{A-1}$$

The gradient operator grad_x is used to denote that derivatives are taken with respect to x, y, z. Similarly, grad_ξ is the gradient operator that differentiates with respect to ξ, η, ζ.

THEOREM: Let the surface S be covered with a variable dipole distribution of intensity μ. (The dipole axes are along $\vec{n}$) The velocity at (x,y,z) due to the dipole sheet is equal to the sum of the velocities due to a certain vortex sheet of strength $\vec{\omega}$ on S and due to a vortex filament of strength Ω along c. The strength of the vortex filament is just the local (edge) value of the doublet strength, i.e.,

$$\Omega = \mu \quad (\text{on} \quad c) \tag{A-2}$$

The vorticity in the sheet is a vector everywhere tangent to the curves of constant μ and has an intensity equal to the magnitude of grad μ. Specifically, if $\vec{\omega}$ is the vector vortex strength on S, then

$$\vec{\omega} = - \vec{n} \times \text{grad}_{\xi}\ \mu \tag{A-3}$$

Since μ is defined only on S, only the tangential component of its gradient is defined. However, it is clear from the form of (A-3) that the normal component of the gradient does not affect the result.

DISCUSSION: The Biot-Savart law gives the velocity at (x, y, z) due to a vortex filament of variable strength Ω lying along any curve c as

$$\vec{V} = \int_c \frac{\vec{t} \times \vec{R}}{R^3}\ \Omega ds \tag{A-4}$$

where s denotes arc length along c. Thus, the velocity due to the vortex filament whose strength is given by (A-2) and which lies along a closed curve c is

$$\vec{V}_{\Gamma} = \oint_c \frac{\vec{t} \times \vec{R}}{R^3}\ \mu ds \tag{A-5}$$

The expression for the velocity due to a vortex sheet is obtained from (A-4) by writing the vector vortex strength $\vec{\omega} = \Omega\vec{t}$, so that (A-4) becomes

$$\vec{V} = \int_c \frac{\vec{\omega} \times \vec{R}}{R^3}\ ds \tag{A-6}$$

Now simply redefine $\vec{\omega}$ as a surface density instead of a linear density and change (A-6) to a surface integral over S. This gives the velocity at (x, y, z) due to a vortex distribution of strength $\vec{\omega}$ on S as

$$\vec{V}_\omega = \iint_S \frac{\vec{\omega} \times \vec{R}}{R^3}\, dS \qquad \text{(A-7)}$$

where dS is an elemental surface area on S. For the particular vortex strength given by (A-3) this becomes

$$\vec{V}_\omega = -\iint_S \frac{(\vec{n} \times \operatorname{grad}_\xi \mu) \times \vec{R}}{R^3}\, dS \qquad \text{(A-8)}$$

or

$$\vec{V}_\omega = -\iint_S \frac{(\vec{n} \cdot \vec{R})\operatorname{grad}_\xi \mu - (\vec{R} \cdot \operatorname{grad}_\xi \mu)\vec{n}}{R^3}\, dS \qquad \text{(A-9)}$$

To obtain the velocity due to the dipole sheet, start with the point source potential

$$\phi_S = \frac{1}{R} \qquad \text{(A-10)}$$

and generate the dipole potential

$$\begin{aligned} \phi_D &= \vec{n} \cdot \operatorname{grad}_\xi \phi_S \\ &= \frac{\vec{n} \cdot \vec{R}}{R^3} \end{aligned} \qquad \text{(A-11)}$$

where $\vec{n}$ is the unit vector along the axis of the dipole, and in this application the axis is along the normal vector to S. The velocity due to the dipole is

$$\begin{aligned} \vec{V}_D \text{ (point)} &= -\operatorname{grad}_x \phi_D = -\operatorname{grad}_x \left(\frac{\vec{n} \cdot \vec{R}}{R^3}\right) \\ &= -\frac{1}{R^3} \operatorname{grad}_x (\vec{n} \cdot \vec{R}) - (\vec{n} \cdot \vec{R}) \operatorname{grad}_x \left(\frac{1}{R^3}\right) \end{aligned} \qquad \text{(A-12)}$$

The first term above may be evaluated with the help of a standard vector differentiation formula taking advantage of the fact that $\vec{n}$ is independent of x, y, z and the fact that $\operatorname{curl}_x \vec{R} = 0$. The result is

$$\vec{v}_D \text{ (point)} = -\frac{1}{R^3}(\vec{n}\cdot \text{grad}_x)\vec{R} - (\vec{n}\cdot\vec{R})\,\text{grad}_x\left(\frac{1}{R^3}\right)$$
$$= -\frac{\vec{n}}{R^3} + 3\,\frac{\vec{n}\cdot\vec{R}}{R^5}\vec{R} \qquad \text{(A-13)}$$

The simple form of the second form of (A-3) is due to the simple form of $\vec{R}$. Thus, the velocity at (x, y, z) due to a normal dipole distribution of strength μ on S is

$$\vec{v}_D = \iint_S \left[-\frac{\vec{n}}{R^3} + 3\,\frac{\vec{n}\cdot\vec{R}}{R^5}\vec{R}\right]\mu dS \qquad \text{(A-14)}$$

The proof of the theorem consists of showing that $\vec{v}_D$ from (A-14) equals the sum of $\vec{v}_\Gamma$ from (A-5) and $-\vec{v}_\omega$ from (A-9). This is done by starting with (A-5) and: (a) writing out the line integral explicitly in terms of components, (b) applying Stoke's theorem to each component separately to obtain surface integrals over S, and (c) manipulating the result to obtain the desired equality. The details are somewhat lengthy. A more concise proof should be possible.

DETAILS OF THE PROOF: For a point on the curve c ξ, η, ζ are functions of the arc length s along the curve. The unit tangent vector to c is

$$\vec{t} = \frac{d\xi}{ds}\vec{i} + \frac{d\eta}{ds}\vec{j} + \frac{d\zeta}{ds}\vec{k} \qquad \text{(A-15)}$$

Taking the cross product with $\vec{R}$ from (A-1) and putting the result in (A-5) gives

$$\begin{aligned}
\vec{v}_\Gamma = \vec{i} &\oint_c \left[\;0\; d\xi + \frac{\mu}{R^3}(z-\zeta)d\eta - \frac{\mu}{R^3}(y-\eta)\,d\zeta\right] \\
\vec{j} &\oint_c \left[-\frac{\mu}{R^3}(z-\zeta)d\xi + \;0\; d\eta + \frac{\mu}{R^3}(x-\xi)\,d\zeta\right] \qquad \text{(A-16)} \\
\vec{k} &\oint_c \left[+\frac{\mu}{R^3}(y-\eta)d\xi - \frac{\mu}{R^3}(x-\xi)d\eta + \;0\; d\zeta\right]
\end{aligned}$$

Differentiation gives

$$\frac{\partial}{\partial\xi}\left(\frac{\mu}{R^3}\right) = \frac{1}{R^3}\frac{\partial\mu}{\partial\zeta} + 3\,\frac{x-\xi}{R^5}\,\mu \tag{A-17}$$

and similar formulas for the η and ζ derivatives. These are used below.

Stokes theorem in component form is

$$\oint_C [P d\xi + Q d\eta + R d\zeta] = \iint_S \left[\left(\frac{\partial R}{\partial\eta} - \frac{\partial Q}{\partial\zeta}\right) n_1 + \left(\frac{\partial P}{\partial\zeta} - \frac{\partial R}{\partial\xi}\right) n_2 + \left(\frac{\partial Q}{\partial\xi} - \frac{\partial P}{\partial\eta}\right) n_3\right] dS \tag{A-18}$$

where

$$\vec{n} = n_1\vec{i} + n_2\vec{j} + n_3\vec{k} \tag{A-19}$$

This theorem must be applied to the components of (A-16) separately. The result is

$$\begin{aligned}
\vec{v}_\Gamma = \vec{i} \iint_S \Bigg\{ & -\left[(y-\eta)\left(\frac{1}{R^3}\frac{\partial\mu}{\partial\eta} + 3\,\frac{y-\eta}{R^5}\,\mu\right) - \frac{\mu}{R^3}\right. \\
& \left. + (z-\zeta)\left(\frac{1}{R^3}\frac{\partial\mu}{\partial\zeta} + 3\,\frac{z-\zeta}{R^5}\,\mu\right) - \frac{\mu}{R^3}\right] n_1 \\
& + \left[+ (y-\eta)\left(\frac{1}{R^3}\frac{\partial\mu}{\partial\xi} + 3\,\frac{x-\xi}{R^5}\,\mu\right)\right] n_2 \\
& + \left[+ (z-\zeta)\left(\frac{1}{R^3}\frac{\partial\mu}{\partial\xi} + 3\,\frac{x-\xi}{R^5}\,\mu\right)\right] n_3 \Bigg\} dS \\
+ \vec{j} \iint_S \Bigg\{ & \left[+ (x-\xi)\left(\frac{1}{R^3}\frac{\partial\mu}{\partial\eta} + 3\,\frac{y-\eta}{R^5}\,\mu\right)\right] n_1 \\
& -\left[(z-\zeta)\left(\frac{1}{R^3}\frac{\partial\mu}{\partial\zeta} + 3\,\frac{z-\zeta}{R^5}\,\mu\right) - \frac{\mu}{R^3}\right. \\
& \left. + (x-\xi)\left(\frac{1}{R^3}\frac{\partial\mu}{\partial\xi} + 3\,\frac{x-\xi}{R^5}\,\mu\right) - \frac{\mu}{R^3}\right] n_2 \\
& + \left[+ (z-\zeta)\left(\frac{1}{R^3}\frac{\partial\mu}{\partial\eta} + 3\,\frac{y-\eta}{R^5}\,\mu\right)\right] n_3 \Bigg\} dS
\end{aligned} \tag{A-20}$$

$$
\begin{aligned}
+\vec{k}\iint_S \Bigg\{ & \left[+(x-\xi)\left(\frac{1}{R^3}\frac{\partial\mu}{\partial\zeta}+3\,\frac{z-\zeta}{R^5}\,\mu\right)\right]n_1 \\
& \left[+(y-\eta)\left(\frac{1}{R^3}\frac{\partial\mu}{\partial\zeta}+3\,\frac{z-\zeta}{R^5}\,\mu\right)\right]n_2 \\
& -\Bigg[+(x-\xi)\left(\frac{1}{R^3}\frac{\partial\mu}{\partial\xi}+3\,\frac{x-\xi}{R^5}\,\mu\right)-\frac{\mu}{R^3} \\
& \quad +(y-\eta)\left(\frac{1}{R^3}\frac{\partial\mu}{\partial\eta}+3\,\frac{y-\eta}{R^5}\,\mu\right)-\frac{\mu}{R^3}\Bigg]n_3\Bigg\}\,dS
\end{aligned}
\tag{A-20}
$$

Certain terms can be collected at once. The μ/R^3 terms add to give

$$
2\iint_S \frac{\mu}{R^3}\,\vec{n}\,dS \tag{A-21}
$$

The coefficient of $n_1\vec{i}$ includes the term

$$
-\frac{3\mu}{R^5}\left[(y-\eta)^2+(z-\zeta)^2\right] = -3\,\frac{\mu}{R^3}+3\mu\,\frac{(x-\xi)^2}{R^5} \tag{A-22}
$$

Similar terms occur in the coefficients of $n_2\vec{j}$ and $n_3\vec{k}$. Separating these terms and collecting gives

$$
\begin{aligned}
\vec{v}_\Gamma = {} & 2\iint_S \frac{\mu}{R^3}\,\vec{n}\,dS - 3\iint_S \frac{\mu}{R^3}\,\vec{n}\,dS \\
& + 3\iint_S \frac{\mu}{R^5}\Bigg\{\vec{i}\left[(x-\xi)^2 n_1+(x-\xi)(y-\eta)n_2+(x-\xi)(z-\zeta)n_3\right] \\
& \qquad +\vec{j}\left[(y-\eta)(x-\xi)n_1+(y-\eta)^2 n_2+(y-\eta)(z-\zeta)n_3\right] \\
& \qquad +\vec{k}\left[(z-\zeta)(x-\xi)n_1+(z-\zeta)(y-\eta)n_2+(z-\zeta)^2 n_3\right]\Bigg\}dS \\
& - \iint_S \frac{1}{R^3}\Bigg\{\vec{i}\Bigg[\left((x-\xi)\,\frac{\partial\mu}{\partial\xi}\,n_1\right)+(y-\eta)\,\frac{\partial\mu}{\partial\eta}\,n_1+(z-\zeta)\,\frac{\partial\mu}{\partial\zeta}\,n_1 \\
& \qquad -\left((x-\xi)\,\frac{\partial\mu}{\partial\xi}\,n_1\right)-(y-\eta)\,\frac{\partial\mu}{\partial\xi}\,n_2-(z-\zeta)\,\frac{\partial\mu}{\partial\xi}\,n_3\Bigg]
\end{aligned}
\tag{A-23}
$$

$$+ \vec{j}\Big[(x-\xi)\frac{\partial\mu}{\partial\xi}n_2 + \Big\{(y-\eta)\frac{\partial\mu}{\partial\eta}n_2\Big\} + (z-\zeta)\frac{\partial\mu}{\partial\zeta}n_2$$

$$-(x-\xi)\frac{\partial\mu}{\partial\eta}n_1 - \Big\{(y-\eta)\frac{\partial\mu}{\partial\eta}n_2\Big\} - (z-\zeta)\frac{\partial\mu}{\partial\eta}n_3\Big]$$

$$+ \vec{k}\Big[(x-\xi)\frac{\partial\mu}{\partial\xi}n_3 + (y-\eta)\frac{\partial\mu}{\partial\eta}n_3 + \Big\{(z-\zeta)\frac{\partial\mu}{\partial\zeta}n_3\Big\}$$

$$-(x-\xi)\frac{\partial\mu}{\partial\zeta}n_1 - (y-\eta)\frac{\partial\mu}{\partial\zeta}n_2 - \Big\{(z-\zeta)\frac{\partial\mu}{\partial\zeta}n_3\Big\}\Big]\Big\}\,dS$$

(A-23)

In the fourth (last) integral the terms in dotted brackets { } have been added and subtracted. In the third integral, if $(x-\xi)$ is factored from the first line, $(y-\eta)$ from the second line, and $(z-\zeta)$ from the third line, the remaining terms are identical in all three cases, namely $(\vec{n}\cdot\vec{R})$. In the fourth integral, the odd numbered lines are identical except for the component of $\vec{n}$, and these three lines add together to give $(R \cdot \mathrm{grad}_\xi \mu)\vec{n}$. In the fourth integral the even numbered lines are identical except for the differentiation variable, and these three lines add together to give $\cdot(\vec{n}\cdot\vec{R})\,\mathrm{grad}_\xi\mu$. Using all these results (A-23) becomes

$$\vec{v}_\Gamma = -\iint_S \frac{\mu}{R^3}\vec{n}\,dS + 3\iint_S \frac{(\vec{n}\cdot\vec{R})}{R^5}\vec{R}\,\mu\,dS$$

$$-\iint_S \frac{1}{R^3}\left[(\vec{R}\cdot\mathrm{grad}_\xi\mu)\vec{n} - (\vec{n}\cdot\vec{R})\,\mathrm{grad}_\xi\mu\right]dS \qquad \text{(A-24)}$$

Thus using (A-3) and (A-14)

$$\vec{v}_\Gamma = \vec{v}_D - \vec{v}_w \qquad \text{(A-25)}$$

as required.

APPENDIX B

LITERATURE REVIEW OF SHAPES OF TRAILING VORTEX WAKES

As part of the present work a literature search has been conducted into the problem of locating the trailing vortex sheet. The idea is that the more information that can be collected on this matter the more accurate will be the specification of the wake to the program and thus the more accurate will be the calculated pressures. In view of the results of section 8.5, it appears that the location of the wake of a lifting body is not very important as far as the surface pressures on that body are concerned. Wake position may be of greater interest in the case where one body is generally downstream of another lifting body.

It is fortunate that the position of the wake does not appear to be critical, because the literature has proved very disappointing in this regard. First, there are very few articles on this subject. Second, most of those few deal with the asymptotic wake location many chord lengths behind the wing. This is the important region for determining the effects of a wake on another aircraft, but the wake position at such remote locations seems unlikely to affect the surface pressures. Third, the handful of articles that discuss the wake in the first few chord lengths behind the wing are to some extent contradictory. Some of the applicable articles are discussed below.

Reference 17, an experimental study of straight wings of fairly high aspect ratio on a fuselage, reports that the wake vorticity is essentially all concentrated into the tip vortices right from the beginning. The tip vortices separate from the wing tip at about the quarter-chord (not the trailing edge) and go straight downstream parallel to the freestream direction, i.e., they do not follow what are normally thought of as the streamlines of the flow.

Reference 18 proved very encouraging. The configuration was a swept wing on a fuselage, and the study was both theoretical and experimental. The wake behind the wing was examined from the trailing edge downstream to a distance equal to one span. Various theoretical models were considered. One model consisted of exactly the model used in many of the cases of this report.

Specifically, the wake was taken to lie straight back in the wing midplane and the spanwise vorticity distribution was the same as at the wing trailing edge. Downwash computed by this model gave excellent agreement with experiment - much better than a model that considered the wake to be rolled up into tip vortices.

Reference 19 presented the results of numerical computations for wake locations behind isolated wings, both straight and swept. The rolled up portions of the wake near the tips lay essentially straight back in the freestream direction. The wake center line lay much lower, but the vorticity was quite weak in the whole region near the centerline.

However, reference 20 contradicted this last result. Based on experimental studies of swept wings, the authors showed that the wake centerline lay essentially straight back. This report contains a large amount of downwash data that is difficult to apply to wake-shape estimation. This occurs in many reports.

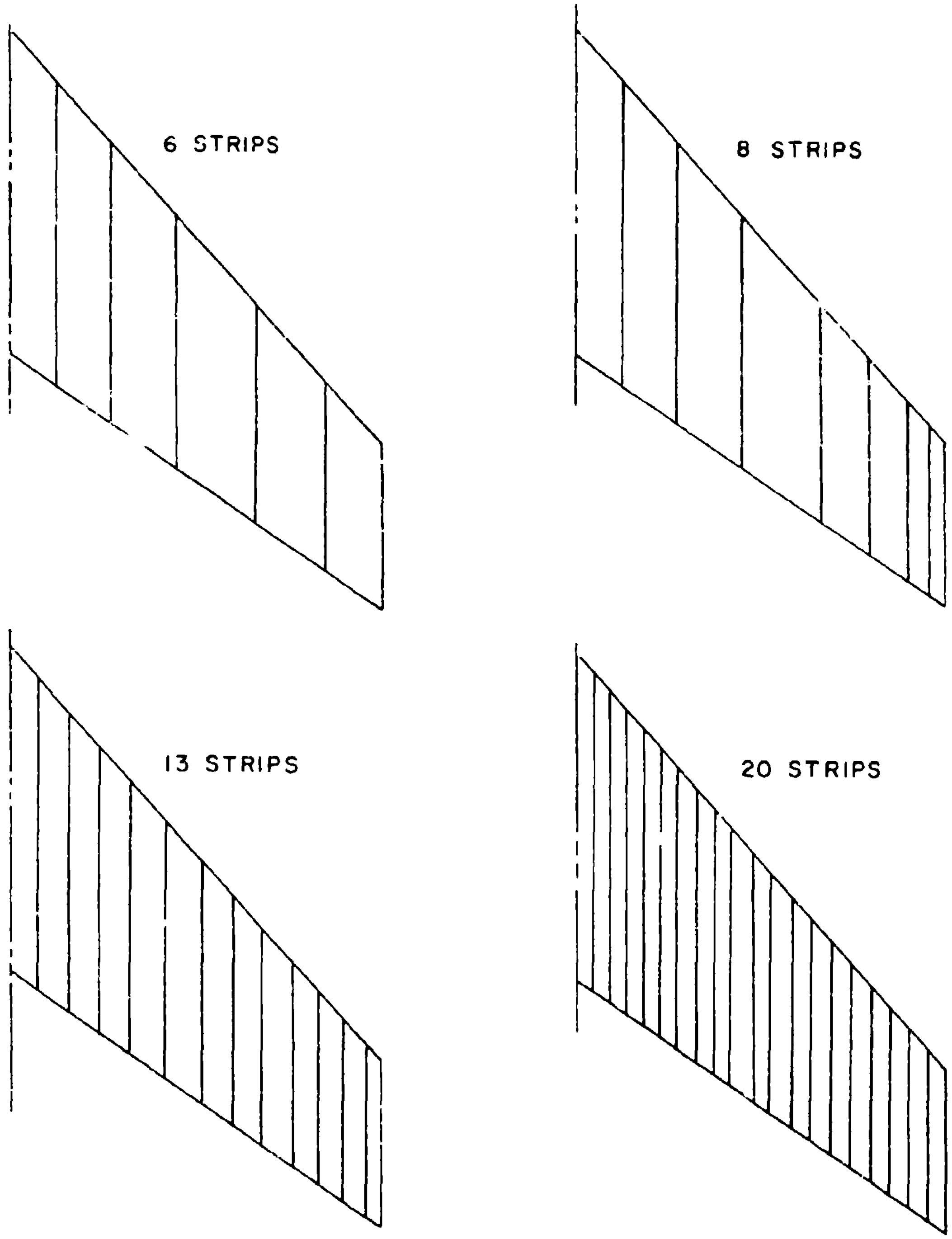

Figure 25. Planform of a swept tapered wing showing lifting strips used in the calculations.

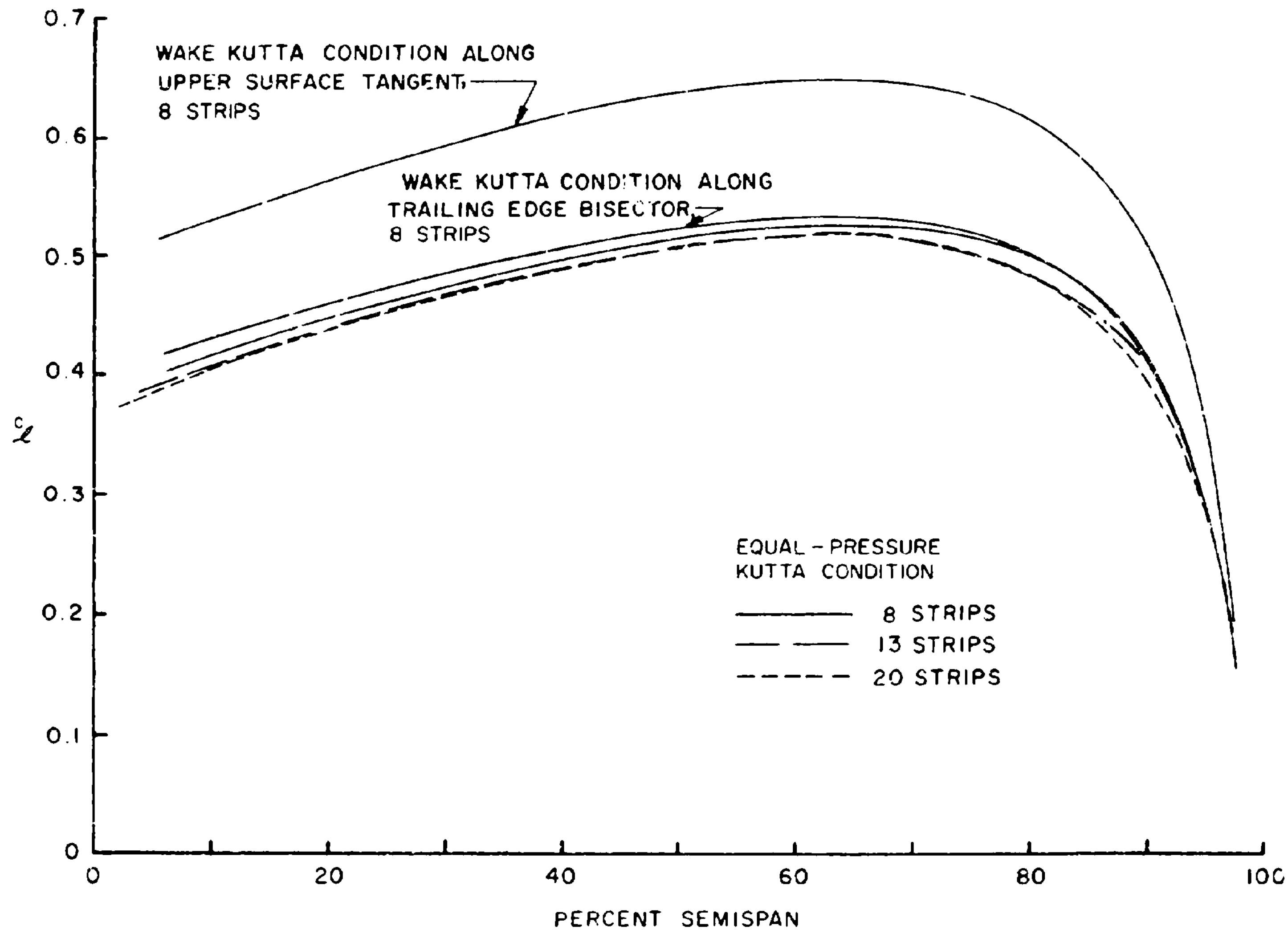

Figure 26. Spanwise distributions of section lift coefficient calculated for a swept tapered wing at 8 degrees angle of attack using various numbers of lifting strips.

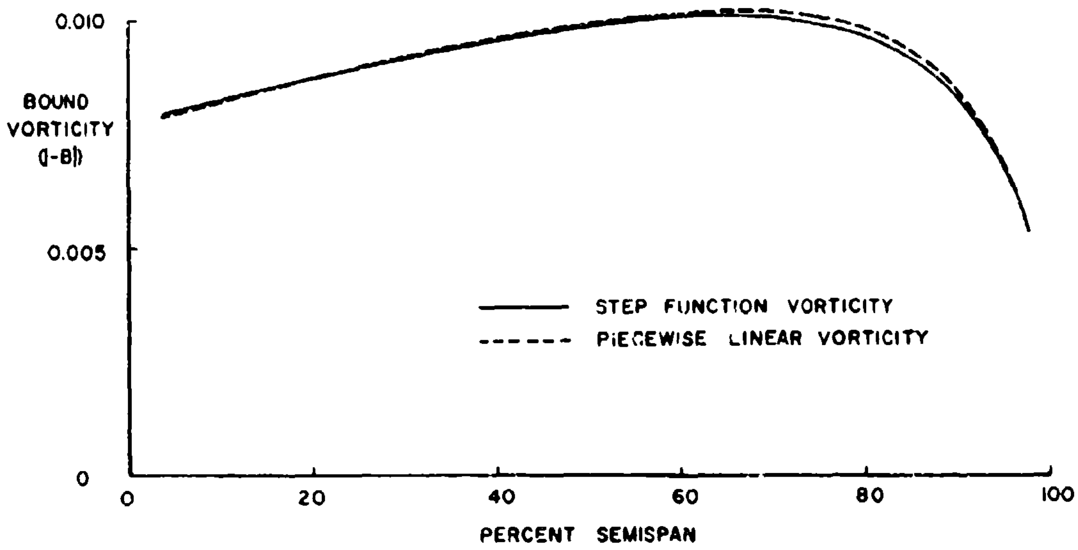

Figure 27. Spanwise distributions of bound vorticity on a swept tapered wing at 8 degrees angle of attack computed by the two bound vorticity options.

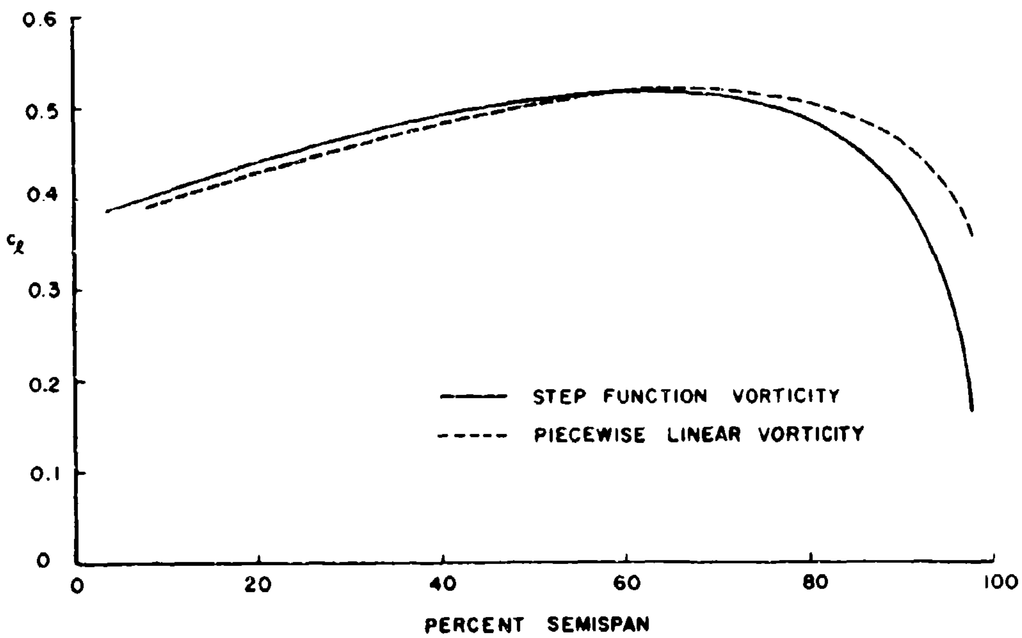

Figure 28. Spanwise distributions of section lift coefficient on a swept tapered wing at 8 degrees angle of attack computed by the two bound vorticity options.

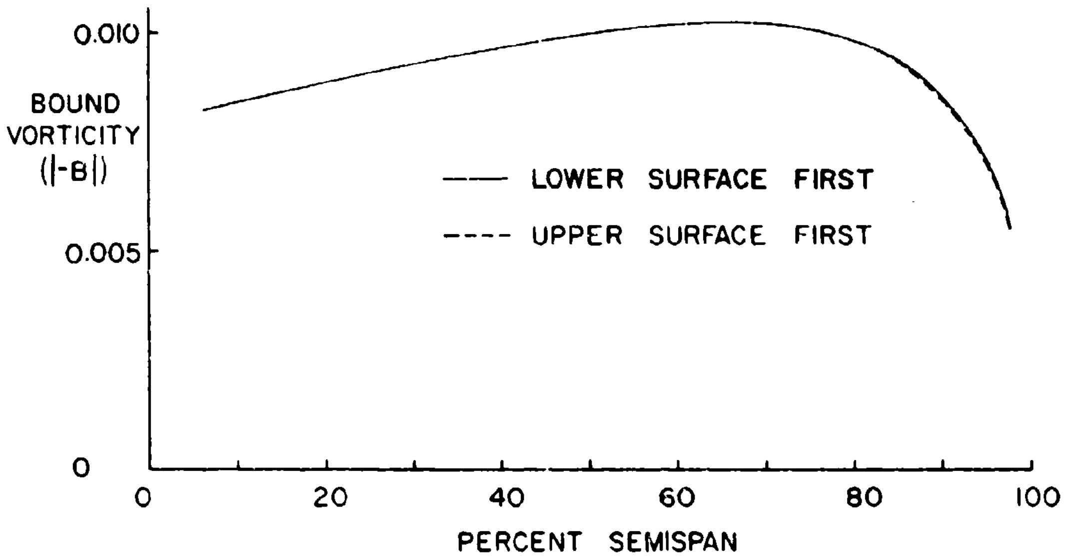

Figure 29. Spanwise distributions of bound vorticity on a swept tapered wing at 8 degrees angle of attack computed with two orders for the input points.

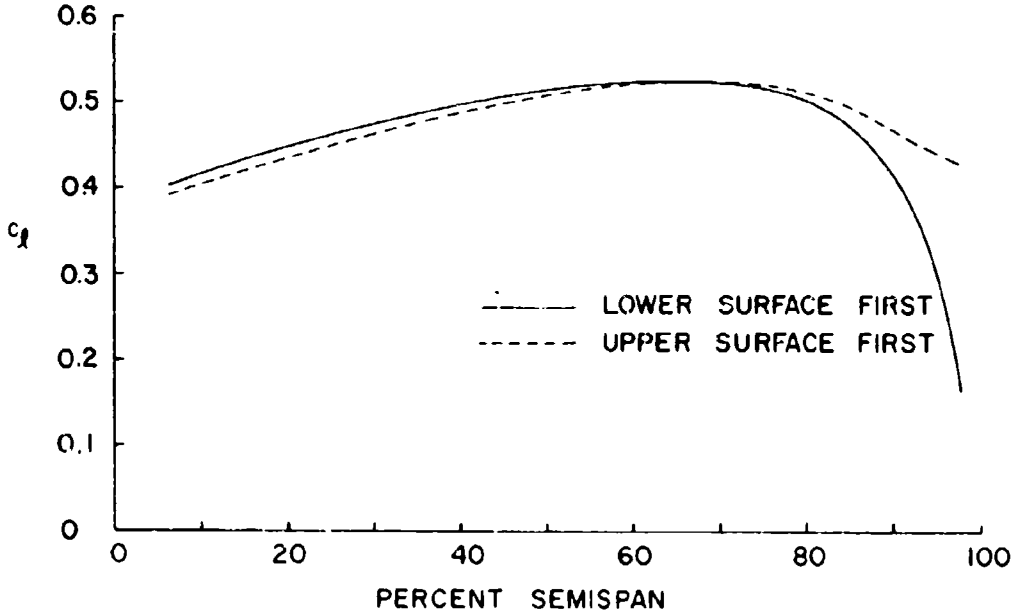

Figure 30. Spanwise distributions of section lift coefficient on a swept tapered wing at 8 degrees angle of attack computed with two orders for the input points.

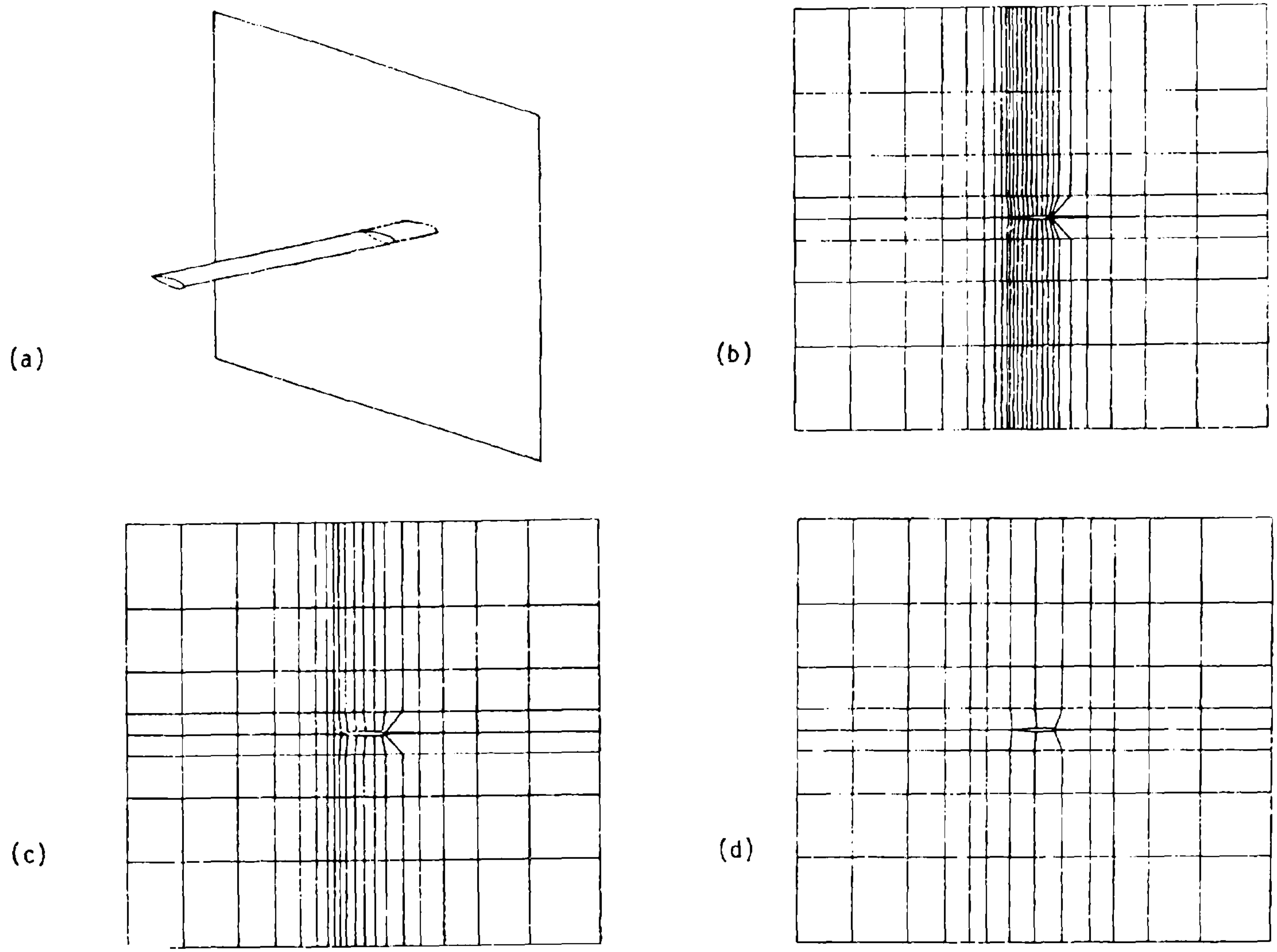

Figure 31. A wing protruding from a plane wall showing three element distributions used for the wall.

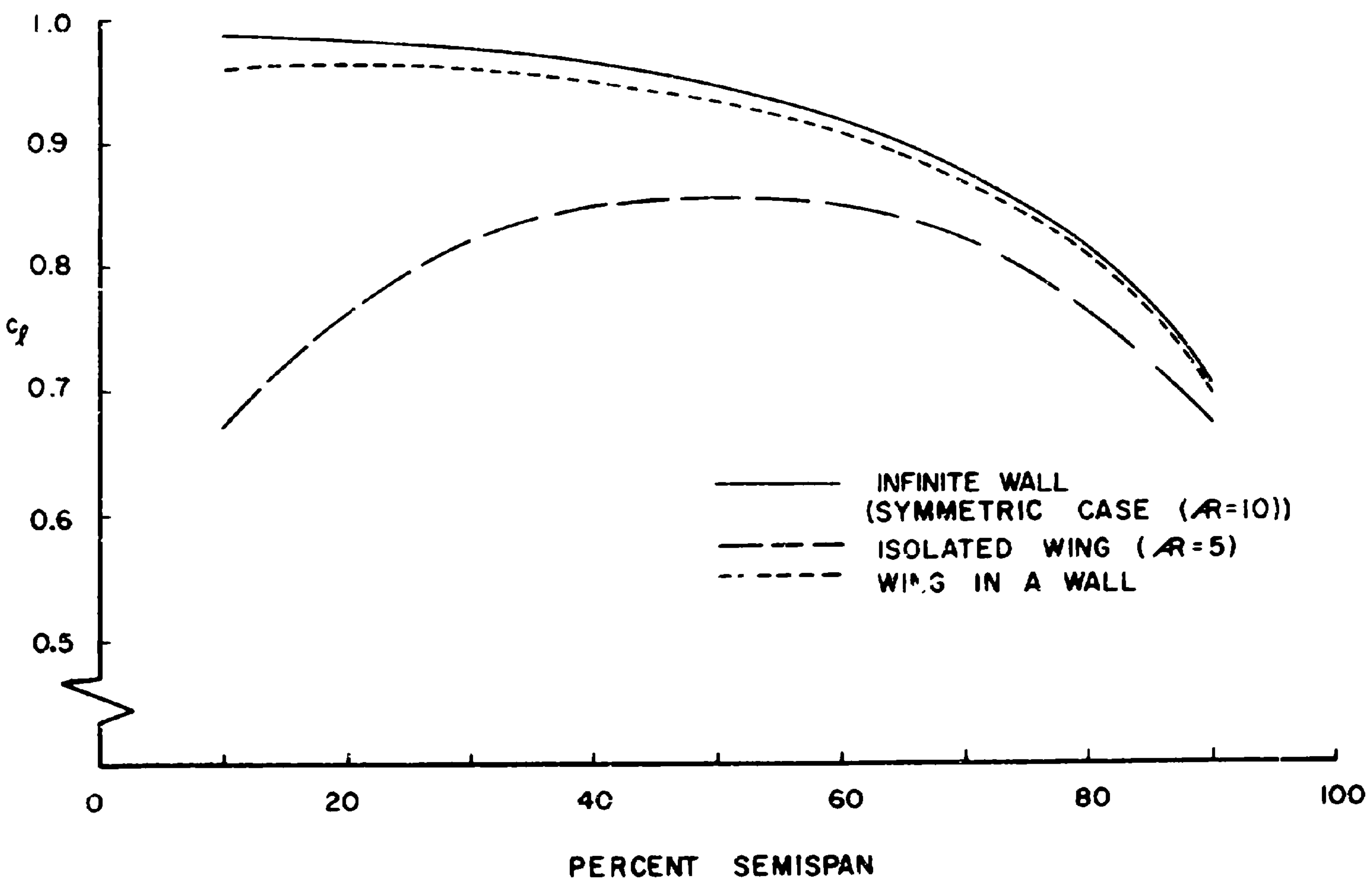

Figure 32. Calculated effects of a finite and an infinite plane wall on the spanwise distribution of section lift coefficient for a wing of rectangular planform at 10 degrees angle of attack.

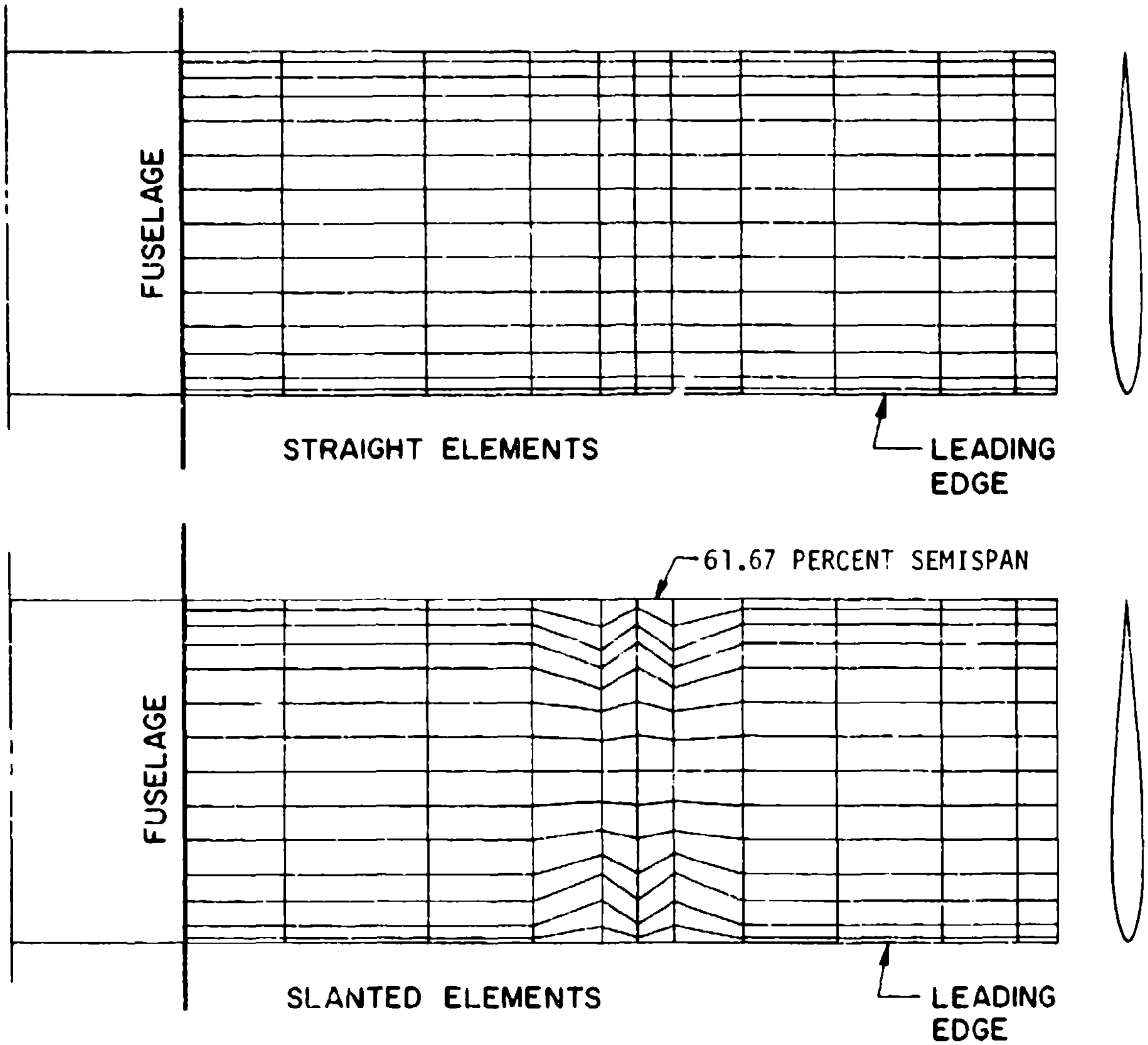

Figure 33. Two element distributions on a wing of rectangular planform mounted on a round fuselage.

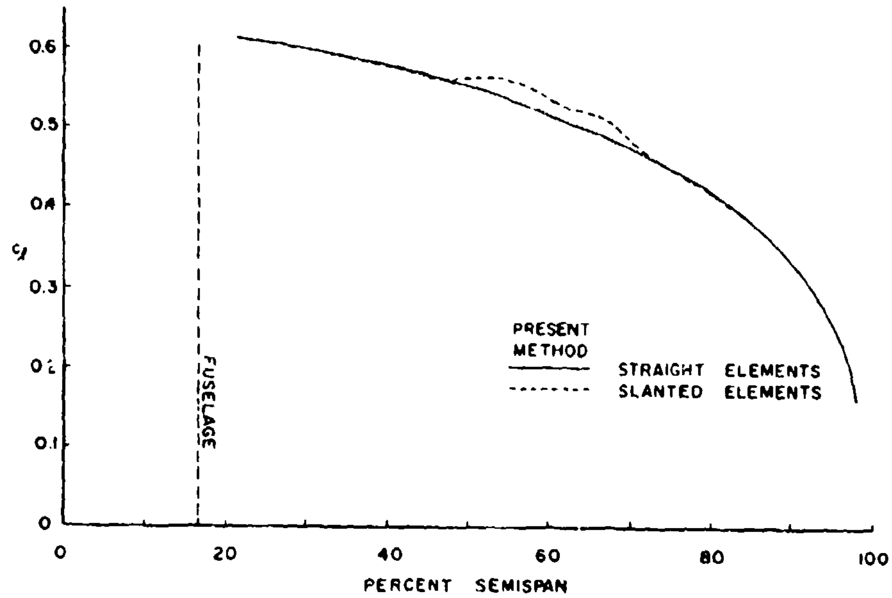

(a)

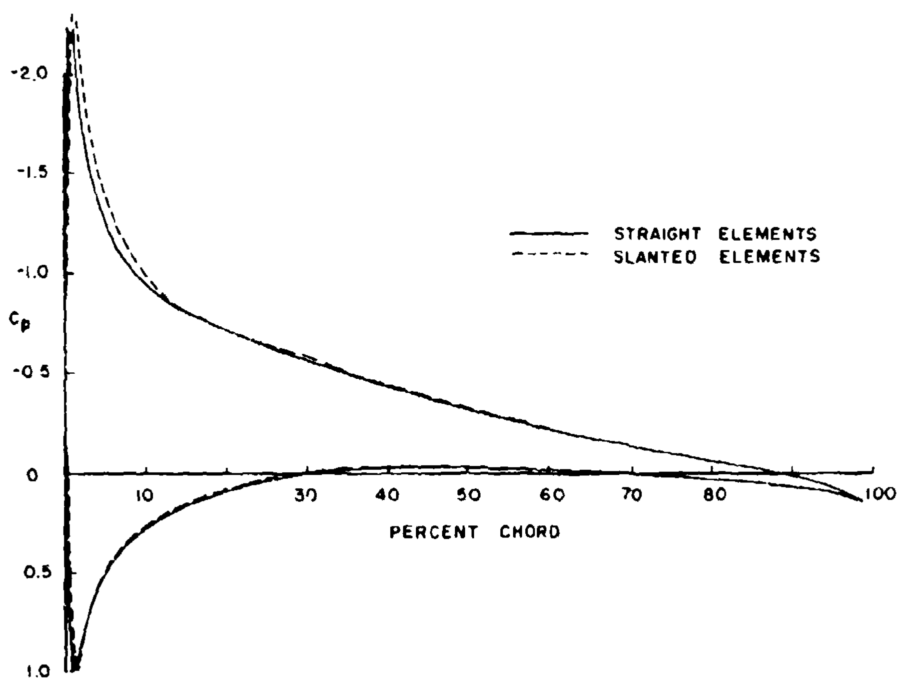

(b)

Figure 34. Comparison of results calculated for a rectangular wing mounted on a round fuselage using two different element distributions at 6 degrees angle of attack. (a) Spanwise distributions of section lift coefficient. (b) Chordwise pressure distributions at 61.67 percent semispan.

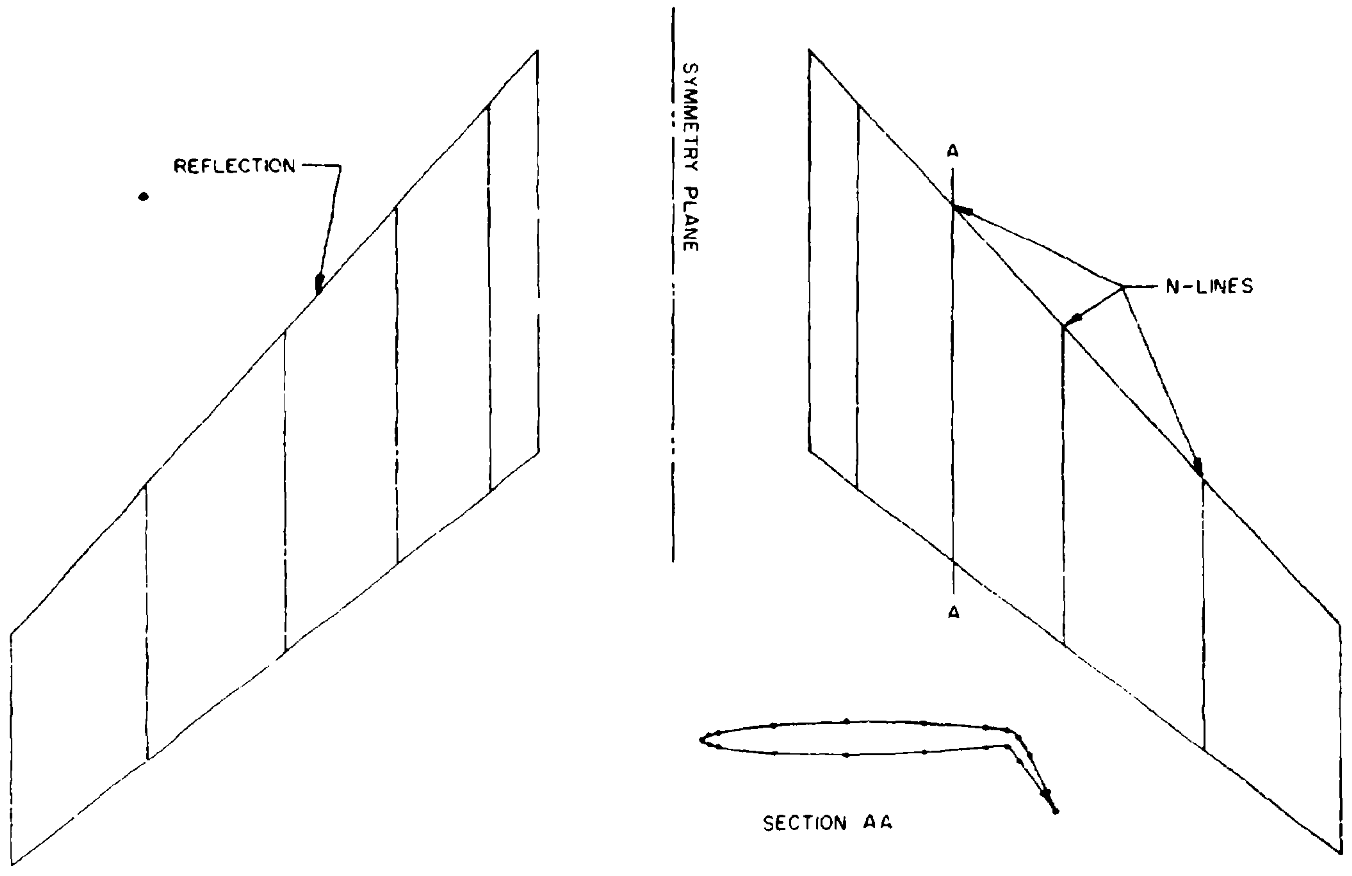

Figure 35. Geometry of an extreme test case with a large flap deflection.

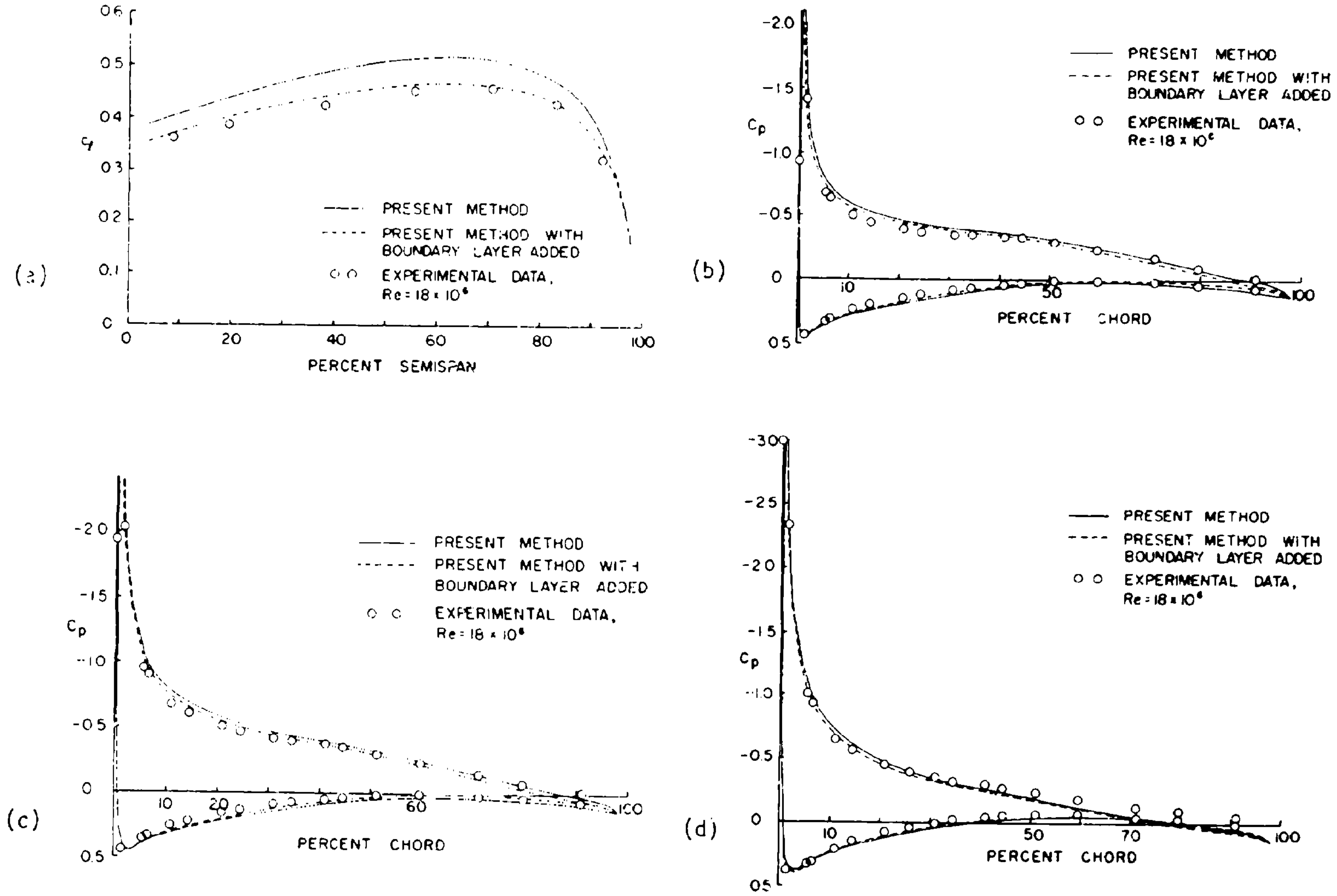

Figure 36. Comparison of calculated and experimental results on a swept tapered wing at 8 degrees angle of attack. (a) Spanwise distributions of section lift coefficient. Chordwise pressure distributions at: (b) 19.5 percent semispan, (c) 55.5 percent semispan, (d) 92.4 percent semispan.

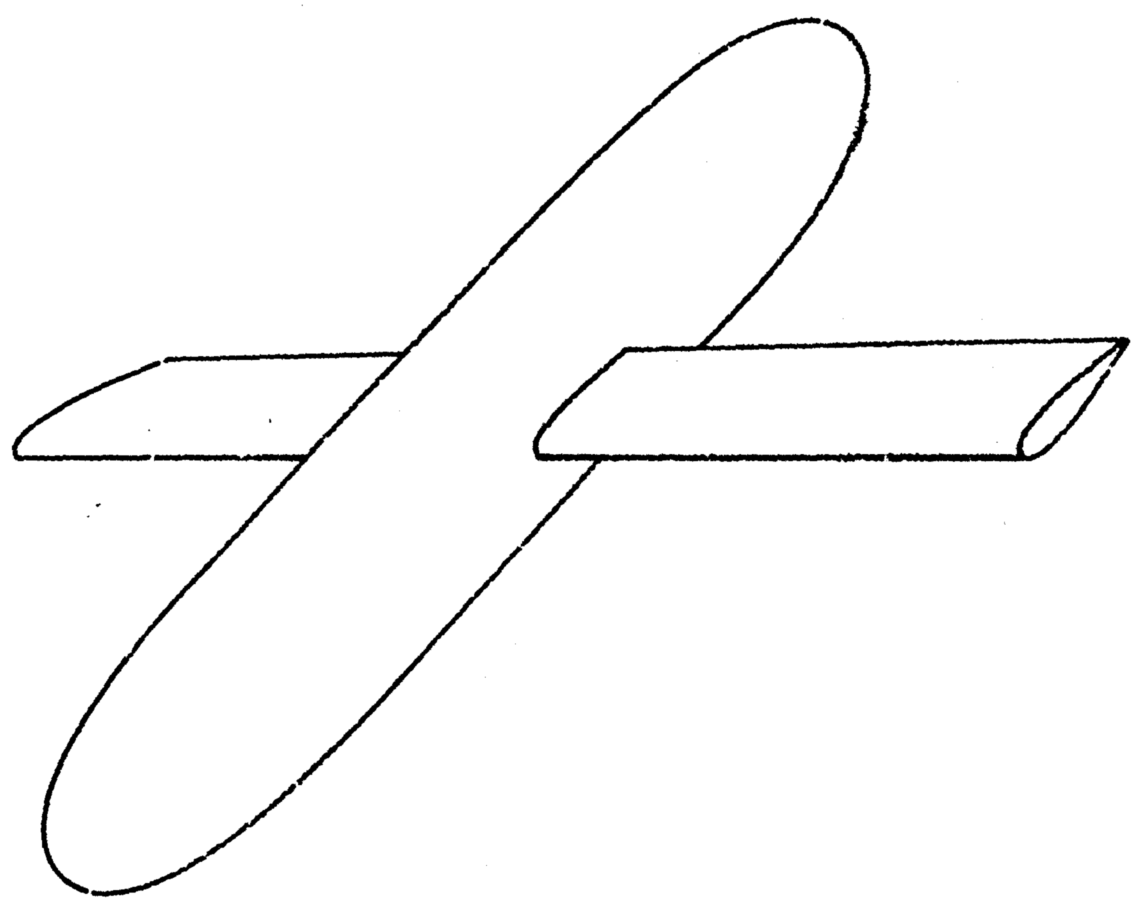

Figure 37. A rectangular wing mounted as a midwing on a round fuselage.

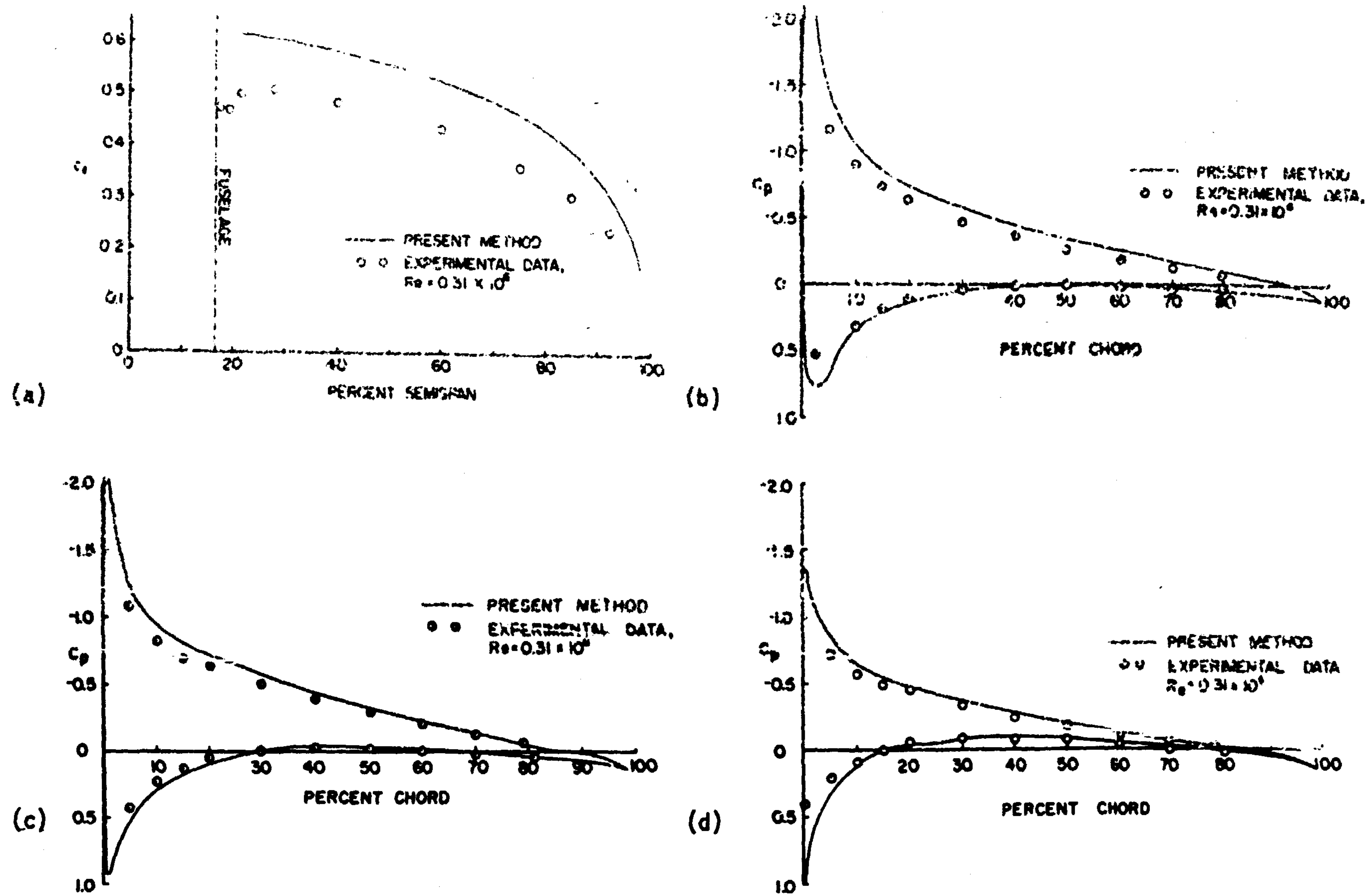

Figure 38. Comparison of calculated and experimental results on a rectangular wing mounted as a midwing on a round fuselage at 6 degrees angle of attack. (a) Spanwise distributions of section lift coefficient. Chordwise pressure distributions at: (b) 19.3 percent semispan, (c) 60.0 percent semispan, (d) 92.4 percent semispan.

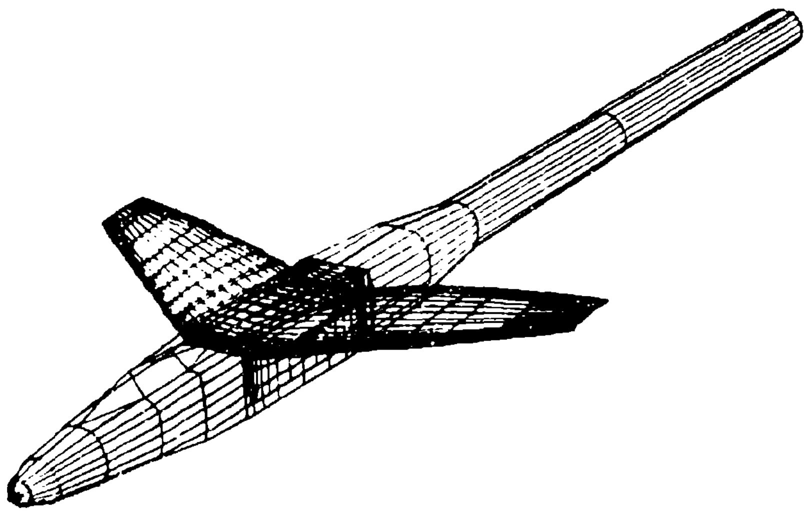

(a)

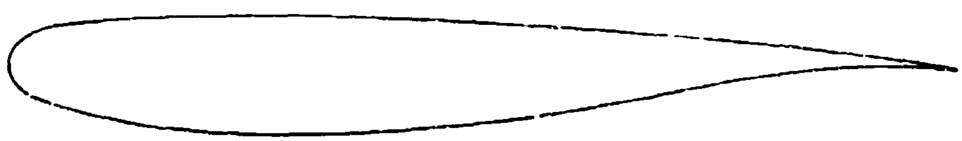

(b)

Figure 39. A supercritical wing mounted as a high wing on a fuselage. (a) The complete configuration. (b) Airfoil section of the wing.

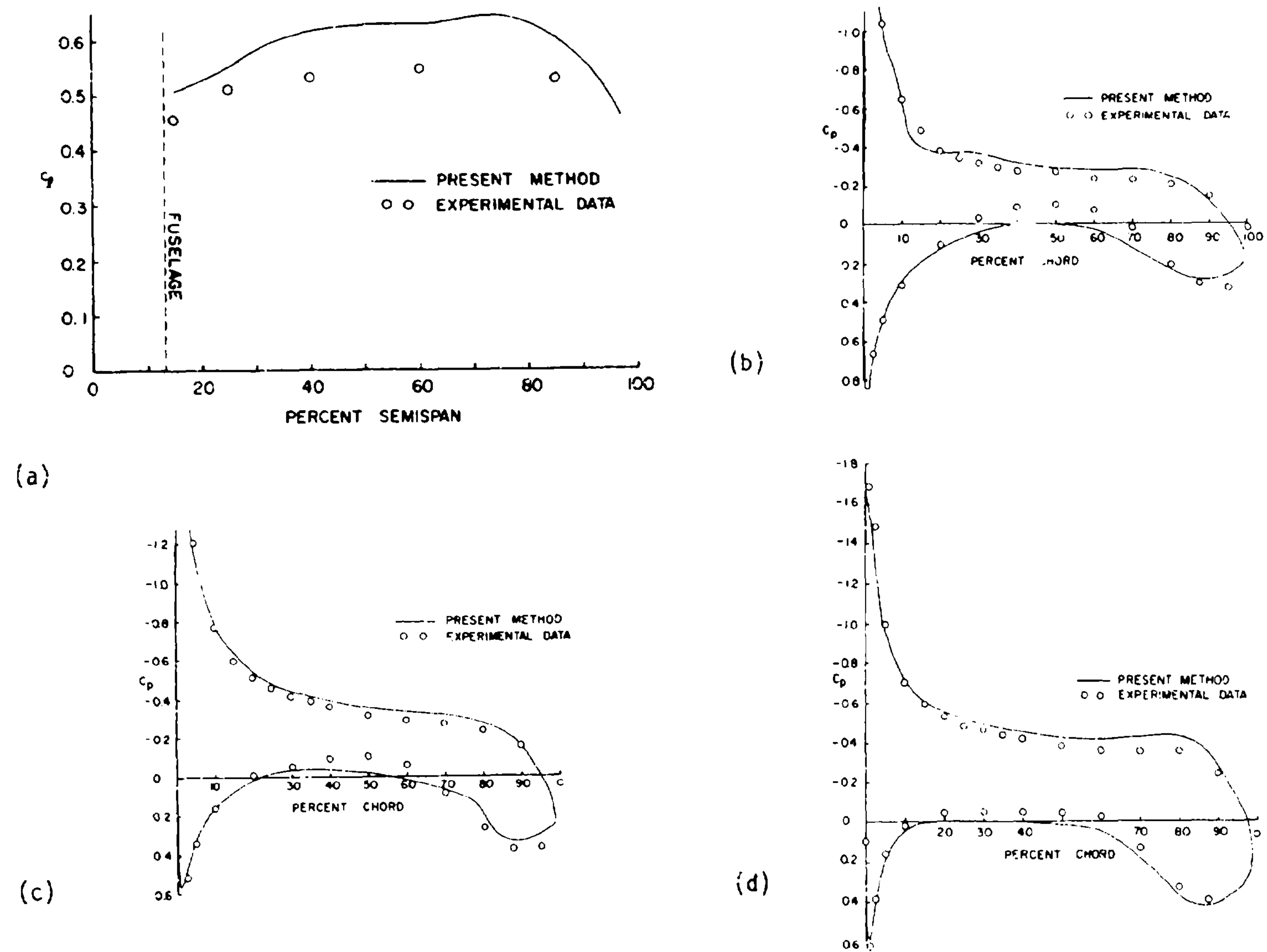

Figure 40. Comparison of calculated and experimental results on a supercritical wing mounted as a high wing on a fuselage at 7 degrees angle of attack. (a) Spanwise distributions of section lift coefficient. Chordwise pressure distributions at: (b) 15 percent semispan, (c) 25 percent semispan, (d) 60 percent semispan.

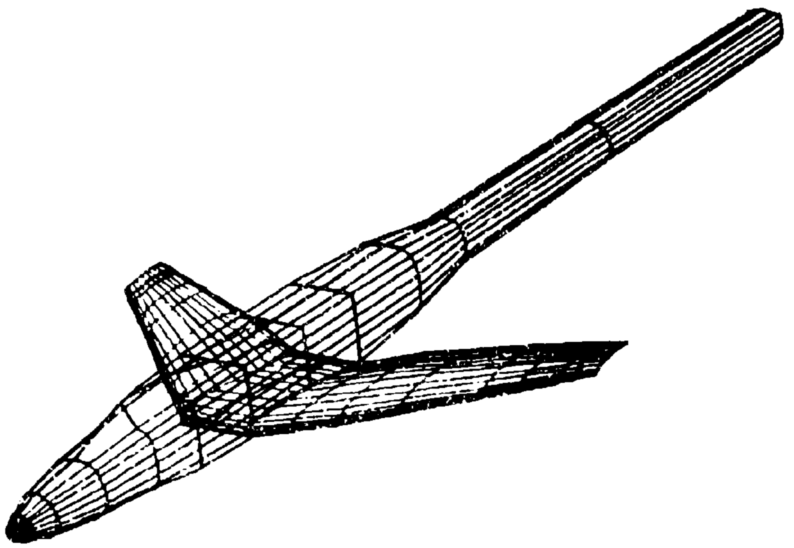

(a)

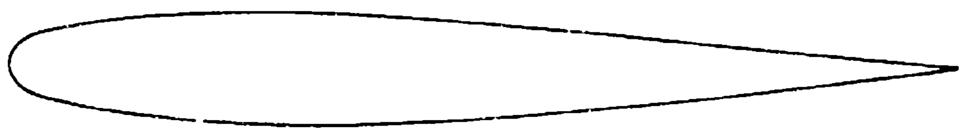

(b)

Figure 41. A conventional wing mounted as a low wing on a fuselage. (a) The complete configuration. (b) Airfoil section of the wing.

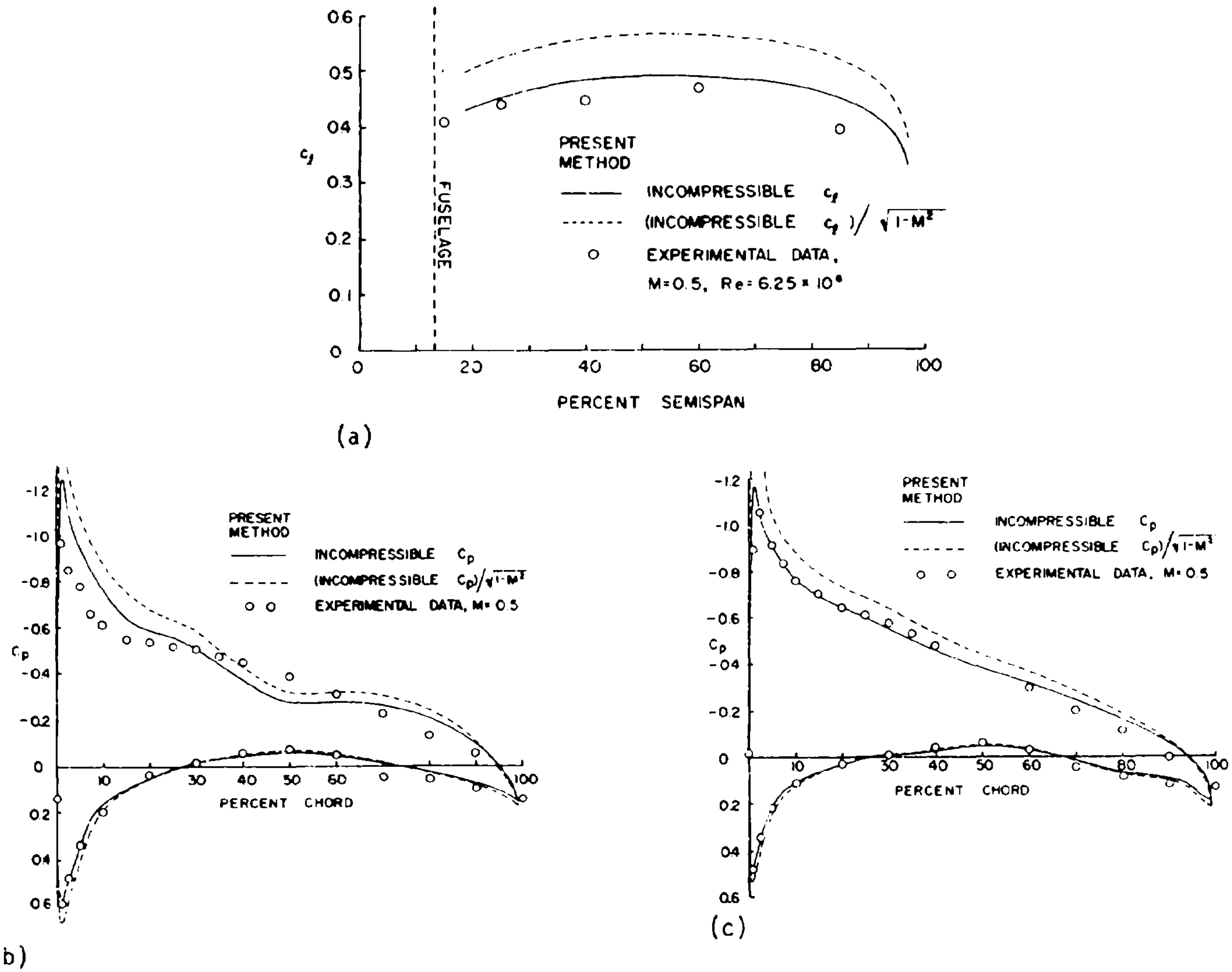

Figure 42. Comparison of calculated and experimental results on a conventional wing mounted as a low wing on a fuselage at 6.9 degrees angle of attack and a freestream Mach number of 0.5. (a) Spanwise distributions of section lift coefficient. Chordwise pressure distributions at: (b) 15 percent semispan, (c) 25 percent semispan.

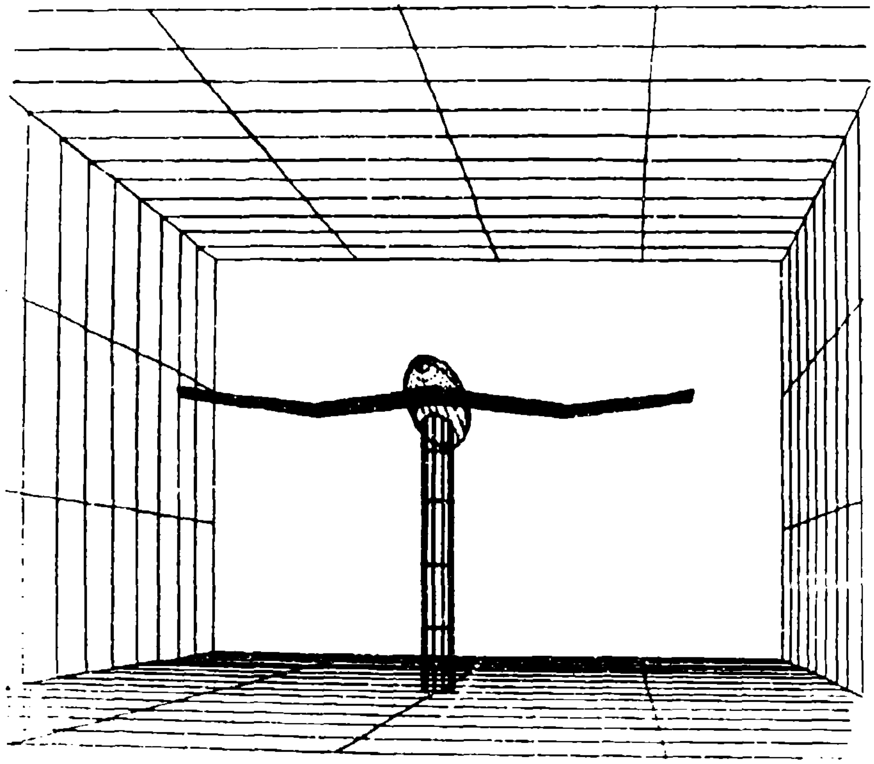

(a)

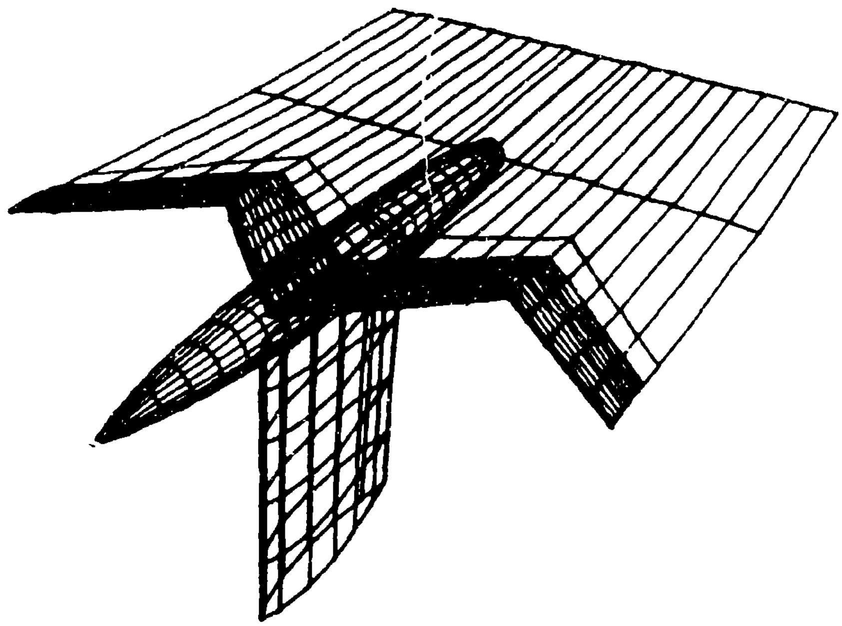

(b)

Figure 43. A W-wing on a fuselage mounted on a strut in a rectangular wind tunnel.

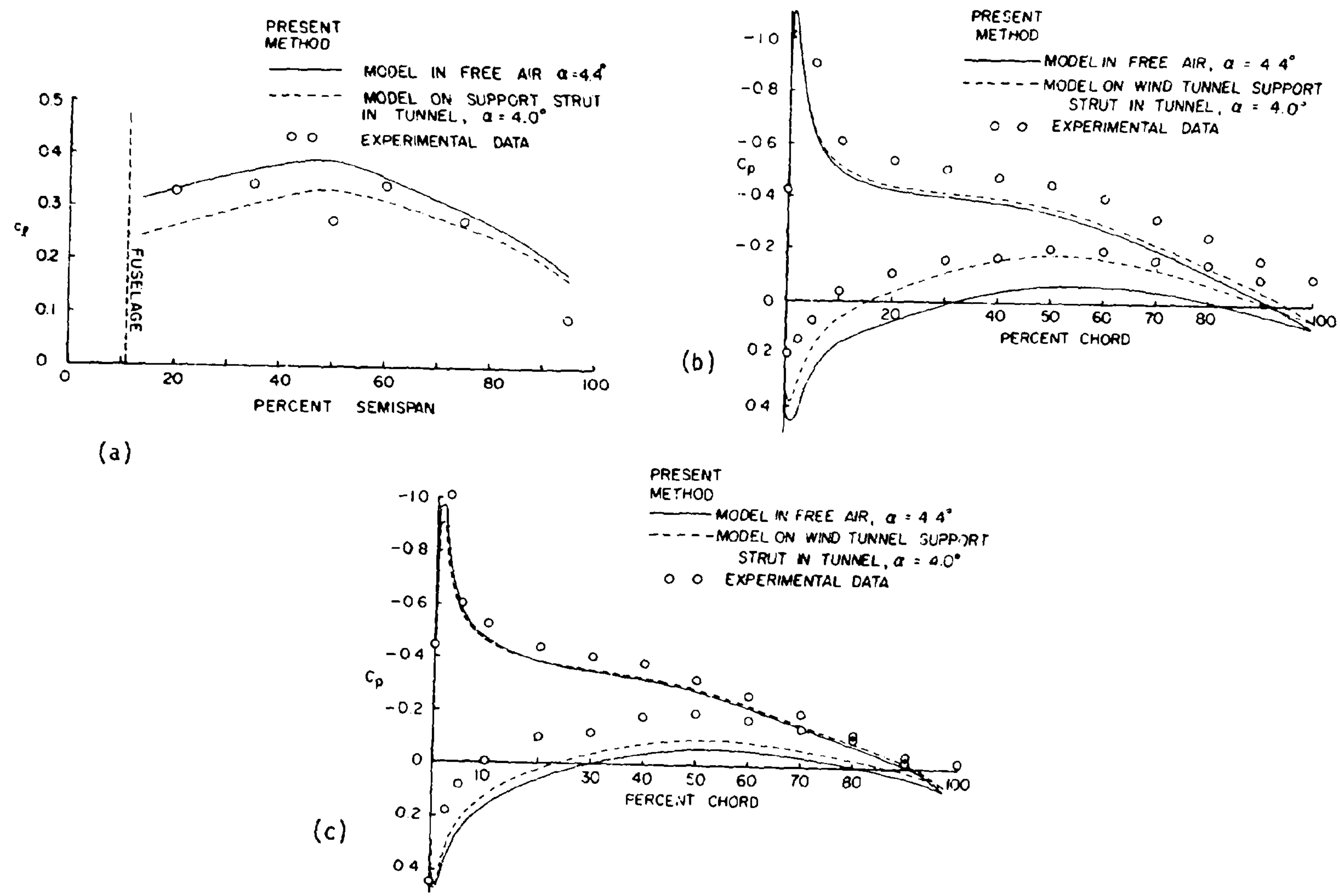

Figure 44. Comparison of calculated and experimental results on a W-wing mounted on a fuselage. Calculations performed with and without support strut and wind tunnel walls. (a) Spanwise distributions of section lift coefficient. Chordwise pressure distributions at: (b) 20 percent semispan, (c) 75 percent semispan.

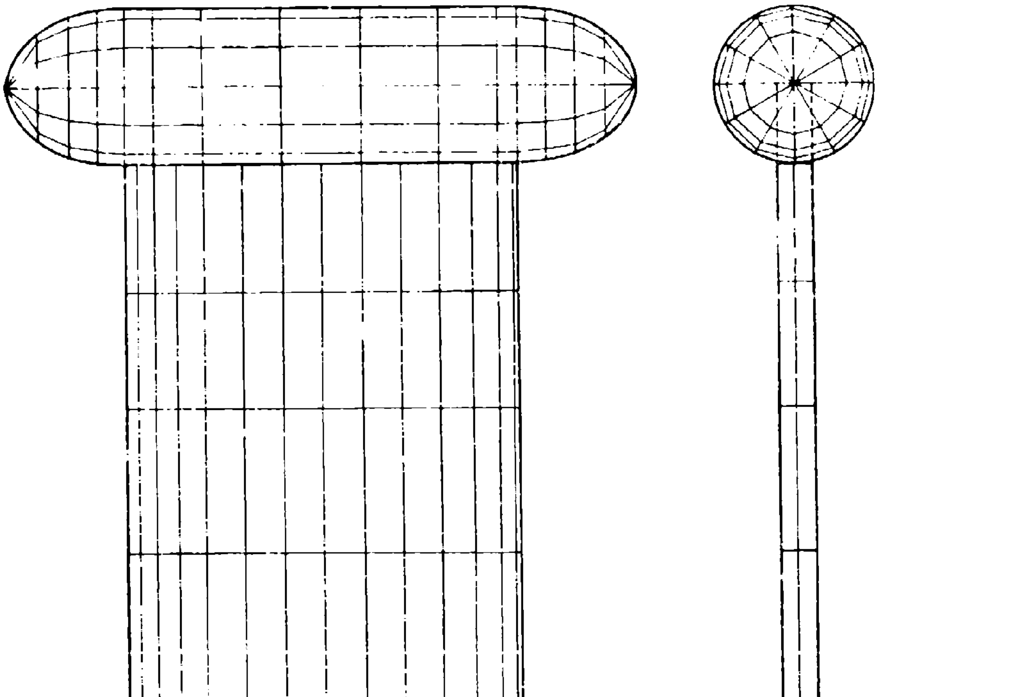

Figure 45. Two external-store configurations. (a) A tip tank.

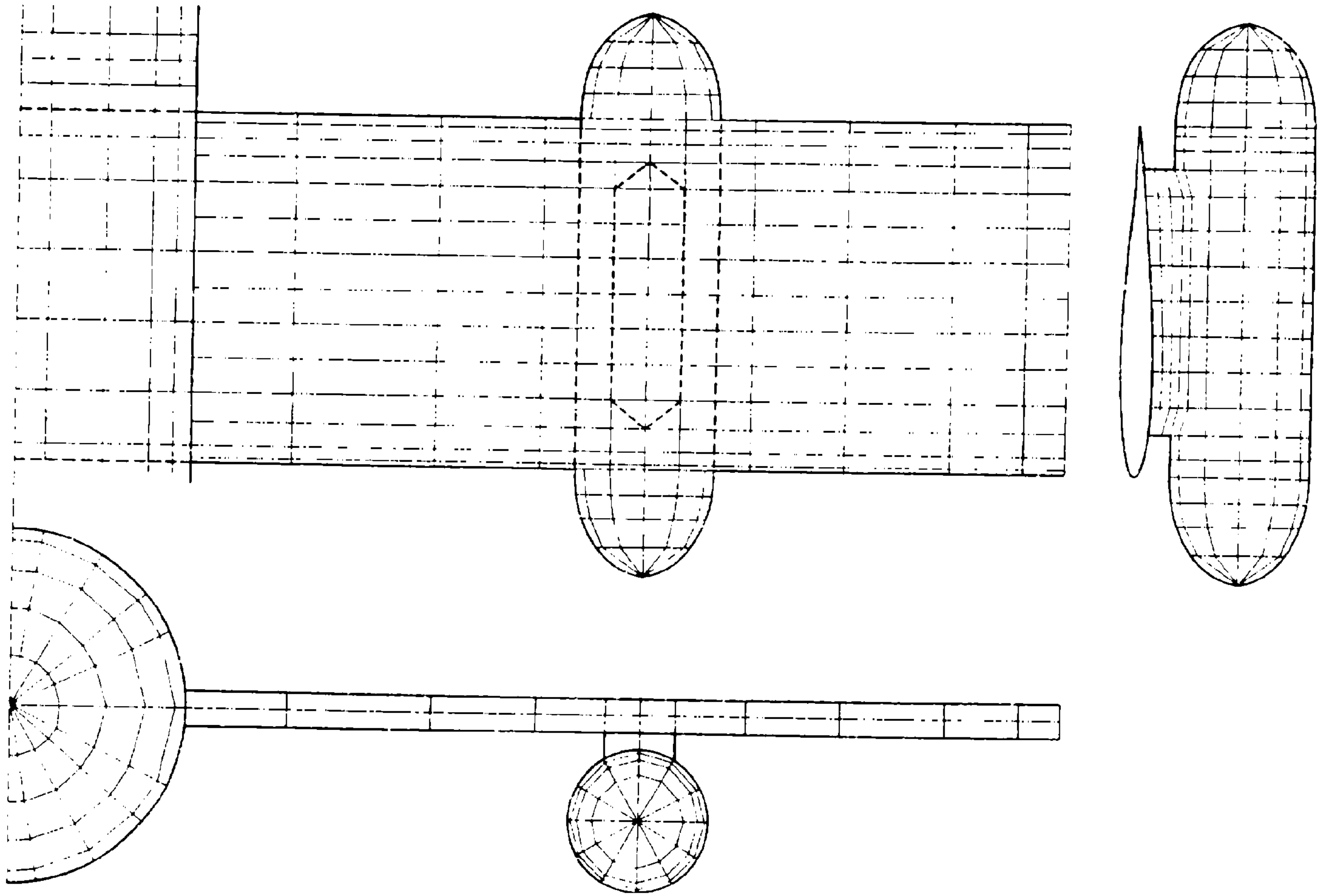

Figure 45. Continued (b) A pylon-mounted external-store.

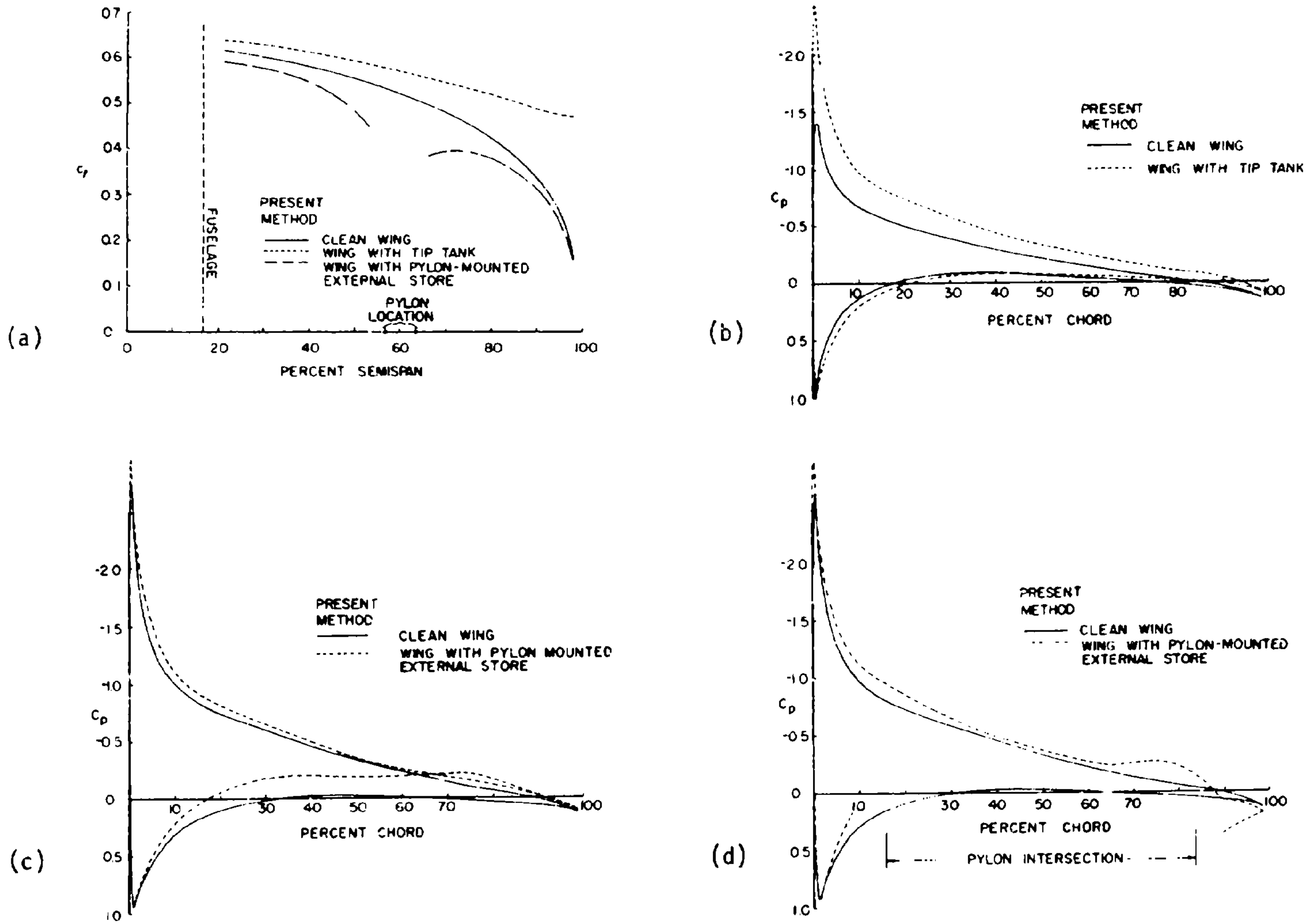

Figure 46. Comparison of calculated results on a clean wing, a wing with tip tank, and a wing with pylon-mounted external store, all in the presence of a round fuselage at 6 degrees angle of attack. (a) Spanwise distributions of section lift coefficient. Chordwise pressure distributions at: (b) 92.4 percent semispan, (c) 53.3 percent semispan, (d) 58.3 percent semispan.

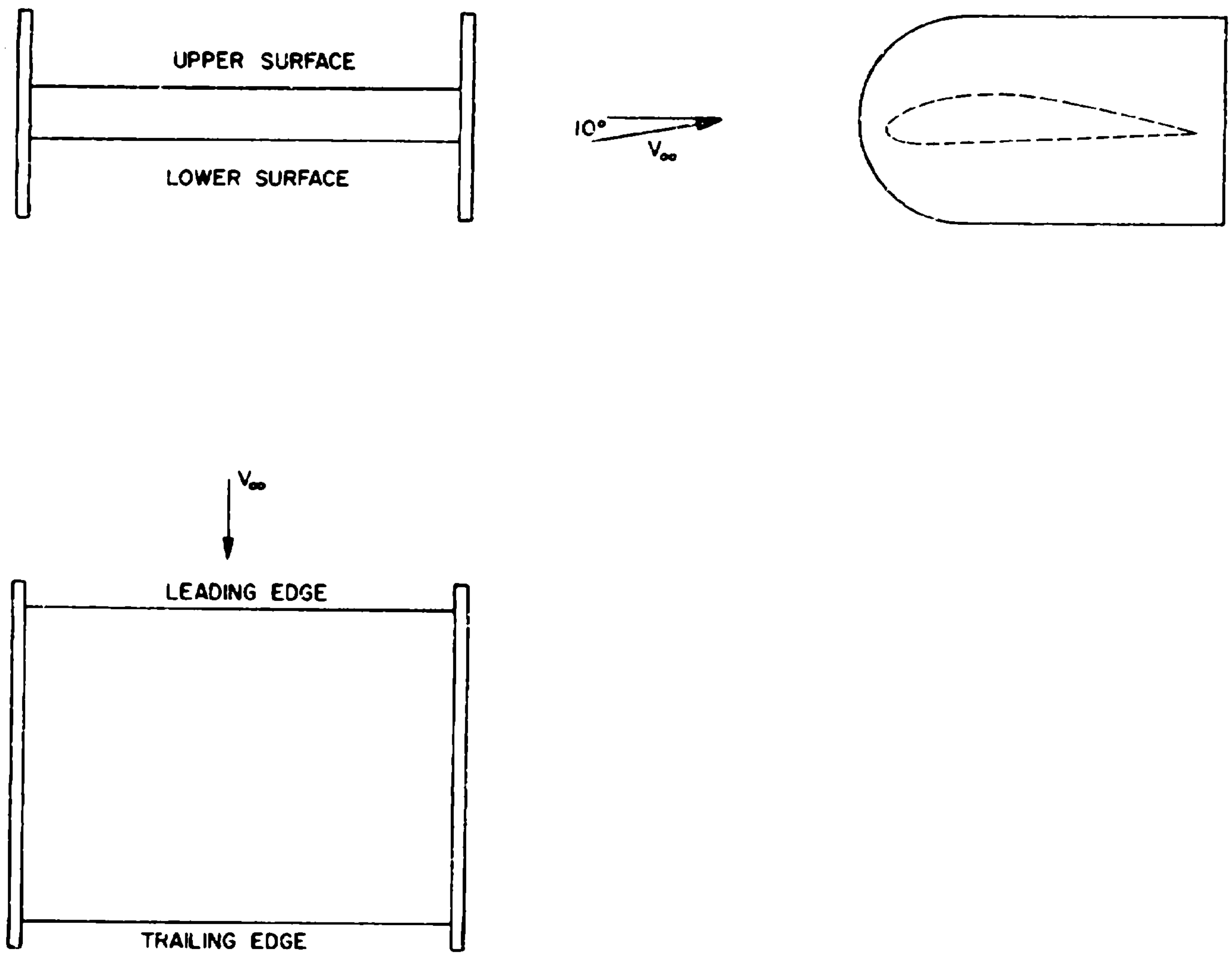

Figure 47. A rectangular wing of aspect ratio 1.4 with endplates.

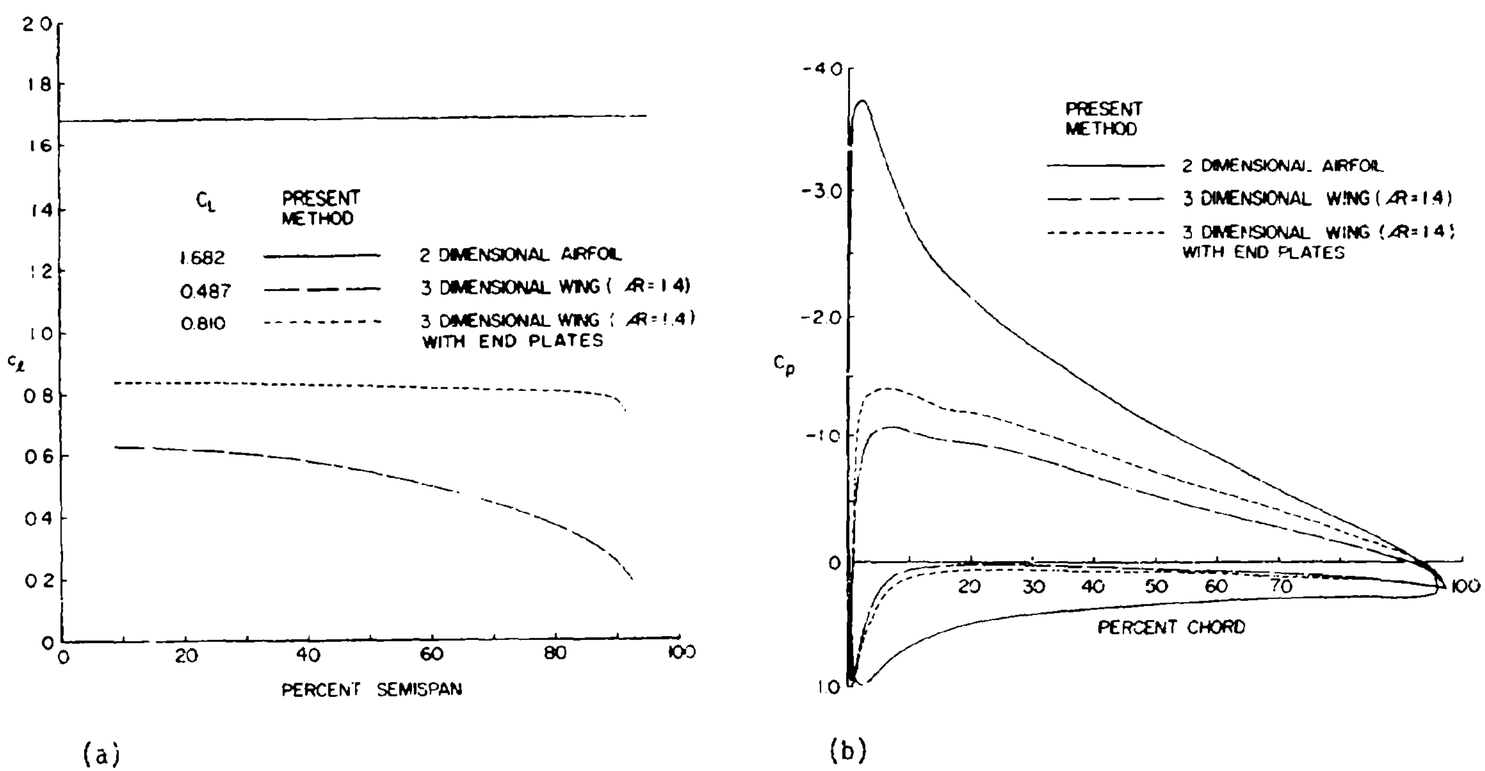

Figure 48. Comparison of calculated results on a rectangular wing at 10 degrees angle of attack with and without end plates. (a) Spanwise distributions of section lift coefficient. (b) Chordwise pressure distributions at the center section.

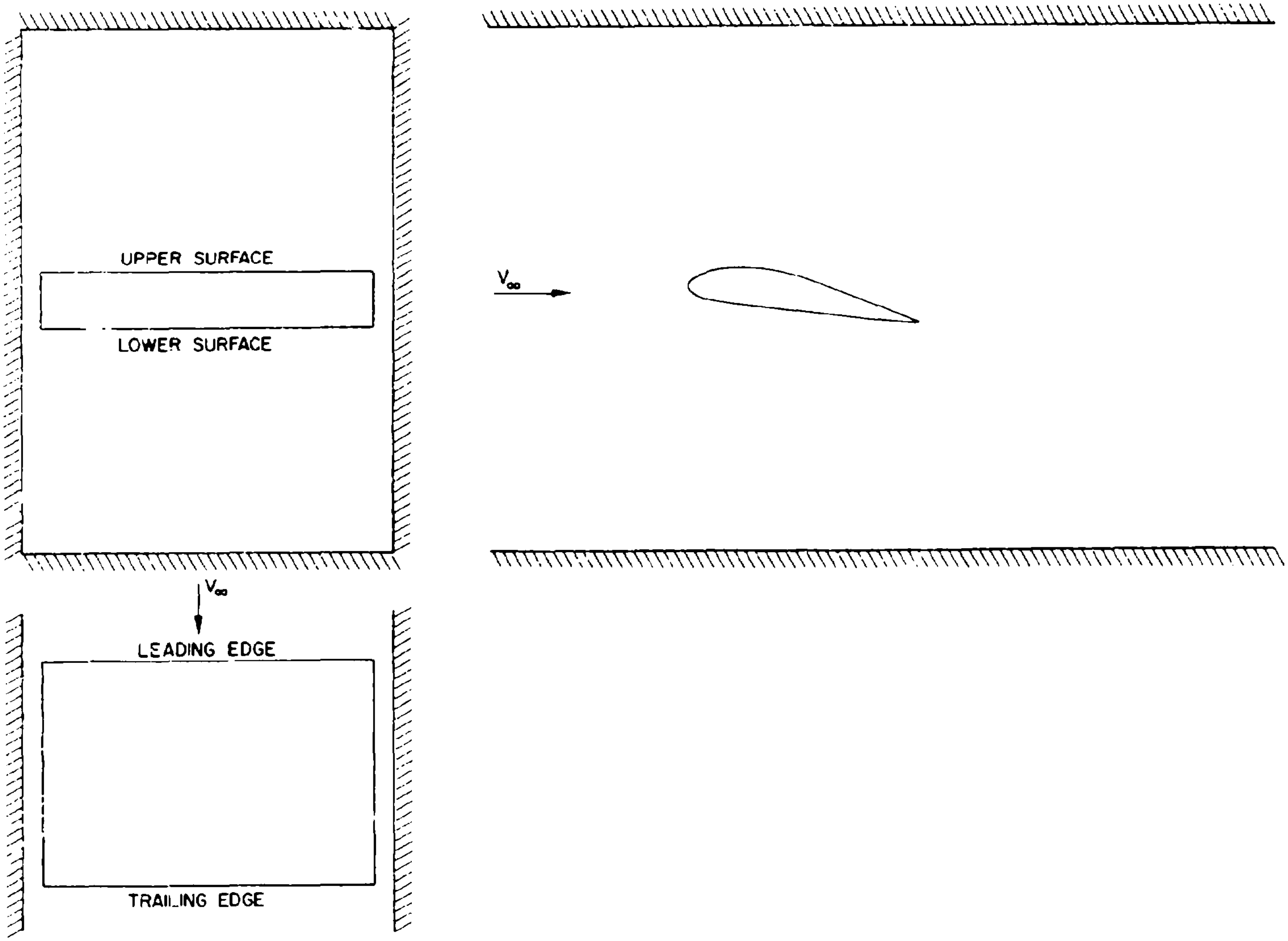

Figure 49. A rectangular wing of aspect ratio 1.4 in a rectangular wind tunnel.

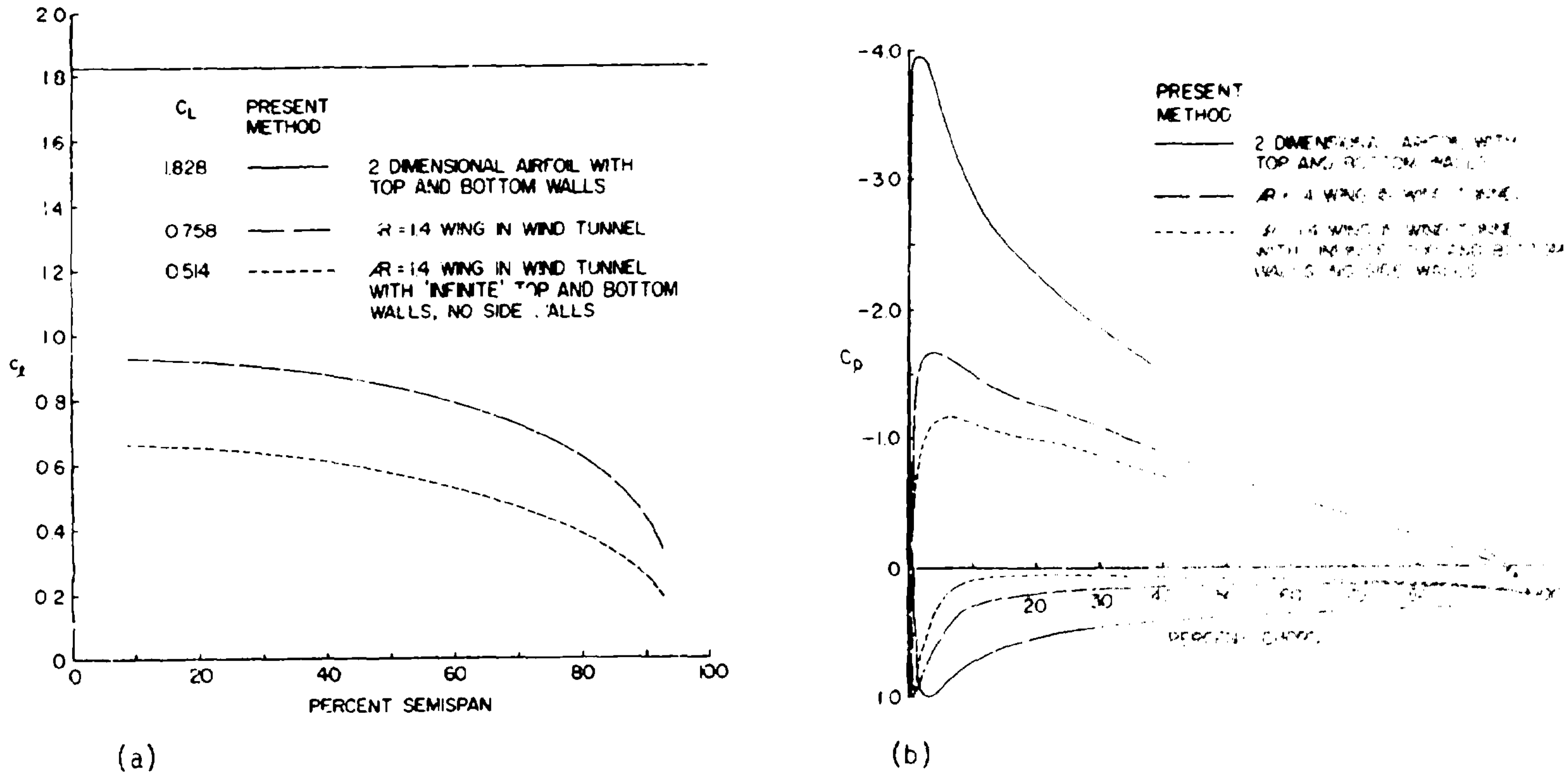

Figure 50. Comparison of calculated results on a rectangular wing at 10 degrees angle of attack with and without the wind tunnel side walls. (a) Spanwise distributions of section lift coefficient. (b) Chordwise pressure distributions at the center section.

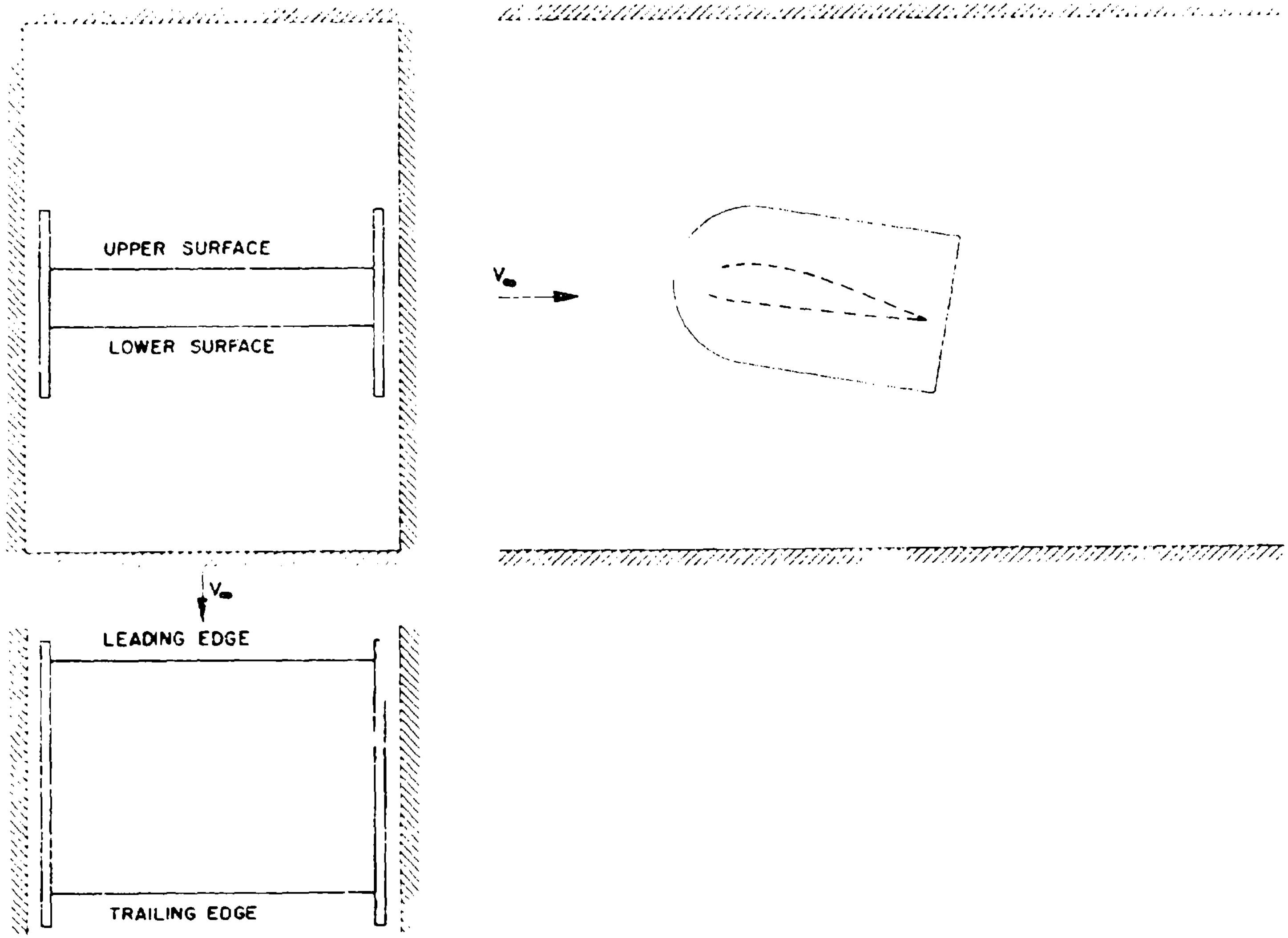

Figure 51. A rectangular wing of aspect ratio 1.4 with endplates in a rectangular wind tunnel.

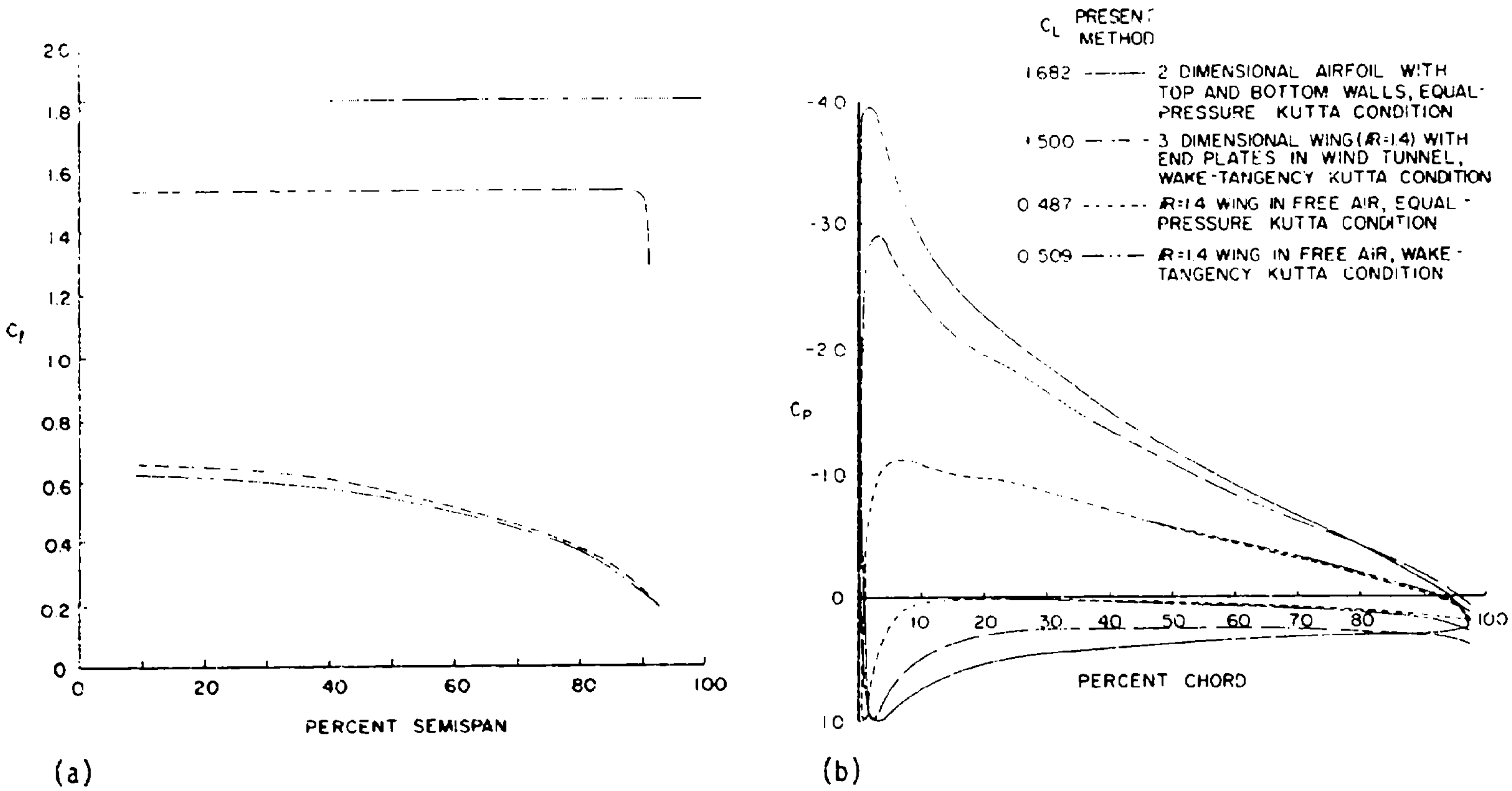

Figure 52. Comparison of calculated results for a rectangular wing at 10 degrees angle of attack in free air with those for the same wing with endplates in a wind tunnel. (a) Spanwise distributions of section lift coefficient. (b) Chordwise pressure distributions of the center section.